REAL TIME CELL METABOLISM BY NMR

JENNIE ROBERTS

[redacted]

A thesis submitted to the University of Birmingham for the degree of

DOCTOR OF PHILOSOPHY

The Institute of Cancer and Genomic Sciences

College of Medical and Dental Sciences

University of Birmingham

2020

ABSTRACT

Metabolism is now widely recognised as an important hallmark of disease. Measuring metabolism is therefore an important endeavour to identify and elucidate disease states. NMR is used for the study of live samples, from cells to whole organisms, due to its non-invasive, non-destructive nature. A variety of different approaches have been proposed for real-time analysis of live samples including bioreactors that perfuse nutrients to sustain cells during acquisition. The purpose of this thesis is to further develop real-time applications for NMR studies of mammalian cell metabolism using an NMR flow system.

ACKNOWLEDGMENTS

I am grateful to Professor Günther and Professor Bonifer for accepting me into their labs, and to Bruker Ltd for providing equipment and support during my studentship. I would like to thank Matteo Pennestri, Martin Hofmann and Pete Gierth for their help and advice while learning NMR and working with the InsightMR flow system. I am thankful also to senior postdocs Anetta Ptasinska and Michelle Thompson for their guidance during my PhD. Daniel Coleman, Sandeep Potluri, Ben Edginton-White, Peter Keane and Sophie Kellaway, thank you all for listening and answering my stupid questions!

I would like to highlight the unsung heroes of HWB·NMR; Sara Whittaker, Mark Jeeves and Sue Rhodes. We should all be grateful for your hard work ensuring that this fantastic facility is available for the NMR community! Mark and Sara your never-ending patience with my project's various trials and tribulations is greatly appreciated.

I would also like to thank Chris Ludwig for his time, effort and patience teaching NMR theory and practice. Your weekly seminars were an invaluable source of information and inspiration.

I was very lucky to share my time in Birmingham with a fantastic group of students; Raquel, Zuhal, Nuria, Gaëlle and Greg. Thank you for all the drinks, dinners and fun times, it was such a pleasure to get to know you all and explore Birmingham together.

Finally, the two smartest, strongest and most determined people I have ever had the honour to befriend: Raquel you've been my rock – the strength and support you gave me was immeasurable. Thank you for always being there and for all the coffee, cake, and travel adventures! Assunta, my long-suffering housemate, thank you for putting up with me, looking out for me, and taking care of me. I hope our beer fuelled late-night chats and scientific discussions continue well into the future.

CONTENTS

List of Figures

LIST OF DEFINITIONS AND/OR ABBREVIATIONS

1D	one-dimensional
1,3-BPG	1,3-biphosphoglyceric acid
2D	two-dimensional
2-DG	2-deoxyglucose
2-HG	2-hydroxyglutarate
2-PG	2-phosphoglycerate
3-PG	3-phosphoglycerate
7-AAD	7-amino actinomycin D
α-KG	α-ketoglutarate
ADP	adenosine diphosphate
ALT	alanine transaminase
CoA	coenzyme A
AML	acute myeloid leukaemia
AMP	adenosine monophosphate
AMPK	AMP-activated protein kinase
ATP	adenosine triphosphate
AUC	area under curve
BCAA	branched chain amino acids
CEBPA	CCAAT/enhancer binding protein alpha
CPMG	Carr-Purcell-Meiboom-Gill sequence
D2O	deuterium oxide
DHAP	Dihydroxyacetone
DNA	deoxyribonucleic acid
DMSO	dimethyl sulfoxide
DSS	Sodium trimethylsilylpropanesulfonate

ECM	extracellular matrix
EDTA	ethylenediaminetetraacetic acid
ETC	electron transport chain
F1,6P	fructose 1-6,diphosphate
F6P	fructose 6-phosphate
FAB	French-American-British
FAD	flavin adenine dinucleotide
FADH2	reduced flavin adenine dinucleotide
FBS	fetal bovine serum
FCR	Fc receptor
FDA	Food and Drug Administration
THF	tetrahydrofolate
FID	free-induction decay
G6P	glucose 6-phosphate
GADP	glyceraldehyde-3-phosphate
GAPDH	glyceraldehyde 3-phosphate dehydrogenase
GDH	glutamate dehydrogenase
GFP	green fluorescent protein
GLS	glutaminase
GSH	glutathione
H_2O_2	hydrogen peroxide
HFPB	hollow fibre perfusion bioreactor
HIF	hypoxia-inducible factor
HK	hexokinase
HMDB	human metabolome database
HPLC	high performance liquid chromatography
HS	horse serum

HSC	hematopoietic stem cell
IDH	isocitrate dehydrogenase
LC	liquid chromatography
LDH	lactate dehydrogenase
LT-HSC	long-term haematopoietic stem cell
MACS	magnetic activated cell sorting
MCT	monocarboxylate transporter
MEM	minimal essential medium
MTHDF	methylenetetrahydrofolate dehydrogenase
NAD+	nicotinamide adenine dinucleotide
NADH	reduced nicotinamide adenine dinucleotide
NADP+	nicotinamide adenine dinucleotide phosphate
NADPH	reduced nicotinamide adenine dinucleotide phosphate
NMR	nuclear magnetic resonance
NaN_3	sodium azide
NOESY	nuclear Overhauser effect spectroscopy
OAA	oxaloacetate
OD	optical density
PBS	phosphate buffered saline
PCR	polymerase chain reaction
PDH	pyruvate dehydrogenase
PEEK	polyether ether ketone
PEP	phosphoenolpyruvate
PFG	pulsed field gradients
PFK	phosphofructokinase
P_i	inorganic phosphate
PHGDH	phosphoglycerate dehydrogenase

PIP_2	phosphatidylinositol (4,5) bisphosphate
PIP_3	phosphatidylinositol (3,4,5) triphosphate
PI3K	phosphatidylinositol 3-kinase
PTEN	tumour suppressor phosphatase with tensin homology
PTFE	polytetrafluoroethylene
PP_i	pyrophosphate
PPP	pentose phosphate pathway
PTM	post-translation modifications
pVHL	von Hippel-Lindau tumour suppressor
R5P	ribulose 5-phosphate
RF	radio frequency
ROS	reactive oxygen species
RNA	ribonucleic acid
RPMI	roswell park memorial institute 1640 medium
SAM	S-adenosylmethionine
SHMT	serine hydroxymethyltransferase
shRNA	short hairpin RNA
siRNA	small interfering RNA
TCA	tricarboxylic cycle
TMSP	3-(Trimethylsilyl)propionic-2,2,3,3-d4 acid sodium salt
UNF	Fine Unified Screw Thread
WHO	World Health Organisation

CHAPTER 1

METABOLISM

1. Supporting Life at the Cellular Level

All forms of life are self-propagating chemical systems, and coordinated units of biochemical activity underpin the internal structure of all organisms. In complex multicellular systems these units can be broken down into different organs, each composed of an ensemble of tissues that together fulfil specialised roles. Specific cell types define each tissue, together with a structured extracellular matrix that supports 3D form and function. Each cell can be further deconstructed into subcellular compartments, including membrane bound organelles that perform activities vital for cellular function [1].

Survival at each level involves internalising material from the surrounding environment; animals eat and their organs break down food to process it into smaller units such as proteins, fatty acids and polysaccharides. Individual cells uptake nutrients and process them further, ultimately producing energy from breaking the molecular bonds in sugars, amino acids and lipids. This energy supports cellular activities and can be used to drive biosynthesis of new molecules. In order to proliferate, enough ribonucleic acids, proteins, lipids and membranes must be synthesised to form new cells [2].

Metabolism encompasses the chemical reactions involved in maintaining life that take place on the subcellular level. Core biochemical processes, conserved across a diverse range of prokaryotic and eukaryotic life forms, comprise an integrated network of substrates, enzymes, and products that provide the fuel for bioenergetic demands. The basic architecture of metabolic pathways is well characterised, with over 10,000 reactions and nearly 18,000 metabolites catalogued in the Kyoto Encyclopaedia of Genes and Genomes [3]. The flow of metabolites through these pathways is context dependant, and can be specific to particular organisms, tissues and cell types. Active metabolic

pathways can vary according to health or disease state, or change with alongside other factors such as age, or even circadian rhythm [4,5].

1.1. Energy and Metabolism

Metabolic cycles and pathways are composed of three basic processes; anabolism, catabolism and elimination. In order to support cell growth and proliferation anabolic pathways generate new biomass, whereas catabolic pathways degrade substrates to produce energy and macromolecular building blocks. Elimination removes metabolic by-products, shuttling molecules between cellular compartments, or effluxing material out into the extracellular space through membrane transporters.

Glycolysis is a near-ubiquitous metabolic pathway, found in almost all domains of life [6]. In eukaryotic cells glycolytic metabolites feed into the tricarboxylic acid (TCA) cycle, which takes place inside membrane bound organelles called mitochondria. These two pathways form part of the core of mammalian metabolism, providing molecules for the anabolic and energetic demands of the cell.

Energy is required to drive reactions and a key set of compounds act to transiently store and transfer energy in the cellular environment. These energy carriers, known as adenylates, all have phosphate groups that can be removed in order to release energy for reactions.

1.1.1. Cellular Energy Sources and Electron Carriers

Energy for cellular processes is derived from the cellular energy carrier, adenosine triphosphate (ATP). This nucleotide contains two phosphoanhydride bonds that can be hydrolysed to release energy, inorganic phosphate (P_i) and adenosine diphosphate (ADP)

or adenosine monophosphate (AMP) and pyrophosphate (PP_i), as shown below in equations 1.1 and 1.2 and illustrated in Figure 1.1.

$$ATP + H_2O \rightleftharpoons ADP + P_i \quad (1.1)$$

$$ATP + H_2O \rightleftharpoons AMP + PP_i \quad (1.2)$$

Energy from ATP is coupled to other reactions, and can be used to for a variety of cellular processes including biosynthesis, motion and active transport. For example, motor proteins transform the chemical energy of ATP into discrete movements, such as the contraction of muscle fibres by myosin [7].

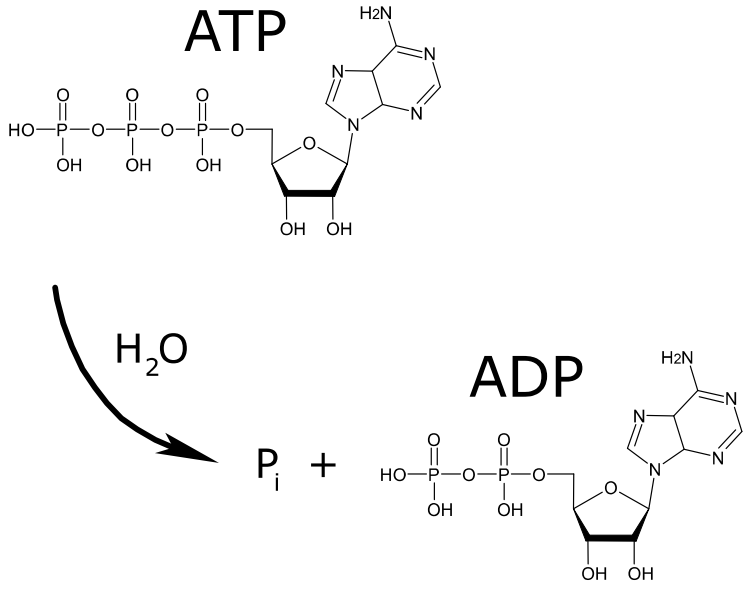

Figure 1.1 Adenylate ATP provides cellular energy for metabolic reactions.
Hydrolysis of the phosphoanhydride bond in ATP (adenosine triphosphate) yields ADP (adenosine diphosphate), inorganic phosphate (P_i) and releases energy that can be used to drive reactions.

Chemical reactions involve the conversion of substrates to products by the flow of electrons between molecules. Substrates are transformed into intermediates and products as bonds are broken and remade. The coupling of multiple reactions allows energy to be transferred from an energetically favourable reaction to another less energetically favourable reaction, usually in the form of electrons or hydride ions [8].

Two key electron carriers, nicotinamide adenine dinucleotide (NAD+) and nicotinamide adenine dinucleotide phosphate (NADP+) act as cofactors for oxidoreductases by accepting electrons from substrates. The reduced compounds formed, NADH and NADPH, act as reducing agents able to donate electrons via enzymatic transfer of a hydride ion from the nicotinamide moiety. Another electron carrier, flavin adenine dinucleotide (FAD), is also involved in core carbon metabolism and forms $FADH_2$ (reduced flavin adenine dinucleotide) by accepting a hydride ions and electrons [9].

NAD+ removes electrons from nutrients in the core metabolic pathways, forming NADH, and is later regenerated (see section 1.3.2). In reductive biosynthesis NADPH is the predominant cofactor that donates electrons, for example to regenerate glutathione (GSH) to combat reactive oxygen species (ROS).

1.1.2. Cellular Redox

ROS production and elimination is a normal part of cellular metabolism, and redox homeostasis is well regulated in order to maintain cellular function [10]. In particular, the mitochondrial respiratory chain generates superoxide (O_2^-) as a by-product of metabolism. This molecule is highly reactive due to a single unpaired electron and a net negative charge.

The formation of superoxide involves the electron transport chain (ETC), embedded in the inner mitochondrial membrane, which transfers electrons through a series of complexes, producing a transmembrane proton gradient. This proton-motive force is used by ATP synthase to produce ATP by rotary catalysis; transmembrane proton flow rotates part of structure, inducing a confirmation change so that active sites containing ADP and P_i are forced together to form ATP [11].

Some electrons can leak out of the electron transport chain and combine with oxygen to produce the superoxide anion [12], which can then be converted to hydrogen peroxide (H_2O_2) by the enzyme superoxide dismutase. H_2O_2 forms hydroxyl radicals (·OH) which can also cause oxidative damage to cellular constituents [13]. Oxidative modifications include altering structure and reactivity of thiols in cysteine residues of proteins [14].

The ROS defence system is composed of a series of enzymes that interact with organic hydroperoxides, radicals and superoxide. Each of these enzymes requires NADPH for activity [15]. A source of NADPH therefore protects the intercellular environment from oxidative damage and redox equivalents can be shuttled throughout the cell, and regenerated in further metabolic reactions.

1.1.3. Glycolysis and the Pentose Phosphate Cycle

During glycolysis the carbon skeleton of glucose is broken down, producing two molecules of pyruvate from the original six-carbon sugar. This anaerobic process can be considered as two phases; initial investment (consuming ATP) and final payoff (producing ATP) [16]. Three key points of allosteric regulation control the overall cascade of ten reactions, involving enzymes hexokinase, phosphofructokinase and pyruvate kinase. Overall, the energy released by the oxidation of one glucose molecule results in a net production of two ATP and two NADH molecules, shown in Figure 1.2.

The glycolytic pathway starts with the uptake of glucose, facilitated by the GLUT family of membrane transporters [17]. Once inside the cell glucose is phosphorylated by hexokinase (HK) to form glucose 6-phosphate (G6P). This decreases the intracellular concentration of glucose, driving uptake, while also trapping G6P inside the cell. At this point G6P can be accepted as a substrate for the pentose phosphate pathway (PPP) or continue along the glycolytic cascade to from fructose 6-phosphate (F6P). Different isozymes of hexokinase have different affinities for glucose, and the main isoform in animal tissues is inhibited by G6P, ensuring that when the cell has high concentrations of G6P no further glucose is phosphorylated. The *K*m for hexokinase is $1x10^{-5}$ M and the enzyme will be working at maximal velocity even at relatively low glucose concentrations [18].

Isomerisation and subsequent irreversible phosphorylation of F6P by phosphofructokinase (PFK) produces fructose 1-6,diphosphate (F1,6P), using a molecule of ATP and ending the investment phase [19]. At this key control point allosteric regulation of glycolysis by PFK results in a rate limiting step. Various small molecules can act as positive and negative allosteric modulators of PFK, including adenylates, citrate and fatty acids. This ensures that the rate of glycolysis is stimulated when ADP or AMP concentrations are high. Equally, when ATP concentrations are high, or other fuel molecules are available, the rate of glycolysis will be inhibited.

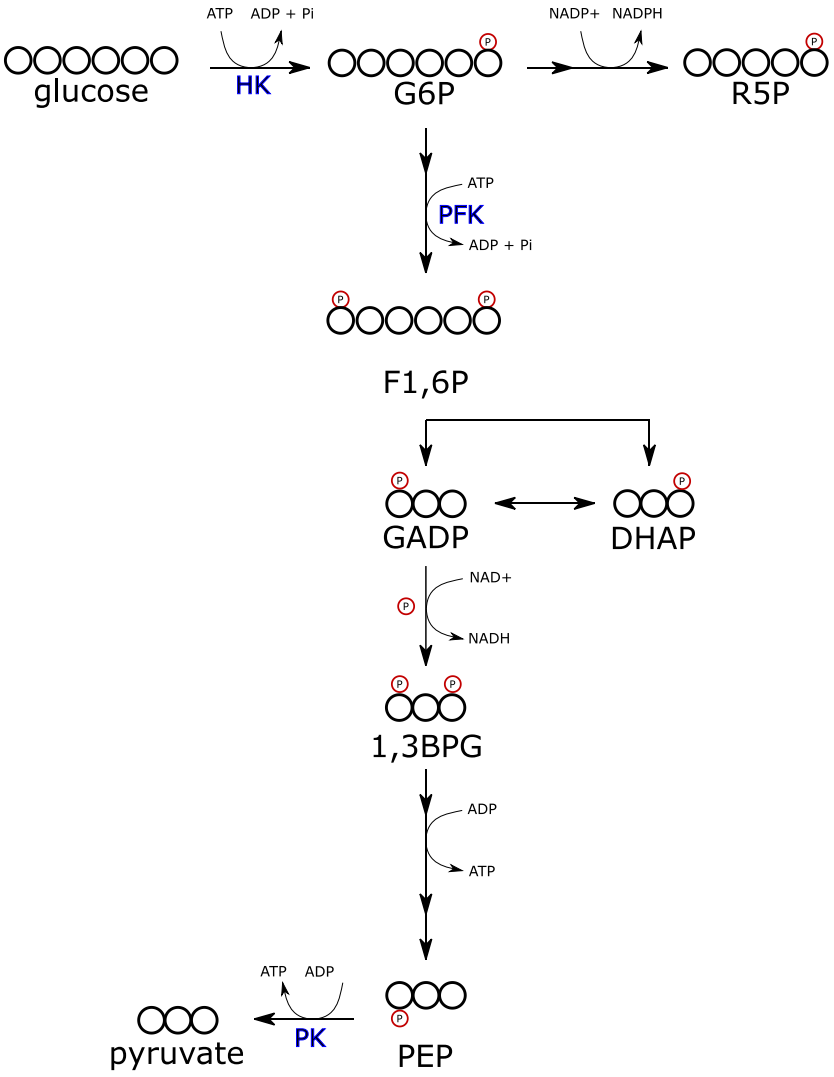

Figure 1.2 The glycolytic pathway

Glycolysis is regulated by three key enzymes; hexokinase (HK), phosphofructokinase (PFK) and pyruvate kinase (PK). The first step generates glucose 6-phosphate (G6P), which can enter the pentose phosphate pathway producing ribose-5-phosphate (R5P), or continue along the glycolytic cascade. A key point in the pathway is formation of fructose 1-6,diphosphate (F1,6P) by PFK which is then cleaved into glyceraldehyde-3-phosphate (GADP) and dihydroxyacetone (DHAP). Phosphorylation of GADP forms biphosphoglyceric acid (1,3-BPG) which undergoes several transformation to produce PEP. Overall, the end product of glycolysis is pyruvate, produced from phosphoenolpyruvate (PEP) by pyruvate kinase (PK).

Two triose molecules are produced by the breakdown of F1,6P, an enzyme catalysed interconversion allowing glycolysis to proceed from glyceraldehyde-3-phosphate (GADP) and enter the payoff phase. Glyceraldehyde 3-phosphate dehydrogenase (GAPDH) oxidises and phosphorylates the three-carbon sugar to form 1,3-biphosphoglyceric acid (1,3-BPG). Subsequent transfer of the phosphate group to ADP yields ATP and 3-phosphoglycerate (3-PG). At this point 3-PG can also be diverted to serine biosynthesis via phosphoglycerate dehydrogenase (PHGDH) [20]. Back in the glycolytic pathway isomerisation converts 3-PG to 2-phosphoglycerate (2-PG), followed by production of phosphoenolpyruvate (PEP) by enolase. The final kinase catalysed reaction produces ATP and pyruvate, which can be transported into the mitochondria where pyruvate dehydrogenase (PDH) converts the three-carbon molecule to acetyl-coenzyme A (acetyl-CoA), which then enters the TCA cycle.

The pentose phosphate pathway branches from glycolysis at the first regulatory point catalysed by hexokinase. In the oxidative stage, dehydrogenation of G6P produces 6-phosphogluconate, which is then oxidised and decarboxylated to form ribulose 5-phosphate (R5P). The NADPH generated in the oxidative stage can be used to detoxify ROS, as described in section 1.1.2.

1.1.4. Tricarboxylic Acid Cycle

Acetyl-CoA, derived from fatty acids, carbohydrates and amino acids, feeds the TCA cycle, shown in Figure 1.3. Overall, each acetyl-CoA will generate two molecules of CO_2 and regenerate the oxaloacetate (OAA) at the end of the cycle. In combination with the electron transport chain, the TCA cycle yields ATP, $FADH_2$ and NADH.

The first step commences with the ligation of OAA and acetyl-CoA, forming the six-carbon compound citrate. Interconversion of citrate and isocitrate occurs via the enzyme

bound intermediate cis-aconitate, followed by oxidation to the five carbon α-ketoglutarate (α-KG). Succinyl-CoA is formed from α-KG by oxidative decarboxylation to produce the four-carbon succinate. A series of transformations follows succinate production, to form fumarate, through the action of succinate dehydrogenase, malate via fumarase and finally OAA by malate dehydrogenase.

Various anaplerotic pathways feed into the TCA cycle, maintaining the cycle function when intermediates are diverted for use in competing biosynthetic pathways [21]. Glutamine, an abundant circulating amino acid, is converted to glutamate by glutaminase (GLS), which is subsequently transformed into α-KG, by glutamate dehydrogenase (GDH). Pyruvate may also enter the TCA cycle, following conversion to OAA through the action of pyruvate carboxylase.

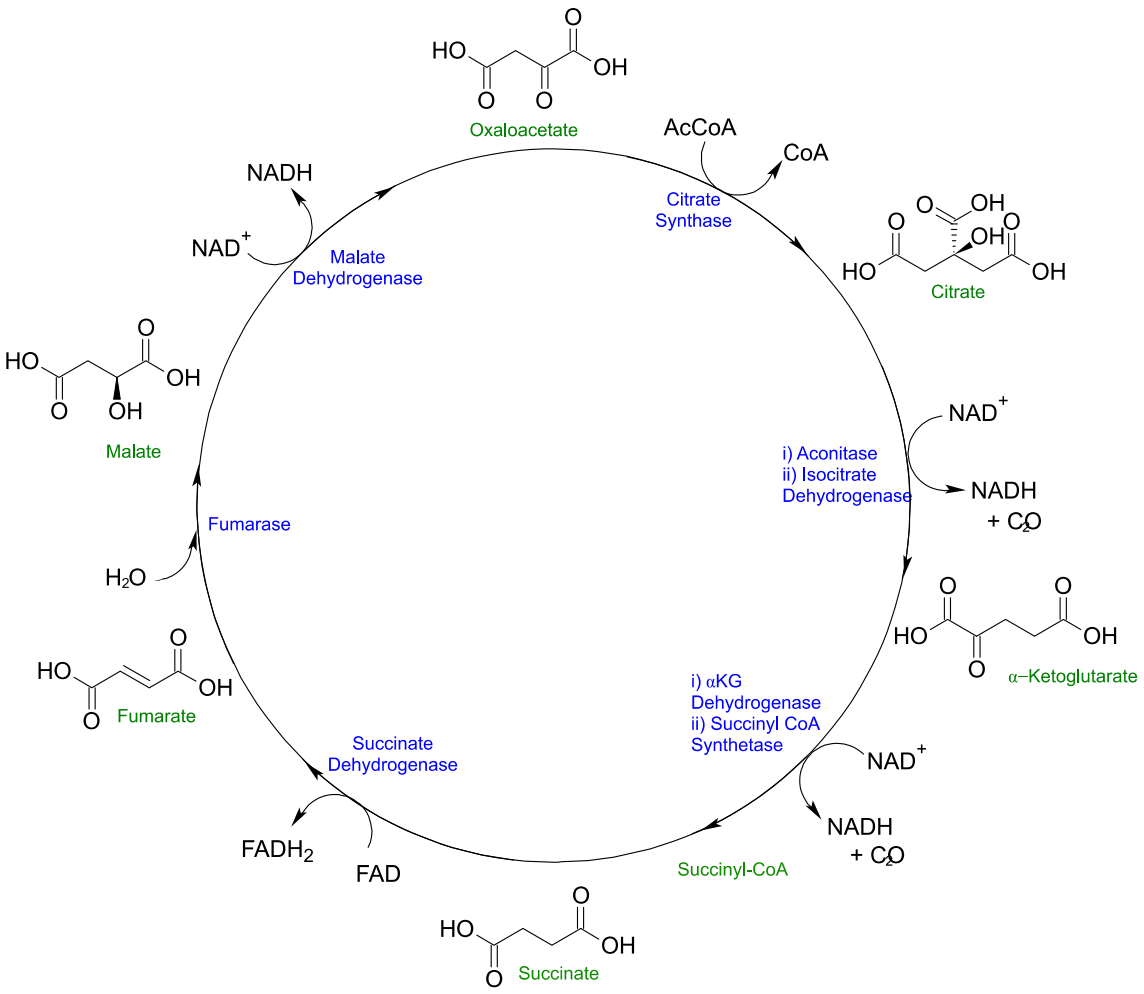

Figure 1.3 The tricarboxylic acid (TCA) cycle.

Acetyl-CoA condenses with oxaloacetate (OAA) to form citrate, which undergoes isomerisation and oxidative decarboxylation to yield α-ketoglutarate (α-KG) and release carbon dioxide (CO_2). A further carbon is lost through succinate formation, which is then oxidised to produce fumarate. Malate formation follows, and finally OAA is regenerated.

1.2. Metabolic Regulation and Nutrient Sensing Mechanisms

Cells must coordinate their growth and division with nutrient availability. Depending on the state of the cell its metabolic requirements will vary, and the activation of cell growth machinery requires certain conditions to be met [22]. For instance, proliferation requires doubling of cellular constituents and therefore new macromolecules will need to be synthesised. This can only take place if there are adequate sources of synthetic precursors, either through breaking down intracellular material or acquiring sources from the extracellular environment. In contrast, other non-proliferating cells may only require sufficient ATP to maintain cellular function and integrity.

Sensing mechanisms therefore exist to evaluate and respond to changing levels of energy sources and nutrients such as sugars, amino acids and lipids. Anabolism and storage can occur during times of abundance, whereas usage of autophagy and catabolism can be initiated during nutrient scarcity [23]. An overabundance of nutrients can also stress cells, as unrestrained metabolic processes produce an excess of toxic by-products, such as ROS [24].

In complex organisms, composed of many different kinds of cells, there must be a simultaneous detection of systemic and intracellular nutrient levels. Individual cell types have specific functions that dictate demand for certain nutrients, and regulation is required to harmonise consumption and usage of fuel substrates between tissues [25]. This is achieved through signalling molecules such as cytokines, growth factors and hormones. These secreted compounds are used to communicate energetic and nutritional status between cells, and to stimulate appropriate responses via signalling cascades. Sensing may involve direct interactions between nutrient molecules and sensor molecules, or indirect mechanisms that use surrogate signals to inform on nutritional status [26].

Post-translation modifications (PTMS), including histone modifications, are a key signal for cellular adaptation. Metabolites act as cofactors for epigenetic modifications, transmitting nutrient availability into cell signalling via chromatin remodelling. These mechanisms provide fine control of gene expression through modifications such as acetylation and methylation [27]. Cell fate can be directed though acetyl-CoA by acetylation of histones [28], or by methylation using the methyl donor S-adenosylmethionine (SAM) to alter chromatin structure and influence transcriptional activity [29].

1.2.1. Energy Sensors

The adenosine monophosphate (AMP)-activated protein kinase (AMPK) is a master energy sensor controlling cellular energetics and allowing cells to manage energy consumption based on the availability of intracellular nutrients and energy stores [30].

The kinase activity is controlled by allosteric binding of the various adenylates, with AMP and ADP competing for access with ATP [31]. As demands for cellular energy are increased ATP levels can become depleted in comparison to AMP and ADP. When ATP levels are low, AMP and ADP will preferentially bind to the kinase, inducing a conformational change [32]. This activation, producing a catalytically competent form of AMPK, results in modification of metabolism through phosphorylation of metabolic enzymes and transcriptional regulators. For example, it promotes glucose uptake through translocation and activation of glucose transporters GLUT1 and GLUT4 to the cell membrane [33]. Glucose usage is also enhanced by the phosphorylation of the glycolytic enzyme PFK, resulting in an increase of flux through the glycolytic pathway.

One downstream effector of AMPK is the mechanistic target of rapamycin (mTOR), which acts as a central point of nutrient sensing and control for many biosynthetic

pathways. There are two distinct multiprotein mTOR complexes, mTORC1 and mTORC2, which integrate a range of extracellular and intracellular cues to control energy metabolism, growth and proliferation [34]. When ATP levels are low AMPK restores the energy balance of the cell by suppressing the mTOR pathway, upregulating usage of catabolic pathways that produce ATP [35]. In contrast, once cellular energy levels are high, the mTOR complexes are activated to promote anabolic processes, such as protein synthesis, and limit catabolic processes such as autophagy.

AMPK is a target in the treatment of metabolic disorders such as diabetes. Drugs, such as biguanides like metformin, can act on AMPK indirectly by influencing mitochondrial production of ATP [36].

1.2.2. Environmental Parameters Affecting Metabolism

In addition to nutrient status, other environmental conditions also influence metabolism. For example, the concentration of molecular oxygen (O_2) has a profound effect on cellular physiology [37]. Oxygen is used as a substrate for numerous biochemical reactions, including the electron transport chain, and cellular systems exist to sense and respond to varying oxygen tensions. Low oxygen tension, known as hypoxia, is a key stimulus that can influence metabolism through transcriptional activity.

The master regulators mediating adaptation to limited oxygen are the hypoxia-inducible factors (HIFs). The transcription factor complex HIF-1, composed of a heterodimer containing α and β subunits, is responsible for gene regulation and cellular signalling in response to oxygen levels and has a direct impact on metabolism.

Under normal conditions, when sufficient molecular oxygen is present, the α subunit is hydroxylated and is recognised by the von Hippel-Lindau tumour suppressor (pVHL) for ubiquitination and degradation by the proteasome. Without molecular oxygen, HIF1α

levels accumulate and lead to the upregulation of key glycolytic enzymes, increasing metabolic flux [38].

The immediate response to hypoxia has been demonstrated in leukemia cells, where metabolic adaptation occurs within minutes of oxygen levels being depleted [39]. Rates of nutrient consumption and metabolite production changed as cells were deprived of oxygen, highlighting the importance of maintaining constant, stable partial pressure of oxygen during in vitro studies, particularly when looking to monitor responses in real time.

In mammalian cells the intracellular and extracellular pH of fluids and tissues is vital to the chemical reactions controlled by enzymes [40]. Physiological pH is maintained by buffering processes, and membrane transport systems regulate movement of protons between cellular compartments. Dysregulated pH can therefore influence cell behaviour as pH sensitive proteins, such as PFK, can have a 10-fold increase in activity with relatively small changes in pH [41].

1.3. Overflow Metabolism

Excretion of metabolic products can occur when substrates are not completely broken down by catabolic processes. Instead they are released from cells in a phenomenon known as overflow metabolism. This occurs in many organisms, and is most familiar as fermentation; the anaerobic process by which yeasts generate alcohol from sugar. Excreting metabolites, rather than breaking them down to yield ATP, may seem wasteful, yet it is often observed in fast growing cells, and thought to be an optimal growth strategy [42].

Overflow metabolism is also observed in proliferative mammalian cells, as they divide rapidly the glycolytic pathway processes glucose to pyruvate, which is then transformed into lactate and effluxed out of the cell. In addition to providing a faster rate of ATP production together, with production of biosynthetic precursors, this also generates redox equivalents [43]. Other overflow metabolites include alanine, formate and pyruvate.

1.3.1. Formate

Excess formate is effluxed from cells and circulating formate in human blood is in the range 10-100 μM [44]. In mammalian systems, formate arises from a number of metabolic pathways, and is a key intermediate in one-carbon metabolism, as shown in Figure 1.4. [45]. It therefore contributes to thymidylate synthesis, the production of methyl groups for S-adenosylmethionine (SAM) and synthesis of purine nucleotides. It is also involved in the metabolism of the amino acids serine and glycine [46]. The release of formate is thought to aid invasiveness of metastatic cells through remodelling of the extracellular matrix [47]

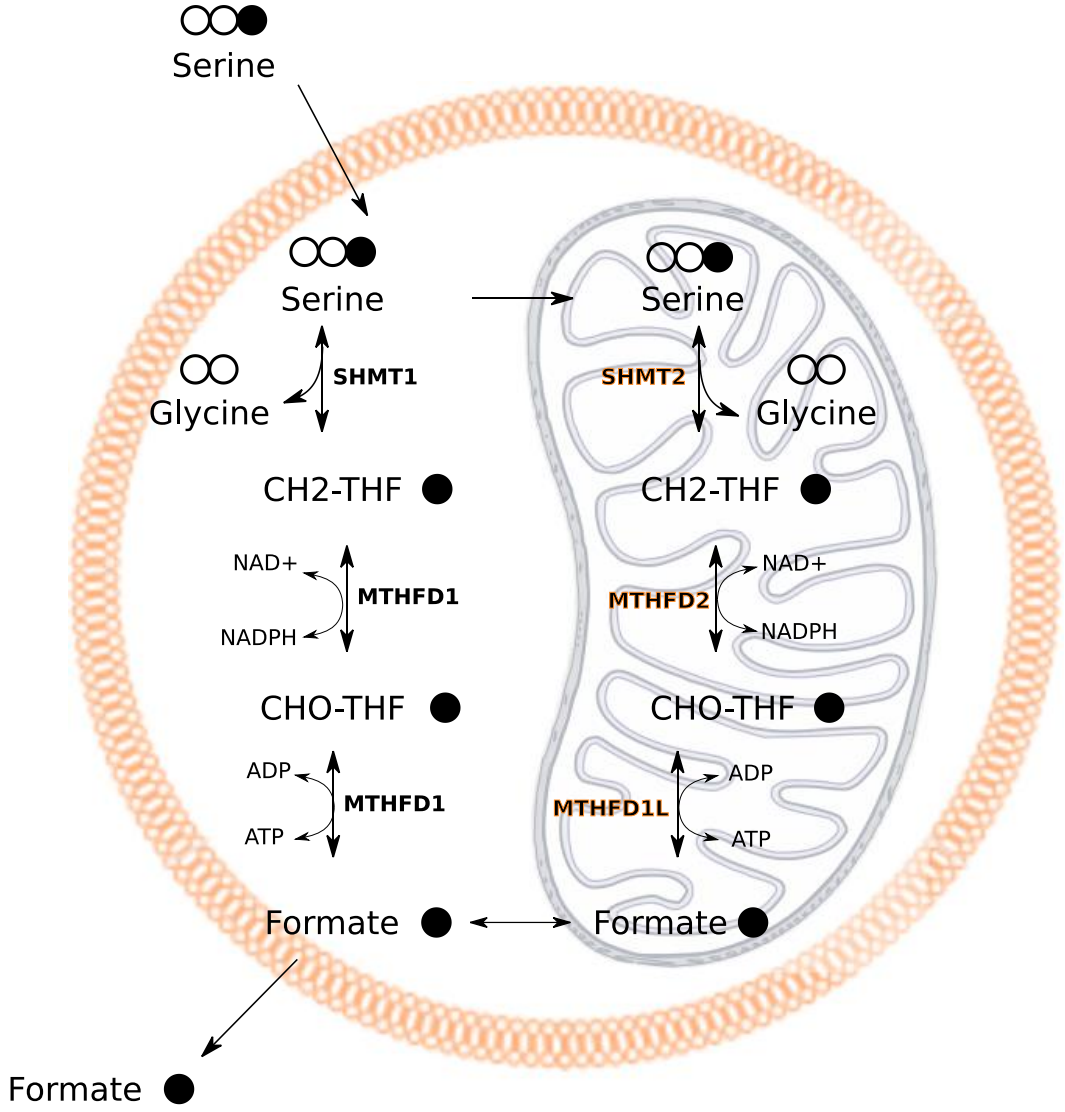

Figure 1.4 Formate efflux and parallel pathways of one carbon metabolism.

Formate release is derived from extracellular serine via catabolism to glycine and tetrahydrofolate (THF) in the cytoplasm and mitochondria. The one carbon unit is transferred from serine to glycine by serine hydroxymethyltransferase (SHMT) and further metabolised by action of methylenetetrahydrofolate dehydrogenase (MTHFD).

1.3.2. Lactate

A build-up of lactate inside cells would result in an acidic environment. A low cytosolic pH (pH_i) would reduce the rate of glycolysis through inhibition of the PFK, and if pH_i becomes too low it could prevent other vital cellular processes from occurring [48]. Lactate (p*K*a 3.86) dissociates completely under physiological conditions, and therefore cannot cross membranes by diffusion. Instead, transport is facilitated by the bidirectional proton-linked monocarboxylate acid symporters (MCTs), with stoichiometric transfer of the dissociated acid and a hydrogen ion [49]. The main isoform expressed in the majority of tissues, is MCT1, has a K_m in the region of 3.5-10 mM and therefore has a high affinity for L-lactate and can maintain efflux even at relatively low intracellular levels [50]. MCT4 is also associated with lactate export, but does not import lactate. It has a much lower affinity of 22-30 mM and therefore acts when intracellular concentrations are high [51].The overflow of lactate as a typical signature of the Warburg effect has been well documented in proliferative cells, plasma concentration of lactate for a resting, healthy human is in the millimolar range [52].

1.3.3. Pyruvate

Pyruvate is a major node of central metabolism and it can be converted into lactate, alanine, oxaloacetate, acetyl-CoA, or secreted from cells. Production of alanine occurs in concert with generation of α-KG; alanine transaminase (ALT) catalyses the transfer of an amino group from glutamate to pyruvate. This is most commonly links muscle and liver metabolism in a recycling and scavenging pathway known as the Cahill cycle.

Release of pyruvate into the extracellular space occurs by the monocarboxylate transporter family [53]. Data suggests that elevated expression of MCT1 promotes pyruvate export in glycolytic cells [54]. The ratio of lactate to pyruvate reflects cytosolic

redox potential, as the ratio of NADH/NAD+ is in part controlled via lactate dehydrogenase (LDH), shown in Figure 1.5. Without sufficient regeneration of NAD+, glycolysis is impaired, as conversion of G3P to 1,3-BPG relies on transfer of a hydride ion from GAPD to produce NADH.

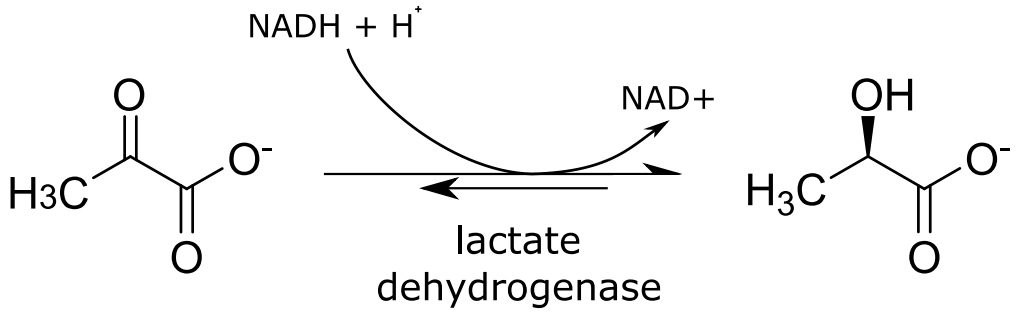

Figure 1.5 Regeneration of redox equivalents by lactate dehydrogenase

The interconversion of pyruvate and lactate by lactate dehydrogenase (LDH) plays a role in redox potential. The NADH/NAD^+ ratio is directly affect by the position of equilibrium of this reaction.

1.4.Cancer Metabolism

Cancer is a condition involving abnormal cell growth, where healthy tissue is damaged and destroyed by invading, diseased cells [55]. Neoplastic disease is recognised as a major health problem worldwide, with 17 million new cases reported in 2018 [56]. Global mortality rates reflect the high incidence of cancer, with 1 in 6 deaths attributed to malignant disease [57]. Treatment outcomes are improving as therapeutics move away from pan-cytotoxic agents to targeted drugs, such as Gleevec and Herceptin. These two drugs inhibit cancer growth via distinct mechanisms; Gleevec prevents proliferation by binding to the protein product of a chromosomal translocation, whereas Herceptin binds to an overexpressed cell membrane receptor.

Exploration of new molecular targets continues in order to achieve the full potential of personalised medicine in the context of cancer [58]. Understanding how these molecules and associated pathways are implicated in this disease is vital to continue to combat morbidity, particularly as populations increase and global cancer burden is projected to rise [59].

Cancer biology has long since recognised the role of altered metabolism in transformed tissues, with the seminal work of Otto Warburg from the 1920s still frequently cited [60,61]. Warburg recognised that the normoxic increase in lactate production was due to glycolytic activity in highly proliferative cells. As malignant cell metabolism is distinct from that of healthy cells metabolic vulnerabilities are therefore a prime target for novel therapies [62]. Research into the cellular alterations that drive cancer actively include the field of cell metabolism and metabolism-modulating anticancer drugs. One example is Enasidenib, which inhibits the mutant TCA cycle enzyme isocitrate dehydrogenase (IDH), decreasing levels of the oncometabolite 2-

hydroxyglutarate (2-HG). Several other metabolic drugs have also been successfully approved by the Food and Drug Administration (FDA) in recent years [63].

1.4.1. Reprogrammed Cellular Metabolism

Some metabolic phenotypes are observed across many types of cancer, regardless of the tissue of origin [64]. Hallmarks of proliferative metabolism include high glycolytic flux, thought to sustain biosynthetic programs and control cell redox. Malignant alterations to metabolism reflect the increased proliferation, as more fuel substrates are required to facilitate uncontrolled cell growth and division. Oncogenes direct enhanced nutrient uptake towards assimilation into biosynthetic pathways, supporting increased proliferation [65,66].

Frequently the phosphatidylinositol 3-kinase (PI3K) signalling pathway is disrupted, leading to aberrant activation of the downstream AMPK-mTOR network [67]. The PI3-kinase is composed of two subunits (regulatory p85 and catalytic p110) that dimerise to generate the active complex, forming phosphatidylinositol (3,4,5) triphosphate (PIP_3) from phosphorylation of phosphatidylinositol (4,5) bisphosphate (PIP_2). These inositol lipids, situated in the cell membrane, recruit downstream effectors that regulate cellular processes in response to external growth factor stimulation. Mutational activation of the PI3K pathway promotes anabolic activities, disconnecting cell growth stimuli from core metabolic networks and driving uncontrolled proliferation [68].

The tumour suppressor phosphatase with tensin homology (PTEN) acts to restrain PI3K signalling by dephosphorylation of the inositol lipids. In addition to modulating cell growth and metabolism through suppressing the PI3K-AMPK-mTOR pathway, PTEN also has key roles in DNA repair and cell cycle regulation [69]. Mutations and

deletions of PTEN therefore lead to perturbations in cellular homeostasis through aberrant metabolism and cell growth, promoting to tumorigenesis [70].

Transformed cells use a range of strategies to compensate for the restrictions of the tumour microenvironment and promote invasiveness [71]. Often tumours do not have adequate vasculature to supply nutrients and need to find other sources of glucose, amino acids and lipids [72]. In addition to upregulating metabolic pathways they can consume their own cellular components via autophagy [73] or use macropinocytosis to ingest extracellular material and provide additional nutrients from protein degradation [74]. The hypoxic environment due to insufficient vasculature drives overflow metabolism in the form of lactate production [75]. Acidic overflow products are thought to aid metastatic migration of cells through remodelling of the extracellular matrix (ECM) [76].

Secreted metabolites can also be used as alternative fuel substrates for neighbouring cells, in particular, monocarboxylate overflow has been linked to lactate and pyruvate being used by adjacent cells [77].

Genetic alterations also drive specific types of cancer, for example, a subset gliomas and glioblastomas are characterised by mutations in the IDH family of enzymes [78]. Isocitrate dehydrogenase 1 and 2 normally catalyse the conversion of isocitrate to α-KG, however due to point mutations at arginine residues they instead produce oncometabolite 2-HG, known to competitively inhibit activity of aKG dependant dioxygenases [79]. This reaction also consumes NADPH that could otherwise be used to neutralise ROS.

1.5. Blood Cells and Haematopoietic Malignancies

The blood system is composed of a variety of different cells, commonly identified by cell-surface markers, each at a distinct point along differentiation from stem cells to specialised, mature cells [80]. In adults, the apex of the hierarchy is the pluripotent, self-renewing, long-term haematopoietic stem cell (LT-HSC). Residing mainly in the bone marrow, LT-HSCs have the unique capacity to reconstitute the entire blood system by generating multipotent progenitors that further differentiate into lineages of committed progenitors and, finally, mature blood cells. While the most potent LT-HSCs are dormant, using a quiescent state to protect themselves from exhaustion, they can reversibly switch to a state of self-renewal in order to maintain homeostatic control of blood production [81].

The maintenance, proliferation and differentiation of stem cells are regulated by a dynamic, intricate network of intrinsic and extrinsic signals throughout the blood and tissues such as bone marrow and spleen. While cytokines and growth factors influence survival and proliferation, lineage decisions are due to the combined effects of transcription factors and epigenetic regulation [82]. Any dysregulation of haematopoiesis, for example, through disruption of regulatory programs due to genetic mutation, can result in an unbalanced population of the blood system.

Malignancies of the blood are commonly associated with chromosomal abnormalities, such as translocations. Leukaemogenesis follows a step-wise evolution where a genetic mutation initiates the condition and activation of a second event is required for full blown disease. The resulting leukaemia can be classified as chronic or acute depending on the proliferation rate of cells. A further subdivision is between myeloid and lymphoid, according to the lineage of the cells.

1.5.1. Acute myeloid leukaemia (AML)

AML is the most common form of myeloid leukemia. It is a complex, heterogeneous disease with many genetically distinct populations of clonal cells co-existing at any one time [83]. The multitude of AML subtypes is classified using the World Health Organisation (WHO) system, based on cytogenetic criteria and the minimum requirement of an accumulation of progenitors that fail to differentiate into functional, mature cells [84].

These neoplastic cells are arrested in an immature state and they can interfere with the process of normal haematopoiesis via the production chemokines [85]. Progression of the disease can be rapid, and the end result is bone marrow failure, with death from infection or haemorrhage [86].

An example of one AML subtype is genetic abnormalities, with a common issue being a t(8;21) chromosomal translocation. The Kasumi-1 cell line carries this genetic mutation that results in oncogenic fusion protein RUNX1/ETO [87]. This protein is a transcription factor that binds to DNA leading to aberrant gene regulation that interferes with normal blood cell development and maturation, deregulating normal haematopoiesis. Myeloid differentiation is blocked and cells show enhanced self-renewal and proliferation.

Ablating expression of RUNX1/ETO, using interfering ribonucleic acids (RNAs), such as small interfering (siRNA) and short hairpin (shRNA), alleviates the block in differentiation [88,89]. RNA interference is a conserved process that defends cells from parasitic nucleotide sequences; exogenous single-stranded RNA is recognised by the multi-protein RNA-induced silencing complex (RISC) and degraded or inactivated, so no translation takes place and no protein product is produced [90].

In the case of shRNA, a double-stranded RNA which contains a loop structure, the Dicer enzyme cleaves the RNA into two single strands. One of these is degraded while the other

acts as a guide template for RISC, which recognises the complementary target mRNA strand. Once loaded into RISC the mRNA molecule is cleaved by the Argonaute proteins and further degraded by endogenous nucleases [91]. Conditional expression of a chosen shRNA can be regulated using tetracycline controlled gene expression systems. The Kasumi-1 cells used in this work (supplied by the Bonifer laboratory) can be induced to express an shRNA against RUNX1/ETO encoding mRNA, under the control of a Tet-On system. Addition of doxycycline induces a conformational change in the tetracycline transactivator protein (tTA), containing bacterial repressor protein (TetR), that allows binding to the Tet Response Element (TRE) at the tetracycline operator sequence (tetO). Subsequent activation of the promotor results in transcription of the genetic product, in this case expression of the shRNA [92]. This leads to silencing of the target gene RUNX1/ETO by sequence specific degradation of the corresponding mRNA, as described above.

CHAPTER 2

NUCLEAR MAGNETIC RESONANCE

2. Overview

NMR involves the manipulation and excitation of nuclei in a magnetic field, probing energy levels through the application of oscillating electromagnetic fields. Once excited the resonant state of a sample will induce a current in a receiver coil, which then decays over time as energy is transferred to the surrounding environment. The signal in the coil provides information on the chemical environment of the nuclei and can be used for structural elucidation and molecular identification.

2.1. Basic Theory

Particles have different types of momentum arising from distinct qualities or motions. For example, classical mechanics describes an electron as having orbital angular momentum as it moves around a nucleus. In contrast, spin angular momentum is intrinsic, an abstract quality that can be interpreted as an atomic-scale angular momentum [93].

Elementary particles are characterised by their spin angular momentum quantum number (***I***), which can be either integer or half-integer. In the case of matter, composed of fermions with half odd integer spins, ***I*** = ½, 3/2, 5/2 etc. Composite particles, like nuclei, have a total spin angular momentum (***S***) calculated from the sum of the component nucleons.

One manifestation of spin is the behaviour of a nucleus in an external magnetic field; half-integer nuclear spins have a magnetic moment and will interact with the surrounding field. These nuclei include the spin ½ isotopes of hydrogen, carbon, phosphorous and nitrogen.

2.1.1. NMR Isotopes

While many NMR active isotopes exist, only a few are used in the study of cellular metabolism. Protons (^{1}H, 99.98% abundant) are ubiquitous in biological systems as they constitute an integral part of organic biomolecules and consequently methods that detect ^{1}H are commonly used in the analysis of biofluids, including cell extracts and cell culture medium [94,95,96].

Phosphorous (^{31}P 100%) is also a major constituent of cells, and ^{31}P can be used to monitor endogenous compounds such as adenylates, providing information on cellular energetics [97]. It has also been used to monitor pH in both the intracellular and extracellular environment [98].

The most abundant isotope of nitrogen (^{14}N 99.63 %) is quadrupolar with $\boldsymbol{I}$ = 1, meaning its charge distribution is no longer spherical and it behaves differently to spin ½ nuclei [99]. Its NMR signals yield broad linewidths and it is therefore rarely used for observation of metabolites. The ^{15}N isotope used to monitor incorporation of labelled substrates provides information into alanine and ammonium [100,101]

In the case of carbon the most abundant isotope (^{12}C 98.9 %) is not NMR active, however, this has the advantage that substrates labelled isotopically with ^{13}C (1.1 % abundant) can be fed to cells. Metabolic transformations distribute the labelled atoms and the resulting molecules can be detected. This provides information on the specific metabolites produced by active pathways, including the exact position of atoms incorporated into synthesised molecules. ^{13}C is commonly used to report on the fate of sugars, amino acids and lipids [102,103].

2.1.2. Magnetic Moments and Gyromagnetic Ratios

Magnetic moments are vector quantities, indicated here by bold italics, and are defined by both a magnitude and a direction. The intrinsic magnetic moment ($\boldsymbol{\mu}$) of a nucleus due to total spin angular momentum ($\boldsymbol{S}$), is defined by:

$$\boldsymbol{\mu} = \gamma \boldsymbol{S} \tag{2.1}$$

where γ is the constant of proportionality, known as the gyromagnetic ratio, with units of $rads^{-1}T^{-1}$. This constant is characteristic of each nucleus and can vary in sign, indicating the alignment of the magnetic moment relative to the spin angular momentum. The gyromagnetic ratio influences the size of the equilibrium magnetisation and consequently nuclei with higher gyromagnetic ratios, such as hydrogen, have higher sensitivities. See Table 1, below, for properties of isotopes commonly used for metabolic studies.

Nucleus	**Spin (I)**	**Gyromagnetic ratio MHz/T (γ)**	**Relative Sensitivity**	**Abundance (%)**
^{1}H	½	42.58	1.0000	99.98
^{2}H	½	6.54	0.0097	0.015
^{13}C	½	10.71	0.0159	1.108
^{14}N	1	3.08	0.0010	99.63
^{15}N	½	-4.32	0.0010	0.37
^{31}P	½	17.24	0.0665	100

Table 1: Properties of some NMR active isotopes used in biological studies

While many isotopes are NMR-active, only a few are relevant for the study of biological molecules [104].

At equilibrium, in the absence of an external magnetic field, the distribution of spin magnetic moments in a sample is isotropic; the magnetic moments of individual nuclei point in all possible directions. Application of a magnetic field to the nuclei will produce a torque on each magnetic moment, the force of which will depend on their orientation relative to the external field. This interaction results in precessional motion and the magnetic moments will rotate around the direction of the external magnetic field as dictated by their gyromagnetic ratio. The direction of rotation will depend on the sign of the gyromagnetic ratio and the frequency of this precessional motion is termed the Larmor frequency (ω_0):

$$\omega_0 = - \gamma \boldsymbol{B}_0 \qquad (2.2)$$

where $\boldsymbol{B}_0$ is the external field strength. The Larmor frequency depends on the nucleus and the external magnetic field.

There is a slight energetic advantage for the magnetic moments to align themselves with the external magnetic field. Overall the transverse components of the magnetic moment's vectors average to zero, leaving a net magnetisation vector along the direction of the field.

Using a radio frequency (RF) pulse, of appropriate frequency and duration, the net magnetisation can be manipulated to rotate around the external field. Following the pulse, the spin system returns to equilibrium via a process called relaxation; energy will be lost to the surroundings and the net magnetisation will return to the z-axis [105].

Precession of the magnetisation in the transverse dimension will induce an oscillating current in the receiving coil. The detected signal is called the free-induction decay (FID). Over time the transverse element will decay to zero and the vertical component will increase back to the equilibrium value. The FID is processed to yield all the component frequencies corresponding to the nuclear spins in the sample, as shown in Figure 2.1.

The spectrum is a plot of signal intensity against chemical shift, where the chemical shift (δ, units ppm) is relative to an agreed reference compound, derived from frequency using the following equation:

$$\delta = \left(\frac{\nu - \nu_{ref}}{\nu_{off}}\right) x10^6 \qquad (2.3)$$

where ν and ν_{ref} are, respectively, the frequencies of the signal of interest, and the relevant chemical shift reference compound. ν_{off} is the offset frequency of the spectrometer. Using this ppm scale the position each resonance is independent of the field strength, so spectra from different spectrometers can be compared.

The frequency of an NMR signal is characteristic of the chemical environment of the nucleus. Higher electron densities shield nuclei from the applied field, in comparison to those with lower electron densities, or deshielded nuclei. The shielded nuclei experience a weaker magnetic field, while the deshielded experience a stronger magnetic field and therefore the resonance will appear at a higher ppm value.

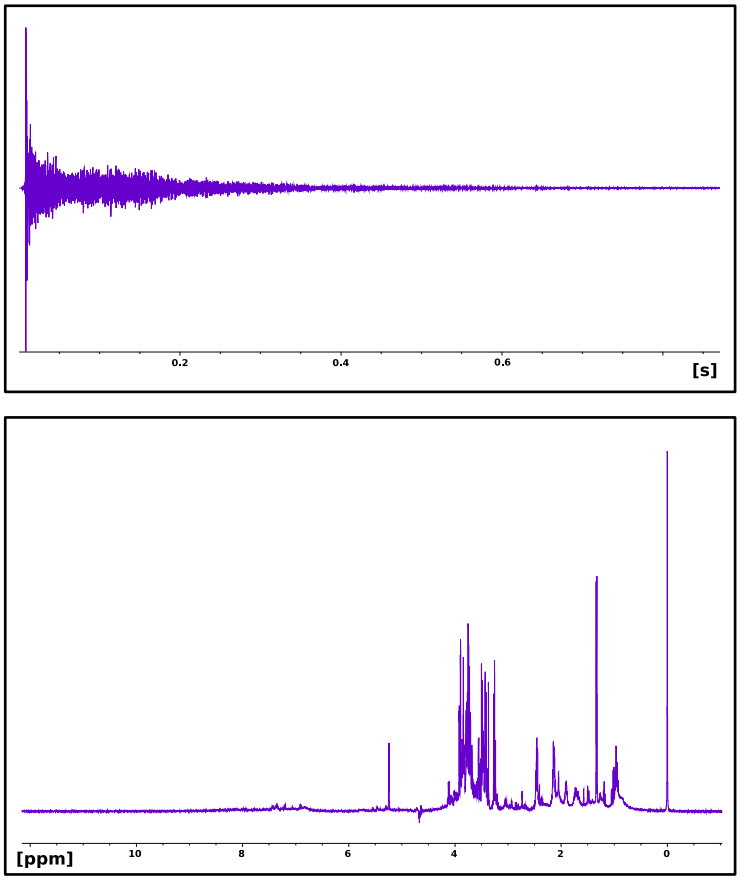

Figure 2.1 NMR Free Induction Decay and Spectrum

Example acquisition demonstrating appearance of the free induction decay (FID) in the time dimension and the corresponding spectrum translated to the chemical shift scale. A mathematical function called Fourier transformation is used to generate the frequency domain spectrum from the FID. Pulse sequence zgesgp, 4 steady-state transients, 64 transients. (Top) zoom of the FID the time-domain signal and (bottom) the corresponding spectrum, with the frequency domain converted to ppm.

2.1.3. NMR Signals and Sensitivity

Interaction of nuclei with an external magnetic field can be described in terms of energy levels, and the frequencies of lines in NMR spectra are a result of allowed energy transitions between these levels. For spin-½ nuclei, such as those commonly found in biological material, the nuclear spin is $(2\boldsymbol{I} + 1)$-fold degenerate. When placed in a magnetic field the degeneracy is broken and the resulting Zeeman splitting produces two energy levels.

The energy of each level is described by:

$$E_m = -m\hbar\gamma\boldsymbol{B_0} \tag{2.4}$$

where m is either +1/2 for the α state or -1/2 for the β state. ħ is Planks constant, γ the gyromagnetic ratio and $\boldsymbol{B_0}$ is the external field strength. The magnitude of the splitting depends on the strength of the magnetic field.

The population of the energy levels is described by the Boltzmann distribution:

$$\frac{N_\beta}{N_\alpha} = \exp\left(\frac{-\Delta E}{kT}\right) \tag{2.5}$$

Where k is the Boltzmann constant and T is the temperature in Kelvin. The N_β population is the upper state and Nα is the lower state. ΔE is the energy difference between the two levels.

Application of a magnetic field at the Larmor frequency ($\boldsymbol{B}_1$, the RF pulse) induces nuclei to "flip" between energy levels. At some point after the RF pulse, the nuclear spins return to equilibrium, via relaxation processes, described in section 2.1.4. The transition will have a frequency equivalent to the energy difference between the levels, and the signal intensity will be directly proportional to the number of nuclei producing it. The NMR signal is relatively weak in comparison to other techniques, as a result the amount of sample required for NMR is generally greater than for other spectroscopic techniques.

2.1.4. Relaxation

The decay of observable magnetisation is a consequence of longitudinal and transverse relaxation. As energy is dissipated to the surroundings the bulk magnetisation vector returns to the equilibrium position.

Longitudinal relaxation (T_1) of spin ½ nuclei occurs as local molecular motions produce magnetic fields oscillating at the Larmor frequency. The random motion of molecular collisions changes the orientation of nuclei relative to both each other and the external magnetic field and thus provides a path for energy transfer between molecules [106].

Transverse relaxation (T_2) is the decay of magnetisation in the transverse plane due to the dephasing of magnetisation vectors as each spin experiences a slightly different magnetic field, and precesses at a different frequency. This effect results from the combination of local magnetic fields arising from the sample and inhomogeneity in the external magnetic field.

Relaxation rates vary between nuclei, and proton T_1 values are in the range of several seconds [107]. For small molecules rapidly tumbling in solution T_1 and T_2 are similar,

whereas large molecules have shorter T_2, due to slow rotational motion and therefore produce in broad resonances.

The duration of time taken to relax is very slow compared to other spectroscopic states. For example, in NMR spectroscopy, excited spins can take seconds or minutes to return to equilibrium, whereas vibrational and rotational excited states relax on a timescale of fractions of a millisecond. The advantage of relatively slow relaxation is that transverse magnetisation survives long enough to be manipulated by further RF pulses. This enables the use of multiple pulses to manipulate the spin system into producing resonances that contain the desired information about the system under study, described in section 2.2. The disadvantage of long longitudinal relaxation times is that quantitative NMR requires the equilibration state to be re-established between successive acquisitions. This increases the total experiment time, as a duration of $5*T_1$ is required for the spins to fully relax back to the equilibrium state [108].

2.1.5. *J*-coupling

Chemical bonds can mediate magnetic interactions between nuclei in a molecule. Bonding electrons are polarised by nuclear spins, which in turn perturb the magnetic moment of any connected nucleus. The magnetic moment can align with or against the external field ($\boldsymbol{B}_0$) and consequently the effective magnetic field experienced by each nucleus is slightly increased or decreased. The resonance of each nucleus will therefore be split by these interactions, giving rise to multiplets in the NMR spectrum. This phenomenon, known as scalar or *J*-coupling, is independent of the external magnetic field strength. The fine detail of each multiplet provides information about the number of connected atoms in a molecule. Coupling constants, measured in Hz, depend on the number and type of bonds connecting nuclei. This information in invaluable when

assigning resonances in complex mixtures, as the splitting pattern of each multiplet (and the associated coupling constants) aids in the identification of molecule.

2.2. Pulse Sequences and Parameters

Most NMR experiments involve a sequence of RF pulses and delays designed to extract specific information from the spin system. They can manipulate just one nucleus or use a series of pulses to transfer magnetisation to coupled nuclei [109]. This can elevate sensitivity and provide complementary information, or just simplify spectra.

Pulse sequences describe the type and order of delays and pulses for each acquisition, along with any other necessary acquisition parameters. Often sequences start with a 90° ($\pi/2$) excitation pulse to generate magnetisation in the transverse plane, while different delays can allow time for refocusing or evolution of chemical shifts during the particular sequence of pulses. A final read pulse generates observable magnetisation in the transverse plane.

Each NMR experiment will be composed of multiple transients, the number of which will depend on the pulse sequence in question and is usually chosen to obtain sufficient signal intensity for a given amount of sample. The total number of transients will also involve balancing the sensitivity of the experiment with efficient use of instrument time.

The signal to noise (S/N) defines the sensitivity of an experiment [110], and increases with the number of transients) according to:

$$\mathrm{S/N} = \frac{\mathrm{N}\gamma_e T_2(\gamma_d \mathrm{B}_0)^{3/2}\sqrt{\mathrm{ns}}}{\mathrm{T}}$$

where γ_e is the gyromagnetic ratio of the excited nucleus, γ_d is the gyromagnetic ratio of the detected nucleus and $\boldsymbol{B}_0$ is the external magnetic field. T_2 is the transverse relaxation time and T is the sample temperature.

2.2.1. Phase cycling and Pulsed Field Gradients

Multi-pulse experiments are tailored to excite specific spins and produce magnetisation that yields a spectrum containing resonances of interest. In many samples there will be a mixture of signals, and it may be advantageous to filter out those associated with undesired resonances as spectral overlap may prevent identification and/or quantitation.

Phase cycling is a procedure used to reduce contributions from unwanted signals. This method repeats the multi-pulse experiment while varying the relative phases of the RF pulses and receiver [111]. The resultant sum of the transients will yield only the signals that constructively combine, while others are cancelled out. This difference method is reliant on using a minimum number of transients and can therefore be time consuming.

Another approach is to introduce a transient inhomogeneous magnetic field along one axis of the sample [112]. These pulsed field gradients (PFGs) dephase spins according to their location along the sample axis. An opposite gradient pulse can then be used to rephase signals from spins of interest.

In practice a combination of phase cycling and PFGs are often used to reduce experiment time while maintaining signal selectivity, allowing for the most efficient use of spectrometer time.

2.2.2. Biological Samples and Water Suppression

The aqueous milieu of biological samples (tissues, cells or reconstituted extracts) provides a measurement challenge in proton NMR spectroscopy. Protons in water (H_2O, 110 M) dominate the spectrum, and a simple pulse acquire experiment would result in the large water resonance obscuring and distorting much smaller analyte peaks in the millimolar range. Pulse sequences use a range of techniques to attenuate the water signal and there is usually a trade-off between completely removing the water and distorting other resonances [113]. The choice of suppression scheme can therefore have a significant impact on the quality of the resulting spectrum [114].

Strategies to eliminate the water signal can selectively excite or refocus the analyte resonances of interest. For example, excitation sculpting uses shaped pulses with a refocusing element [115], while WATERGATE uses a frequency selective pulse train that excites everything but the water [116,117]. In contrast 1D NOESY sequences remove the water with a long, low-power presaturation pulse during the recycle delay, destroying any residual water magnetisation with phase cycling and pulsed field gradients [118].

2.3. One-Dimensional and Two-Dimensional NMR Spectroscopy

Each NMR spectrum can contain a wealth of information, particularly when analysing complex mixtures of multiple spin-active nuclei. One-dimensional (1D) NMR spectroscopy involves a series of pulses followed by data acquisition in a detection period, and can also include a preparation and mixing time. A subsequent Fourier transformation of the FID generates a plot of intensity versus frequency.

In two-dimensional (2D) NMR spectroscopy there two stages after the preparation time, the evolution time and then the mixing time, where magnetisation may be transferred to a second nucleus prior to the detection time. A series of FIDs are acquired at regularly spaced increments in the evolution time. Subsequently, the data is transformed to frequency co-ordinates, much like a topographical map, where peak intensity is represented by contours.

2D experiments can provide additional dispersion in the second dimension and help to resolve peaks that would otherwise overlap in a 1D [119].This is best achieved using pulse sequences like the HSQC and HMQC experiments that correlate the chemical shifts of ^{1}H and ^{13}C [120]. These pulse sequences can also enhance sensitivity by transferring magnetism to the nucleus with a higher gyromagnetic ratio, in this case ^{1}H.

2.4. NMR Spectrometer

High resolution NMR spectroscopy requires a strong and stable, homogenous magnetic field. Superconducting magnets, held at sufficiently low temperatures, are used to generate the $\boldsymbol{B_0}$ field. Concentric Dewars keep the magnet coil cool, using liquid helium (4 K) in the inner chamber to maintain the superconductivity, while liquid nitrogen (78 K) is used as a thermal buffer on the outside [121].

NMR magnets are cylindrical in shape, with a hollow bore along the vertical axis which houses the probe, a combination of RF coils that excite the sample and detect the subsequent response. The sample is seated inside the probe, with an air cushion used to facilitate movement of the sample into and out of the bore.

A deuterium frequency lock coil is also part of the probe. The lock compensates for the slow drift of the field over time by monitoring the ^{2}H signal and using a field-frequency lock to hold the $\boldsymbol{B_0}$ field coil to a constant value. During longer experiments field drift can lead to frequency drift and resonance broadening.

The shims are a set of small coils used to cancel out any inhomogeneity in the $\boldsymbol{B_0}$ field. Imperfections in the field can be corrected for by applying small opposing currents in the shim, improving spectral quality by reducing line width and sharpening resonances [122]. The optimum shim is determined by assessing the linewidth directly, or trying to maximise the lock signal.

A radiofrequency source, the RF transmitter, is responsible for generating the stable, precise frequencies responsible for the $\boldsymbol{B_1}$ field. It can be at room temperature, or cryogenically cooled in order to reduce thermal noise and improve signal-to-noise [123,124].

CHAPTER 3

NMR OF LIVE SYSTEMS

3. Overview

This chapter will begin with an overview of NMR applied to the study of metabolism. The methods used to monitor intracellular molecules will be described and following on from there, the various ways of keeping live samples viable will be summarised, with a focus on bioreactor technology. Finally a brief overview of the aims of this thesis of work will be set out.

3.1. Monitoring Metabolism in Live Systems

The investigation of biochemical processes often requires the use of model systems to recapitulate parts of complex organisms. This can be whole organs, cells or isolated cellular compartments, such as mitochondria. Separation of each component involves disruption of the biological system, and further in vitro or ex vivo study can lose sight of the overall context. While this approach is well suited to the study of isolated aspects of biological mechanisms, it does not provide a holistic view of the intact system. The non-destructive nature of NMR spectroscopy avoids unnecessary perturbations of cellular function, and is consequently an ideal non-invasive tool for the study of live systems. This is exemplified in the use of magnetic resonance imaging (MRI) as a clinical diagnostic tool.

From the first NMR studies on live biological material [125] to the present day, huge advances have been made in the sensitivity and resolution of the technique thanks to the introduction of higher-field magnets, cryo-probes and associated pulse sequences and sampling strategies. Cells, tissues and even whole organisms can be placed inside the spectrometer for in-situ analysis [126,127 ,128, 129].

Various methodologies exist for metabolic studies using in vitro, ex vivo and in vivo NMR approaches. Each experimental setup is tailored to the biological system and

metabolites under study, as the cellular metabolome consists of a variety of molecules present in both the intra and extracellular environment.

Methods that collect samples over a defined time course often involve processes that perturb the live system. Metabolism is very sensitive to environmental changes, and it is therefore important to utilise non-disruptive techniques. This is particularly problematic when taking cell extracts, as cells are separated from the culture medium prior to solvent-based quenching of metabolism [[130]]. This method of sampling can make use of centrifugation or filtration to divide cells from their culture medium, both processes that can take up to several minutes, and therefore mask the dynamics of fast-changing biotransformations taking place over a short time scale.

3.2. In-Cell NMR spectroscopy

The study of biomolecules contained in living cells has in the past focussed on qualitative structural information, to the point that in-cell NMR is often synonymous with structural biology "in the cell". Heteronuclear multi-dimensional NMR is mainly used to monitor resonances associated with protein backbone and side chains [131] and few studies have monitored small molecule metabolism [132]. Otherwise, most studies are concerned with protein interactions and dynamics in the native cellular environment. Overexpression systems and NMR active isotopes enable detection of specific biomolecules in contrast to the unlabelled cellular components [133].Other approaches involve delivery of labelled proteins into the intracellular environment by microinjection [134], electroporation [135] and membrane pore-formation [136]. Time dependent changes in the isotopic signals can be correlated with the biological activities that alter labelled molecules, such as the case of post-translation modifications by small molecule entities [137].

Sample preparation for in-cell experiments can be as simple as pelleting cells into the NMR tube. Typical conditions used for mammalian systems involve high cell densities. The crowding of cells inside sample tubes results in rapid nutrient depletion, and consequently cell viability declines over the course of experiments [138]. Markers of stress have been detected during in-cell NMR, and can be used to monitor cell health in-situ during or at the end of experiments [139]. This is crucial to ensure that valid conclusions are drawn from the biological system.

The short lifetime of in-cell samples due to stress provoked by cell densities has been addressed by the use of specialised vessels (bioreactors) to house and maintain the cells [140], supplying adequate nutrients and maintain appropriate environmental parameters, as explained in the following section.

3.3. Bioreactor Designs for Real-Time NMR

Mammalian cells require a stable environment; a constant temperature of 37 °C, and physiological pH within the range pH 7.2 to pH 7.4. In cell culture laboratory incubators cultures are kept warm at 37 °C, and buffers maintain the pH in the culture medium. Often a bicarbonate buffer is used in conjunction with a controlled carbon dioxide tension inside the incubator, balancing pH with the same mechanism found in human blood (see equation 3.1). Carbon dioxide (CO_2) dissolves in the culture medium and forms carbonic acid (H_2CO_3), which disassociates into bicarbonate (HCO_3^-) and protons (H^+), catalysed by carbonic anhydrases.

$$CO_2 + H_2O \rightleftarrows H_2CO_3 \rightleftarrows H^+ + HCO_3^- \quad (3.1)$$

Cells also require a supply of nutrients to stay viable, and waste products will need to be removed from the surrounding environment before they build up to toxic levels. Cultures are usually passaged in order to replenish nutrients and eliminate waste products. This is achieved by either diluting or resuspending cells in fresh medium, depending on the manner of cell growth. Cells can either grow freely in solution, or adhere to a support matrix. There may be a detachment and/or centrifugation step involved in the media change depending on the cell type and growth. Rate of growth will determine the frequency with which passages are performed and fast growing cells may require medium changes every 48 hours.

Any cultivation system that supports cell growth needs to maintain environmental parameters and keep nutrient levels within an acceptable range. Methods to culture cells cover a diverse range of bioreactor configurations, from small microfluidic devices [141] to large scale setups used in antibody manufacturing [142].

Hardware availability also plays a part in determining the final monitoring arrangement, particularly in NMR spectroscopy, where dedicated spectrometers and probes can be the limiting factor in accommodating live organisms. Bespoke set ups many not be amenable to quick or simple probe or equipment changes, and may need to stay in situ for long term use [143]. There is choice of whether the bioreactor should be adapted for use with a specific probe, and therefore fit within defined dimensions, or if the probe should be modified to house the bioreactor. Probes can be engineered to accommodate the geometry of the bioreactor, however, this is a time-consuming and potentially expensive process.

Other NMR specific considerations include criteria for generating a suitable signal for detection, including a homogenous sample over the volume of measurement. Bubbles in solutions can be problematic, as can sedimentation of cells or debris in the NMR tube [144].

Finding conditions for consistent, successful cultivation of cells is also challenging because each type of cell line will demand unique conditions. The type of cell can therefore limit its suitability for growth systems where cells are forced to be either are immobilised or free floating. Perfusion bioreactors are the predominant design used to maintain cell viability during NMR studies, described in the next section.

3.3.1. Perfusion Systems

Continuous feeding of cell cultures can be achieved by perfusion of fresh cell medium, allowing exchange of nutrients, metabolites and oxygen. This technique is routinely used in commercial production of proteins and antibodies, where intensive bioreactors maintain high cell densities in order to increase productivity [145]. Waste medium is

continuously exchanged for fresh medium, and cells are usually retained within fibres or membranes.

Types of perfusion bioreactors include fixed bed and fluidised bed reactors. Both make use of porous carriers to immobilise cells; fixed bed designs secure cells to a fixed point in the bioreactor while fluidised designs encapsulate cells, but do not limit their movements [146]. The porous materials used to immobilise cells allow liquid to penetrate so nutrient molecules are available to the cells [147]. In the fixed bed design culture medium is perfused over the stationary cells, whereas in the fluidised bed the medium is mixed with the cell encapsulates. One issue with the fluidised approach is cell aggregation, causing oxygen gradients within encapsulates [148]. This results in the internal cells becoming hypoxic as they no longer have adequate exposure to the oxygenated medium. Attempts to improve nutrient perfusion and cell viability include using alginate encapsulation, where dense 3D cultures can be created with seeding densities of tens of millions of cells per ml [149].

Hollow fibre perfusion bioreactor (HFPB) systems are very similar to fixed bed designs, except the medium is channelled through the lumen of fibres, like blood through capillaries [150]. This results in tissue-like densities as cells cluster together between the parallel arrays of fibres. Nutrients from the culture medium are free to diffuse into the cells, while waste products can diffuse away from the cells, back into the fibres. HFPB systems have applications in bioproduction, as well as the pharmaceutical industry [151]. They can be used to stimulate the delivery of therapeutics in vivo, as the drug can be perfused with the medium or injected directly into the cell mass. The disadvantage of the membrane-based systems is the reduction in working capacity compared to encapsulation. Space is taken up by the fibres and therefore fewer cells can be kept in the same volume.

Perfusion bioreactors can also make use of cells in suspension. Since bioreactor geometries can produce nutrient gradients, and allow waste products to build up, mechanical agitation is often used to stir the medium of suspension cultures and maintain homogenous conditions. Homogenous cell populations, with equal nutritional and metabolic states over the whole volume of measurement, are required to provide functional data under realistic conditions of the cellular environment. One problem with stirring cells is the resultant shear force within the fluid that can perturb cell populations. Many cell types are sensitive to shear stress, and fluid shearing is well known to influence cell physiology, and may also stimulate changes in cell morphology and cell state [152,153]. Mechanically stirred configurations are therefore limited to cell lines that require agitation to grow and function, and require some form of mixing to maintain viability. In the context of trying to monitor metabolic parameters of live cultures of human cells or cell lines, these stirred bioreactors are unsuitable. However, they do provide ideal systems to maintain cells that require a microenvironment with directional flow.

The advantage of perfusion systems lie in the maintenance of a steady state culture, in contrast to systems that expose cells to cycles of fresh nutrient-replete medium. In batch fed cultures cells are fed periodic replacements of fresh medium that can have negative effects as sudden change in medium composition can induce differentiation [154].

3.3.2. Physiological Conditions and Cell Numbers

A bioreactor environment may aim to recapitulate conditions associated with certain facets of physiology, however most systems will fail due to cell numbers and environmental parameters inside the bioreactor.

Problems with effects on cell growth due to bioreactor design can stem from immobilisation of cells, as this may prevent them from dividing. Cell to cell signalling, known as quorum sensing, may also be affected.

Alternative approaches use modified hardware to improve detection, using miniaturised NMR detectors and lap-on-chip microfluidics to overcome sensitivity problems associated with very low cell numbers [[155]]. One consideration of bioreactor design is the minimal number of cells required to detect metabolic signatures with NMR. The design of our bioreactor was guided by the desire to recapitulate commonly used lab conditions for growing cells and to minimise cell stress, include shear stress as far as possible. The total volume of the system is 9ml

3.4. Thesis Outline

The aim of this thesis was to develop a methodology to monitor the metabolism of mammalian cells in real-time. This involved the integration of sterile cell culture conditions with flow NMR in a manner amenable to the study of metabolic processes as they occur. The programme of work involved setting up the flow system and finding a suitable approach to keep cells alive and viable over sufficiently long periods of time. Ways of maintaining the equipment were explored with a view to ensuring that cells were kept in a sterile environment for the duration of experiments. Several methods of data acquisition were also tested with a view to finding an appropriate method for monitoring small molecule metabolites in the live cell environment.

A Bruker flow probe insert, termed InsightMR, was supplied for the project. It was originally built for reaction monitoring [156] and is compatible with standard 5mm probes. This system incorporates temperature controlled flow lines that connect a reaction vessel into the flow path and keep the entire system at 37 °C.

Initial experiments investigated cell metabolism in cultured cell lines, monitoring cells and exploring the challenges associated with maintaining cultures away from the sterile cell culture laboratory. Further work explored the suitability of the system to monitor changes in metabolic phenotype through either the administration of therapeutic agents, or the manipulation of transcriptional regulators.

The overall aim was to demonstrate the utility of real-time NMR in the context of correlating the physiological condition of cells with metabolite concentrations with a view to working towards clinical applications.

CHAPTER 4

MATERIALS AND METHODS

4. Materials and Methods

4.1. InsightMR Method Development

Development of the InsightMR flow system, shown below in Figure 4.1, involved a multitude of experiments to optimise the ideal cleaning and sterilisation protocols. These successful methods are outlined in the following sections, while the failed attempts are detailed in Chapter 5.

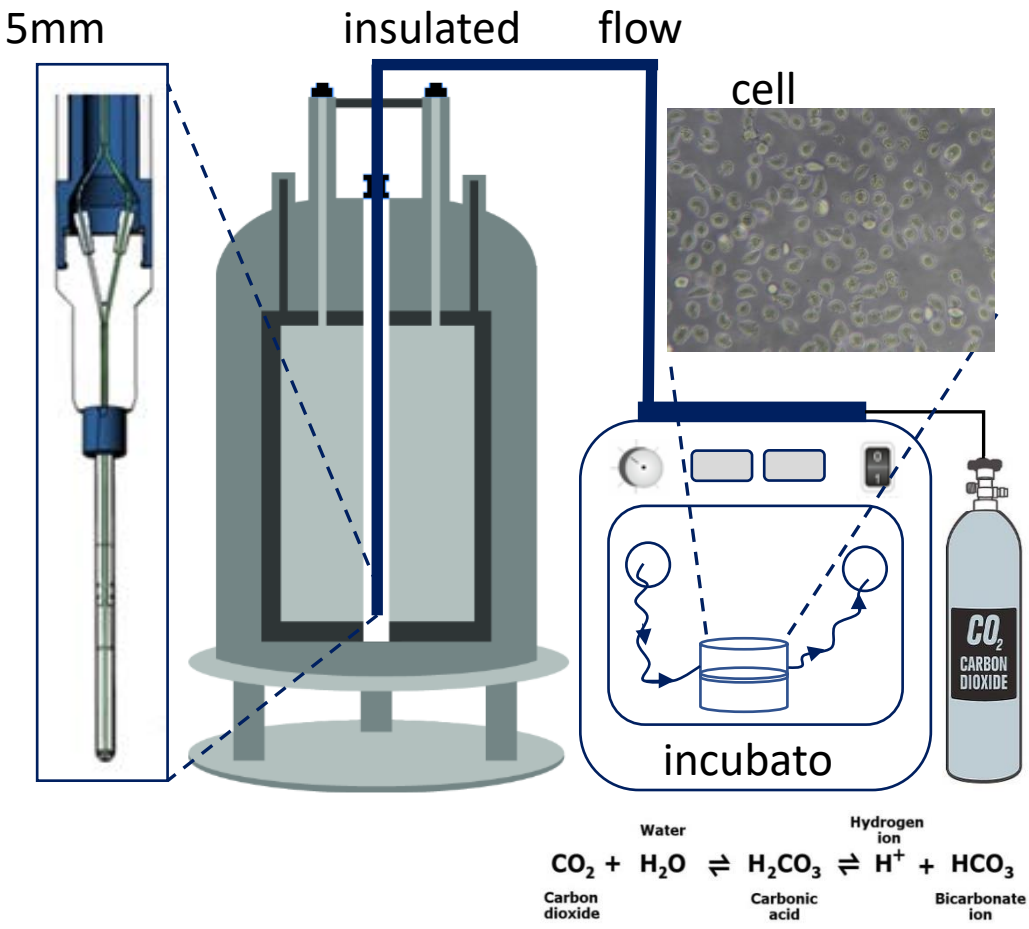

Figure 4.1 Integrating InsightMR and cell culture conditions in the NMR facility

The laboratory setup for monitoring cell metabolism with the flow system. A cell culture incubator is situated adjacent to the spectrometer. Capillary flow lines from the InsightMR enter and exit the incubator via a port in the rear wall and connect to a bioreactor containing the cell culture under observation.

4.1.1. InsightMR System Cleaning Protocol

Removing fluid and any debris from the capillary lines and NMR tube requires several steps of flushing the system (total volume 9 ml). First, any potentially biohazardous sample was flushed out with three systems volume of isotonic phosphate buffered saline (PBS). Biological waste was disposed of via normal autoclave waste streams. Following that, three system volumes of water were used as a final flush and the system was allowed to pump to dryness using a peristaltic pump. The NMR tube was subsequently removed and the lines cleared with compressed air. Air flow was left on until no further fluid exited the lines. The NMR tube was rinsed with water and replaced back onto the tube holder, ready for use.

4.1.2. InsightMR Sterilisation Protocol

The flow system was cleaned, as described in section 4.1.1, prior to sterilisation. The protocol was developed after a series of failed attempts using various chemicals, as described in Chapter 5. Sterilisation was achieved by setting the heater circulator to 95 °C and allowing time for the system and transfer line, containing the capillary flow lines, to equilibrate to temperature. Water was pumped into the flow system and both capillary lines were placed in a large beaker of water, heated to 95 °C on a hot plate. The NMR tube was then lowered into the waterbath of the heater circulator and left for one hour. Once the entire system was at temperature the peristaltic pump was used to circulate the hot water around the system for a further three hours. A protective covering is placed over the NMR tube for the duration of the procedure.

4.2. Cell Based Experiments

4.2.1. Cell Culture Conditions

All cell lines (JJN3, HL-60, SKM-1, MOLM-14 and Kasumi-1) were maintained in a humidified incubator at 37 °C and 5 % CO_2 using supplemented RPMI 1640 medium modified with 10 % fetal bovine serum (FBS), glutamine and pen-strep (Sigma-Aldrich, UK).

Cells were routinely passaged every 2-3 days to maintain cultures in exponential growth (around $5x10^5$ cells/ml). A cell aliquot was taken from culture flasks and counted using trypan blue to establish live cell numbers. Cells were centrifuged (5 mins, 300 g) and resuspended in a suitable volume of fresh culture medium.

4.2.2. Kasumi-1 doxycycline treatment (seven day time course)

The Kasumi-1 cell lines, containing the doxycycline inducible RUNX1/ETO shRNA and mismatch control shRNA, were used to investigate metabolic changes as cells differentiated. Cells were seeded at $5x10^5$ cells/ml and passaged by splitting every 48 hours. Cell suspensions were counted using trypan blue to establish live cell numbers, then centrifuged (5 min, 300 g) and spent medium replace with supplemented RPMI medium with/without 10 mg/ml doxycycline.

4.2.3. RNA isolation, cDNA synthesis and PCR

Cell aliquots (approximately 1 ml containing $1x10^7$ cells) were taken and suspended in triazol prior to storage at -80°C. Samples were defrosted on ice and incubated for 2 to 3 minutes at room temperature following the addition of chloroform (200 µl) to the lysate. After centrifugation (12000 g, 15 min, 4 ºC) the aqueous supernatant was transferred to a new tube, with care taken not to disturb the pink triazol phase.

Precipitation of the RNA was achieved by addition of 2-propanol (500 µl) to the aqueous phase. The sample was vortexed well, incubated at 4 °C for 10 min followed by centrifugation (12000 g, 15 min, 4 °C). The supernatant was removed and the pellet washed with ice-cold ethanol (70 % made in DEPC treated water by addition of 0.1 % DEPC to sterile water). The sample was centrifuged (12000 g, 5 min, 4 °C) and the pellet air dried to remove any residual ethanol and was subsequently resuspensed in DEPC treated water (20 µl). An Rneasy minielute cleanup kit (Quiagen) was then used purify the sample ready for cDNA synthesis.

RNA was treated with DNase1 and incubated (1 hour, 37 °C) with the following:

total RNA (2 µl), 10X DNase1 buffer (2.5 µl), 1 U/µl RQI Rnase free DNase1(1 µl), 40 U/µl RNaseOUT (0.5 µl) and water (1 µl). A NanoDrop spectrophotometer was used to quantify the isolated RNA, with purity ratios at 260/230 nm and 260/280 nm used to assess the quality of the RNA.

1 µg of RNA was used for cDNA synthesis with reverse transcriptase (M-MLV RT). RNA was annealed by heat treatment at 70 °C for 5 minutes, after which a mixture containing nucleoside oligo (dT) primers, 4 µl of 5 x first strand synthesis buffer (Promega), 5 µl of 2mM dNTP, 1 µl of 200 U/µl M-MLV Reverse Transcriptase (Promega), 0.5 µl of 400 U/µl of RNase out (Invitrogen) was added to the RNA and incubated at 37 °C for 1 hour followed by 9 5°C for 5 minutes in a T300 thermocycler (Biometra).

SYBR® Green PCR master mix was used for PCR. Primers were diluted (1:50) from 1 mM stock solutions. Total reaction volume was 10 µl per well (2.5 µl cDNA and 7.5 µl master mix and primers). GAPDH was used to normalise expression of each gene. A standard curve, produced from serially diluted cDNA, was used to determine amplification efficiencies of the different primers.

4.2.4. Preparing Frozen Patient Cells

Culture medium was prepared using alphaMEM (Stemcell Technologies) supplemented with horse serum (HS).

The thawed cell pellet was resuspended in a defrost buffer PBS (5 % HS, DNAase1), initially in 1 ml, followed by slowly adding more buffer over ten minutes. Cells were centrifuged (10 min, 500 g) and resuspended ($5x10^5$ cells/ml) in medium containing 10 % D_2O, ready for transfer to the bioreactor for NMR analysis.

4.2.5. Preparing Patient Cells from Fresh Blood.

A member of the Bonifer lab prepared a peripheral blood sample by layering blood from a patient onto a density gradient medium (Lymphoprep, StemCell Technology) and centrifuging at 600 g. Once the mixture had separated the mononuclear cells were taken from the intermediate layer. Flow cytometry was used to confirm the presence of cell type using the CD34+ stem marker. Cells were incubated with magnetic CD34+ microbeads (500 µl, 15 mins) and then resuspended in 5 ml MACS buffer. Cells were sorted using a LS column (Miltenyl-Biotech) to ensure that a purity of greater than 95 % was achieved in the final sample. An aliquot of cells was used ($5x10^5$ cells/ml) for real-time analysis. Medium was perfused around the flow system at 1 ml/min and the metabolic footprint was monitored over 12 hours.

4.2.6. Patient Cell Line Culture

An aliquot of the patient cell line was defrosted as described in section 4.2.4, above. Cells were centrifuged (10 min, 500 g) and resuspended in MACS (PBS, 0.5 % BSA, 2mM EDTA) buffer ready for purification. Cells were sorted to yield the CD34+ fraction using magnetic beads (Miltenyl-Biotech, USA). An Fc receptor (FcR) blocking agent

was added to avoid non-specific binding together with EDTA (4mM) was added to prevent cell clumping. The solution was gently agitated onto the column and washed three times (3 ml), prior to eluting (5 ml). Cell count post-bead purification was $1x10^6$ cells. Cells were plated out onto MS5 stromal cells and left to expand for two weeks.

4.3. Flow Cytometry

4.3.1. Cell Viability

Apoptosis and cell death was assessed using the AnnexinV-FITC Apoptosis Detection Kit (BD Pharminogen™). The 10X Binding Buffer was diluted 1in10 prior to use. Cell aliquots were collected ($5x10^5$ cells), centrifuged (300 g, 5 mins) and supernatant discarded. The cell pellet was washed with cold PBS, re-pelleted (300 g, 5 mins). Cells were resuspended in 1X binding buffer (500 µl) and aliquoted into flow cytometry tubes (100 µl). The relevant stain was added, and the tubes were gently mixed and left for 15 mins in the dark. 1X binding buffer (400µl) was added to the tubes and analysis was conducted using a CyAn™ ADP flow cytometer.

Sample	Stain
Control	None
Apoptotic	5ul FITC AnnexinV
Dead	5ul propidium iodide
Apoptotic and Dead	5ul each stain

Table 2: reagents for flow cytometry

4.3.2. Cell cycle analysis

A cell aliquot was collected ($1x10^6$ cells) and centrifuged (300 g, 5 mins). The supernatant was discarded and the pellet resuspended in PBS (250 µl). Ice cold ethanol was added dropwise (750 µl) to fix the cells. The aliquot was left at 4 °C for 30 min after which the cells were washed in PBS, pelleted (300 g, 5 mins), resuspended in PBS (1 ml) and left for 20 minutes to hydrate cells. Cells were pelleted (300 g, 5 mins) and resuspended in fresh PBS (500 µl) with RNaseA (100 µg/ml) and incubated for 20 minutes at RTP. The cell aliquot was washed again, resuspend in PBS (400 µl) with 7AAD (4 µl from 1 mg/ml stock). analysis was conducted using a CyAn™ ADP flow cytometer.

4.4. Metabolic Analysis using NMR

4.4.1. InsightMR Development Experiments

All experiments with the InsightMR system used the modified 5 mm NMR tube, with a 500 lµ volume, supplied with the system. Data was acquired at 310K using a 500 MHz Bruker Avance III spectrometer with a 5 mm z-PFG TXI probe. Spectra collected during modifications and protocol developments used the standard Bruker noesygppr1d sequence with parameters as follows: number of transients 32 or 64 (depending on sensitivity required), steady-state transients = 4, relaxation delay 5 s. The number of transients was increased during the development to ensure that all relevant metabolites could be detected. The probe was tuned and matched, with pulse widths in the range 11 µs and the frequency offset was set to 4.7 ppm.

4.4.2. Medium Aliquots

Spectra collected to establish changes in medium composition under standard cell culture conditions, described in Chapter 6.1, were acquired using a 600 MHz Bruker Avance III spectrometer with a 5 mm z-PFG TCI probe and Samplejet autosampler. Samples were transferred to 3 mm NMR tubes, to minimise the amount of medium used, with a final concentration of 10 % D_2O for analysis. The probe was tuned and matched, with typical 90 °C pulse widths in the range 8.5 µs and the frequency offset was set to 4.7 ppm. Parameters were as follows: number of transients = 64, steady-state transients = 4, relaxation delay 5 s. All spectra were acquired at 300 K as there was no requirement to heat the sample to physiological temperatures.

4.4.3. Water Suppression

Comparison of methods to supress the water signal used a 2 mM sucrose standard at 310 K on a 500 MHz Bruker Avance III spectrometer with a 5 mm z-PFG TXI probe. The three standard Bruker pulse sequences, detailed in section 2.2.2, were used with the following parameters: number of transients = 8, steady-statey transients = 4, relaxation delay 5 s. Pulse widths were 7.2 µs, the frequency offset was set to 4.704 ppm.

4.4.4. CPMG – NOESY comparison for real-time acquisition

Spectra were acquired with the flow system set to 37 °C and measurements were carried out after locking on the deuterium frequency. Interleaved acquisitions used the two standard Bruker pulse sequences below with the following parameters: relaxation delay 5 s. Pulse width was in the range 10 µs, the frequency offset was set to 4.698 ppm.

1. noesygppr1d. number of transients = 128, steady-state transients = 4,

2. cpmgpr1d. number of transients = 16, steady-state transients= 16, looping parameter L4 = 100, repetition rate of the echo delay = 400 μs.

L4 is the counter for the CPMG (Carr-Purcell-Meiboom-Gill sequence) element which occurs twice in the pulse sequence.

4.4.5. Real-Time Metabolism

Metabolite profiles, described in Chapter 7, were established using the InsightMR system with a peristaltic pump. The flow rate was set to 0.5 ml/min and the system temperature was set to 37 °C, controlled by the incubator and heater-circulator pump. Measurements commenced after locking on the deuterium signal and after shimming yielded an acceptable spectrum, as determined by the glucose anomeric doublet resolution (5.2 ppm). Sequential ^{1}H 1D spectra were acquired using a 500 MHz Bruker Avance III spectrometer with a 5 mm z-PFG TXI probe at 310 K. The standard Bruker noesygppr1d sequence was used with parameters as follows: number of transients = 128, steady-state transients = 4, relaxation delay 5 s. Pulse widths were in the range 11 μs and the frequency offset was set to 4.7 ppm.

4.4.6. NMR Data Processing

All 1D spectra were processed using NMRlab [157] and MetaboLab [158] in MATLAB (MathWorks, USA). An exponential window function of 0.3 Hz was used to apodize the free induction decay signal, followed by zero-filling prior to the Fourier transform. All spectra were phased and referenced using the chemical shift reference TMSP signal at 0 ppm. The TMSP peak area (AUC) was used to align spectra and normalise peak areas of other proton resonances over the time courses. Assignments were made using the human metabolome database (HMDB) [159] and Chenomx NMR Suite (Chenomx, Canada).

4.4.7. Statistical Analysis

An unpaired t-test was chosen to compare the mean values for each triplicate time point between cell lines. GraphPad Prism (GraphPad, USA) was used to carry out comparisons between metabolites using multiple unpaired t-tests with the two-stage set-up method of Benjamini, Kriger, Yekutieli.[160]. The initial concentration of each metabolite was normalised to unity so that the final values in a course could be compared to establish any differences in the ultimate consumption or production of each metabolite.

4.5. MATLAB scripts

The following scripts were used to automatically process the spectra acquired during time courses.

4.5.1. Spectral Overlay Colours

This script renders a time course into a coloured overlay

```
%NMRDAT is a 1x2 array with second element=total number of spectra
nospec=size(NMRDAT,2)
start=1
stop=nospec;
MAP=colormap(jet(nospec));
for N=1:length(NMRDAT)
    NMRDAT(1,N).DISP.PLOT=0;
end
counter=1;
for N=start:stop
    NMRDAT(1,N).DISP.PLOT=1;
    NMRDAT(1,N).DISP.Color{1} = MAP(counter,:);
    counter=counter+1;
end
clear counter
dr2('plot')
```

4.5.2. Histidine Imidazole Resonances Used to Calculate pH

A pH calibration curve was generated in MATLAB using NMR data of RPMI media samples, with pH values from pH 3 to pH 8.5, acquired by K. Koczula as part of her doctoral thesis [161]. The pH was calculated from the frequency difference between resonances corresponding to the imidazole protons of histidine using equation 4.1 [162].

$$pH = pKa + \log10\,[(\Delta\delta - \delta BH)/(\delta B - \Delta\delta)] \quad (4.1)$$

where $\Delta\delta$ is the chemical shift difference between the H2 and H5 ring protons, δBH is the limiting value at acid pH and δB is the limiting value at basic pH (i.e. chemical shifts when the sites are either fully pronated or unprotonated). The following script was used to pick the relevant peaks for each spectrum in NMRlab and write the ppm values to a .csv file.

```
  %NMRDAT is a 1x2 array with second element=total number of spectra
  nospec=size(NMRDAT,2)
  %number of picked peaks calculated from first spectrum
numpeaks=numel(NMRDAT(1,1).MANINT.peakMaxPPM)
  %script only works for two peaks; use manual int to select H2 and H5
proton
     if numpeaks > 2
         error('Clear peak integrals! Only pick Histidine H2 and H5
peaks!')
     else
         disp('ppm shift values calculated')
     end
  %ppmMax array holds all ppm values for manually picked peaks
  %create nospecxnumpeaks array (all zeros) ready for H2 and H5 ppm
values
```

```
   ppmMax=zeros(nospec,numpeaks);
   %assigns each row in ppmMax the values of picked peak's ppmMax
   for k=1:nospec
      ppmMax(k,:)=NMRDAT(1,k).MANINT.peakMaxPPM;
   end
   %transpose and subtract
   shift=diff(ppmMax')
   %create and open a csv file called pHshifts, 'w' discards exisiting
contents
   fid =fopen('pHshifts.csv','w');
   for k=1:nospec
   fprintf(fid,'%d\t',shift(:,k));
   fprintf(fid,'\n');
   end
   fclose(fid);
```

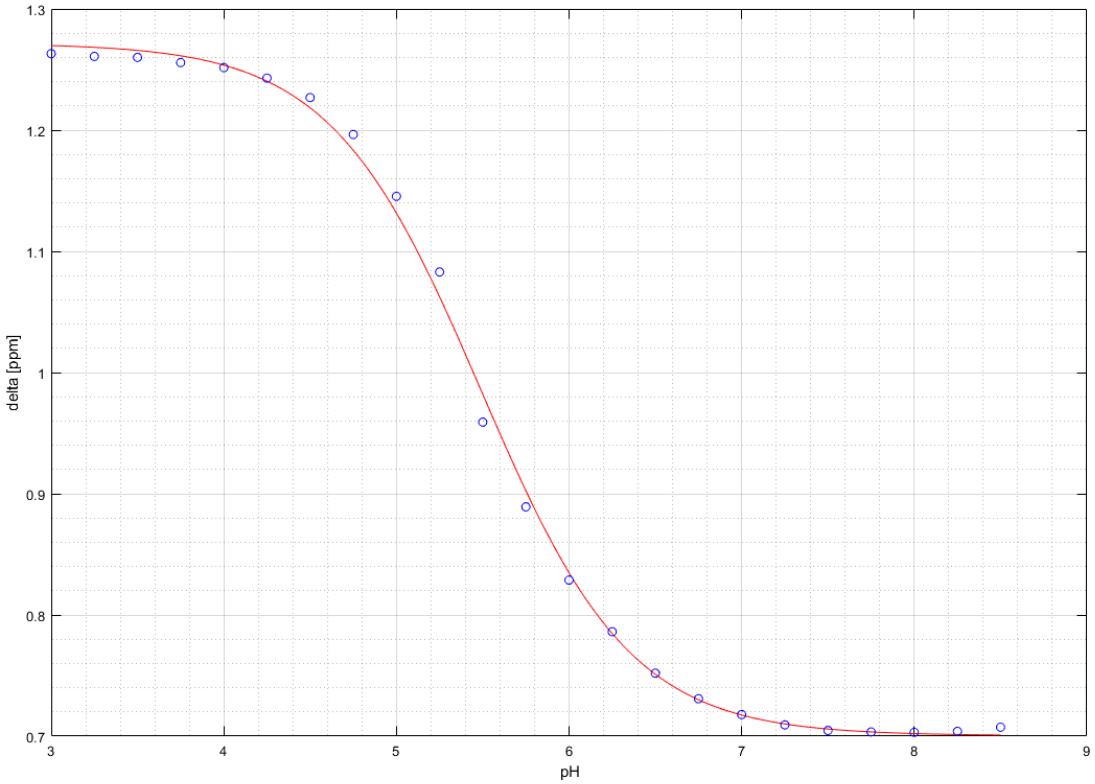

Figure 4.2 pH calibration curve generate from histidine imidazole resonances

Data acquired from a series of RPMI media samples, with pH values from pH 3 to pH 8.5, was used to generate a pH calibration curve.

CHAPTER 5

INSIGHTMR FLOW SYSTEM DEVELOPMENT

5. Reaction Monitoring with Flow NMR

This chapter describes the set-up and modifications made to the InsightMR flow system, and its integration with cell cultures under optimal conditions. Initial experiments focused on understanding the flow system, and how live cells would respond to being kept outside the normal cell culture laboratory while exposed to flow.

The system itself had to be maintained to provide a suitable environment for cell based experiments. Further experiments in this chapter describe the cleaning, disinfection and sterilisation of the system, as appropriate for cell culture under sterile conditions. Finally, data acquisition is considered in the context of the flowing sample in the NMR tube. Pulse sequences are assessed for water suppression and suitability for acquisition of data during time course experiments.

5.1. Overview

NMR can be used to monitor reactions at low and high field, yielding comprehensive structural and quantitative information on chemical species in solution. Current low field benchtop spectrometers operate in the range 60-80 MHz, while high field magnets are typically 500-800MHz, with the current highest field superconducting magnet at a field of 1.2MHz [163]. It can elucidate reaction mechanisms and generate kinetic data from reactant, intermediate and product concentrations [164,165]. Analysis of complex mixtures is possible using a variety of 1D and 2D acquisition strategies. The technique is only limited by the requirement for NMR-active nuclei in the sample, which need to be present in sufficient concentration.

Methodologies can simply use normal NMR tubes, with no requirements for specialised hardware, or make use of flow cells and flow probes, whereby a flowing stream of reaction mixture is pumped through the detection area of the spectrometer.

Broadly speaking there are two approaches to chemical reaction monitoring, split into static or stop-flow and flow methods. The distinction is dictated by the method of data acquisition, with a method being categorised as flow if the sample is flowing during the measurement process. While some static methods can be inexpensive and accessible, as they only require standard NMR tubes, they do have major drawbacks. Static reaction monitoring involves either sequential sampling of the reaction mixture, or completion of the reaction inside the NMR tube where reactants are added at time zero. However, sampling an ongoing reaction introduces a source of error and a time lag between taking the aliquot and analysing the mixture. Other considerations come into play when considering biological reactions, as it may not be permissible to sequentially sample from a limited aliquot of cells or tissue. The disadvantages of in-tube reactions are limited sample volume, as the entire reaction mixture must fit into the NMR tube, and the limited mixing of components, as the reactants are left unstirred during data acquisition [166]. In contrast, flow NMR connects a reaction vessel to the probe area of the magnet, allowing a flowing stream of reaction mixture to be transferred to the detection region.

5.1.1. Flow NMR

There are a variety of applications where it is advantageous to use liquid flow as a means of transport to a chemical detector, for example in liquid chromatography-NMR studies (LC-NMR), where analysis takes place immediately after separation. Providing a means to immediately monitor unstable analytes or track industrial flow processes [167].

Flow NMR techniques generally take advantage of specialised probes with specific RF coil geometry, optimised for flow, with built-in flow cells that directly connect to liquid handling or chromatographic systems. A reaction vessel is linked to the spectrometer bore and material pumped into the NMR tube. Flow is either halted, in order

to monitor the static sample (known as stopped-flow), or the reaction mixture can flow continuously (online monitoring). Both designs require a connection from an outside vessel into the spectrometer bore, and often necessitate bespoke probes to accommodate non-standard NMR tubes or samples sizes.

In contrast, the InsightMR system is intended for use in a conventional probe and therefore offers a more flexible and less expensive approach to flow studies than dedicated flow probe systems.

5.2. Flow System Design

A flowing stream of reaction mixture is pumped from a reaction vessel, via capillary flow lines, to the NMR tube in the bore of the magnet (illustrated in Figure 5.1). Reaction conditions can therefore be maintained throughout the volume of the system. The NMR tube is modelled on a standard 5mm tube and spinner, allowing its use across a multitude of spectrometers and probe types. Two separate capillary lines are used to transfer the reaction mixture to and from the NMR tube; fluid enters via the inlet line and leaves via the outlet line (as detailed in Figure 5.2).

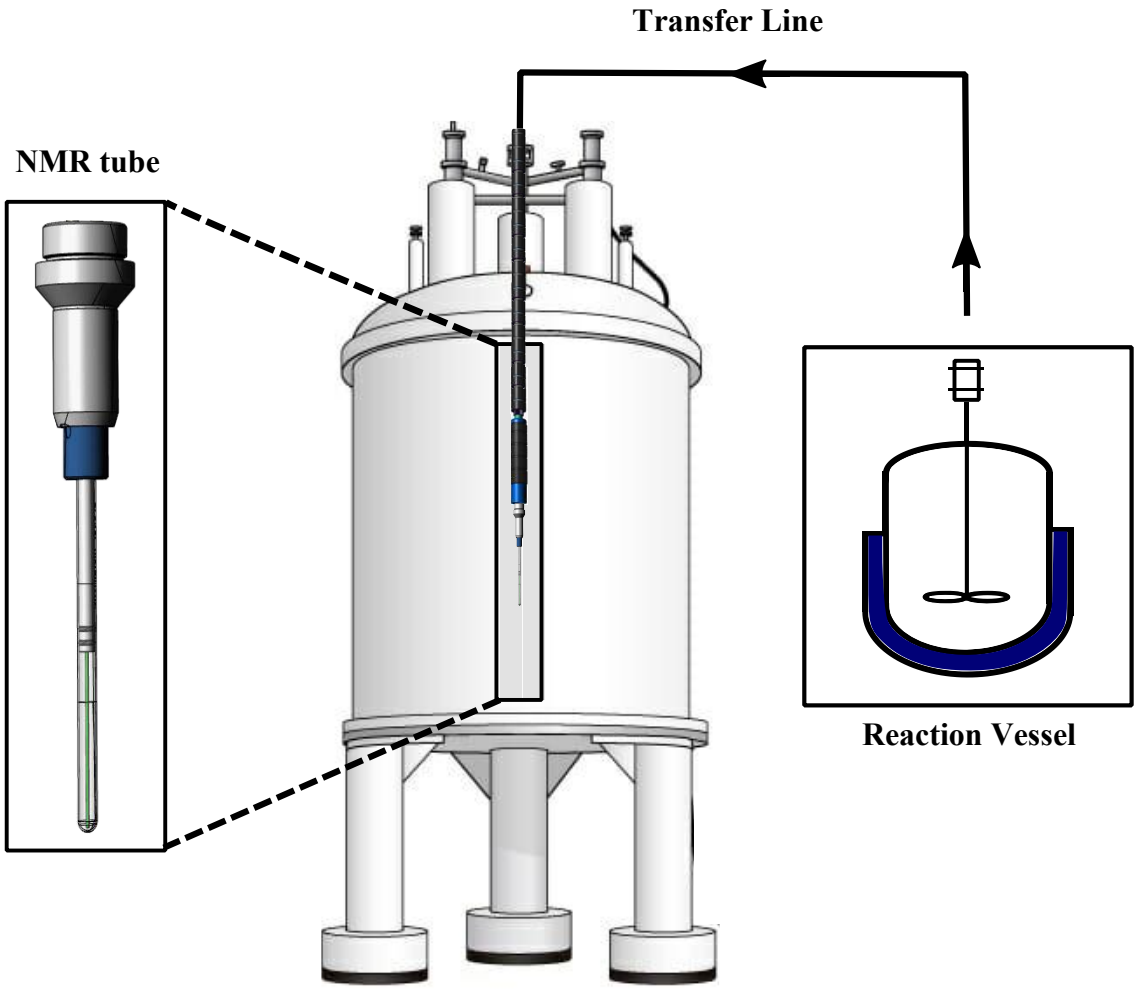

Figure 5.1 Reaction monitoring with InsightMR

An external reaction vessel is connected to a modified 5 mm NMR spinner and tube seated in the detection region of the spectrometer. Reaction conditions are constant throughout the volume of the system while fluid is pumped from the vessel into the NMR tube for analysis. NMR tube and holder image supplied by Martin Hofmann, Bruker Ltd. The spectrometer graphic in this image sourced from WikiCommons [168].

The inlet capillary (C) enters along the centre line of the NMR tube and descends to the bottom, while the outlet capillary (D) is positioned at the top of the tube, slightly over to one side of the holder (E). Both capillary lines connect into the tube holder via the transfer line (F). A thermally controlled sheath fluid, entering the transfer line at the connection block (G) maintains a constant temperature around the capillary lines. The fluid enters via the inlet sheath (I) and returns via the outlet sheath line (J). The tubing inside the transfer line is coaxial, composed of two concentric tubes, enabling the inlet sheath flow to descend down to the NMR tube in the smaller tubing that houses the capillary lines. The return flow is via the larger tubing, flowing up at the outside of the transfer line. Both sheath lines connect to an adjacent heater circulator, filled with an ethylene glycol-water mixture. The capillaries exit the Insight block at point (H) and connect to a reaction vessel containing the fluid under analysis.

Depending on the requirements of the experiment the system can be arranged to recirculate the reaction mixture, back to the vessel in a closed-loop configuration, or direct it to waste after analysis. This is facilitated by a flow control valve on the connection block.

The small diameter of the transfer lines, and close proximity of the reaction vessel to the NMR tube, ensures a minimum transfer time between the vessel and the point of detection inside the spectrometer. This guarantees that the flowing reaction mixture is representative of the bulk sample inside the reaction vessel.

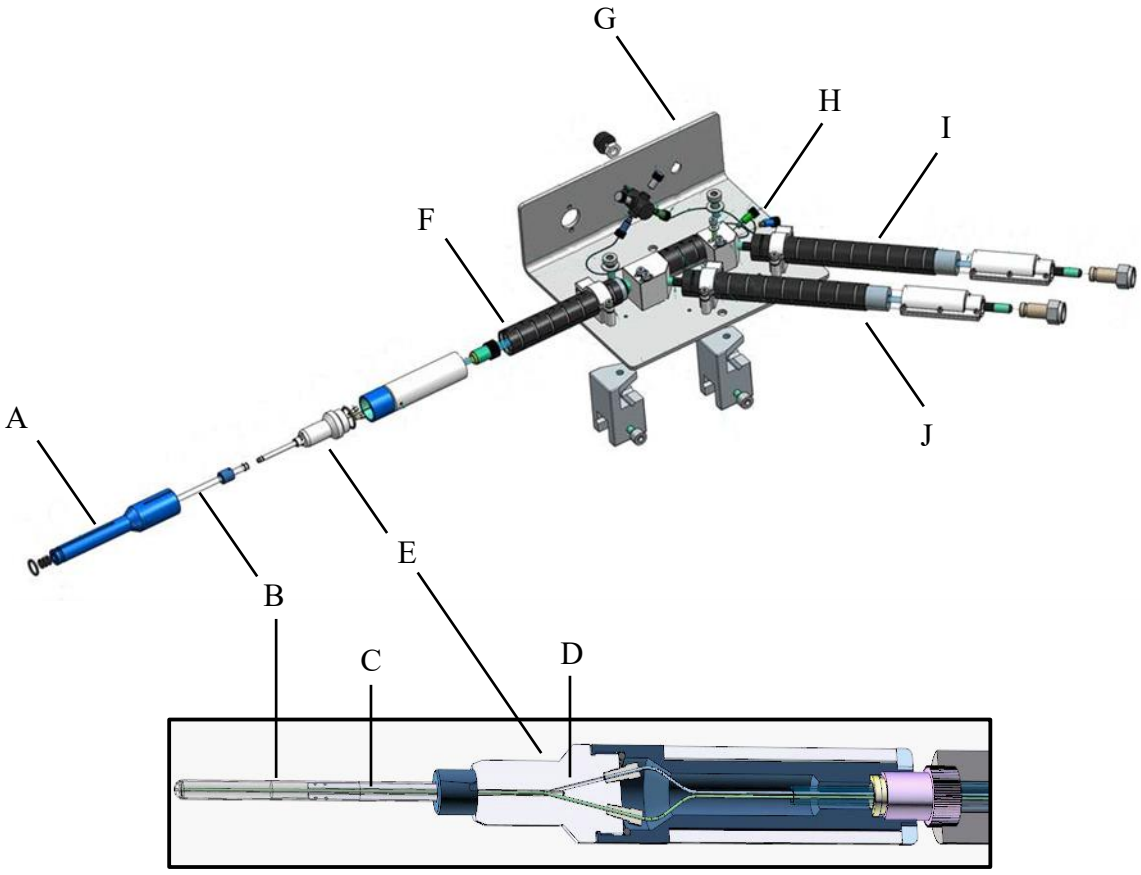

Figure 5.2 InsightMR connection block and flow tube assembly.

(A) protective covering for NMR tube when system is not in use (B) adapted 5mm NMR tube (C) inlet line (D) outlet line (E) tube holder (F) transfer line containing lines concentric sheath tubes and capillary lines (G) connection block (I) sheath water line inlet (J) sheath water line outlet. A heater circulator is connected to the sheath lines, delivering a fluid maintained at a constant temperature. The capillary lines exit the block and connect to the reaction vessel at point (H). Images courtesy of Martin Hofmann, Bruker Ltd.

5.3. Pumps

The InsightMR flow unit is suitable for use with a variety of different pumps, and compatibility is only limited by the available connectors between the capillary flow lines and the pump lines. The choice of pump involves consideration of several factors, including pumping mechanism, rate of flow, stability of flow, and pumping direction. The ability to change flow speed is very important, as different experiments may require faster or slower flow rates around the system. Flow stability is related to the pumping mechanism and the consistency of pressure applied to the fluid. Some positive displacement pumps use alternating pistons that can cause a variable pressure profile, resulting in pulsed or uneven fluid movement along the flow lines. The ability to reverse direction of the flow is useful when flushing out the system, although not strictly required for experimental monitoring of the reaction mixture.

For the purpose of this project a key requirement was the ability to clean and sterilise any part of the system in contact with the reaction fluid. Biological samples may be classified as biohazardous material, depending on species of origin and associated risk of infection. Moreover, any microbial growth within the system will confound results regarding metabolic turnover.

Three pumps were chosen to test with live cells and the flow system.

- A high performance liquid chromatography (HPLC) quaternary pump (Dionex Ltd, UK) provides fine control of flow rates with real-time information on system parameters, such as pressure.
- An M-series positive displacement, syringe-free pump (VICI, USA) offers computer controlled flow rates and bidirectional pumping.

- A peristaltic pump (Masterflex, UK) avoids direct contact between the fluid and pump, reducing risk of shearing forces from pistons or other components. This is advantageous when pumping suspensions of live cells.

While both the HPLC and M series pump performed well (consistent, programmable flow rates), neither were ultimately suitable for the application of monitoring real-time cell metabolism. Unfortunately the M series pump failed, likely as a result of repeated exposure to aqueous and solvent fluids in the presence of air bubbles. The HPLC pump was difficult to permanently locate close to the spectrometer due to space restrictions. Constantly moving the large pump into and out of the laboratory was not an optimal solution. The long sections of tubing running from the HPLC to the flow system also greatly increase the whole system volume.

The peristaltic pump had the advantage of maintaining a sterile environment, as fluid is not in contact with any pump mechanisms and tubing can be autoclaved. It is also very small, light, and easy to situate adjacent to the spectrometer. Chemically resistant tubing is readily available and can used for hundreds of hours before being replaced. While the pump itself did not offer any programmable flow rates or detailed system information, such as flow rate and pressure, it is be possible to upgrade to a model with greater functionality.

5.4. Flow Patterns and Signal Intensity

The residence time of the reaction fluid inside the NMR tube depends on the flow rate and the flow pattern inside the tube (i.e. plug, laminar, turbulent). Ideal plug flow is characterised by a constant fluid velocity over the cross-sectional area of the tubing with no interactions between the fluid and the tubing walls. Laminar flow has a parabolic velocity profile, smooth layers of flow result from the fluid element at the centre traveling faster than at the tubing walls. In contrast, the primary feature of turbulent flow is chaotic mixing of the fluid due to non-uniform velocity across the tubing [[169]].

A coloured tracer was used to characterise the flow pattern inside the NMR tube in order to investigate mixing of the fluid inside during peristaltic pumping. Aqueous fluid dynamics and slow flow rates of the peristaltic pump, together with the low system volumes were expected to produce a laminar flow [[170]].

For this experiment the capillary flow lines were flushed with water and a red tracer dye was used to visualise the movement of fluid in and out of the NMR tube. The tracer flowed via the inlet capillary to the NMR tube, then out to waste via the outlet capillary. Once the system was filled with dye a bolus of water was pumped in, flushing out the dye. Total volume of the system was approximately 8.5 ml (0.5 ml in the NMR tube and 8 ml in the 1/16 ” polyether ether ketone (PEEK) capillary lines).

Appearance of the tracer dye in the NMR tube was asymmetric, due to the PEEK tubing bending slightly towards one side of the glass tube (see Figure 5.3) which resulted in one side of the tube taking longer to fill, and empty than the other side. Several system volumes of fluid were therefore required to completely flush the dye from the NMR tube. As the final visible traces of the dye disappeared from the tube a pulsed-flow pattern was observed, resulting from peristalsis of the pumping mechanism.

While this type of flow dynamics would not be a suitable methodology for monitoring rapid reactions, as the sample would not be well mixed inside the NMR tube, it is sufficient for the application of real-time cell metabolism where flow rates are very slow. Here long acquisition times are used as metabolic products build up over hours of data collection, therefore the slight disturbance of the flow profile has little impact on the final kinetics being measured. The volume of fluid required to displace the dye was set as the minimum flush volume for the cleaning protocol (see methods section 4.1).

Although PEEK tubing is rigid, it was not possible to keep it centred in the middle of the NMR tube. The inlet line would always bend slightly towards the glass, possibly as a consequence of the angle of direction of entry into the tube holder. PEEK had been selected for use on the basis that a larger bore, rigid tubing might be more compatible with a flowing suspension culture. Smaller capillary lines could become blocked if cells clumped together as they flowed around the tubing. Less rigid tubing could also develop bends and kinks as it moves and twists during relocation of the transfer line in and out of the magnet.

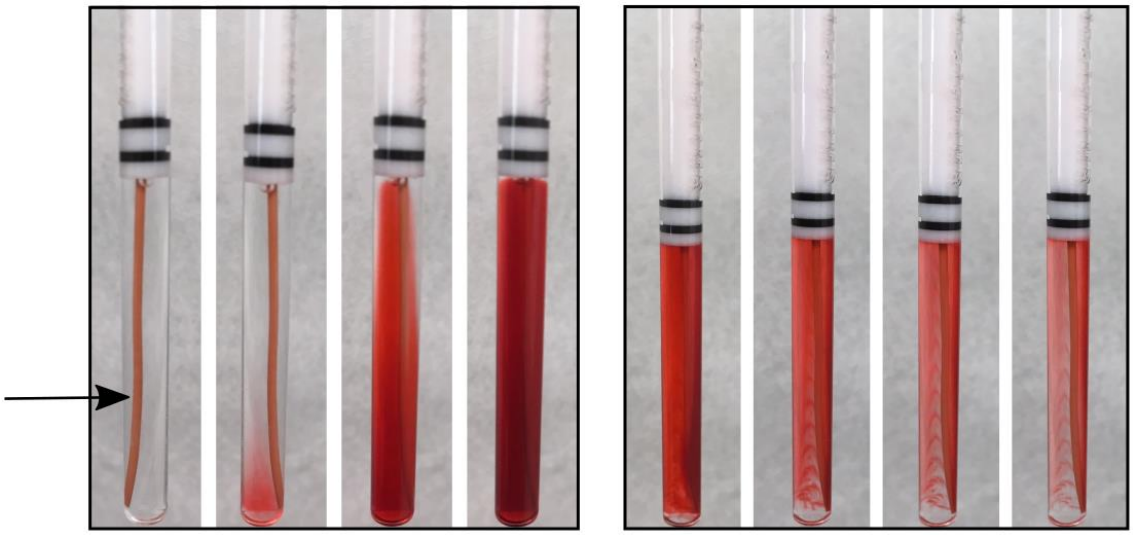

Figure 5.3 Peristaltic flow pattern inside the NMR tube.

Flow regime patterns inside the InsightMR tube are illustrated using a red tracer dye, demonstrating residence of an aqueous fluid at a low flow rate (1 ml/min) using a peristaltic pump. The pumping mechanism resulted in a pulsed flow profile, seen as alternating bands of dye and water during the flushing out of the dye. A bend in the inlet capillary line results in a slightly asymmetric distribution of flow into the tube, marked by an arrow in the above photo. Laminar flow is indicated by the dye progressing up the interior of the tube faster than the peripheral regions.

The presence of the capillary line inside the NMR tube disturbs the otherwise cylindrical symmetry of the flow tube assembly, contributing to non-homogeneity of the sample. This phenomenon can impact the NMR lineshape in comparison to a standard NMR tube and reduce the overall spectral quality (as shown in Figure 5.4). However this does not have a significant impact on the integration of metabolite resonances as at least one peak from each relevant metabolite could still be adequately resolved.

A flowing sample can significantly change quantitation due to flow effects on signal intensity; residence time inside the NMR tube must be sufficient for full magnetisation of the nuclei under investigation [171]. It is possible to establish a compensation factor by comparing spectra with flow off and then flow on. The difference between peak integrals serves as a reference for percentage attenuation due to the flow rate used for acquisition, with each proton resonance having its own factor due to variation in longitudinal relaxation rate (T_1).

Optimal flow rates were established by monitoring a solution and recording intensity of the signals as a function of flow rate. Up to the maximum flow rate of the peristaltic pump (1 ml/min) there was no significant difference between the static signal intensity and the flowing sample intensity. Higher flow rates would likely induce a change in signal intensity [172].

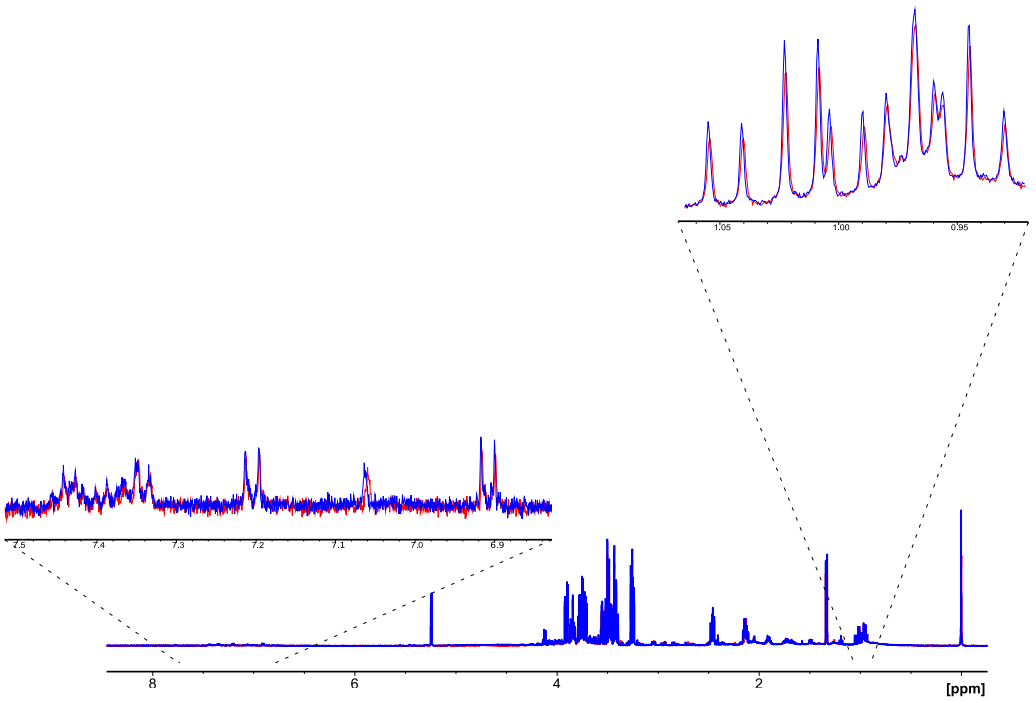

Figure 5.4 Differences in spectral quality due to the capillary line in NMR tube

Presence of the capillary line inside the InsightMR tube (blue trace) results in a minimal increase in linewidth compared to a normal NMR tube (red trace). Zoom of resonances corresponding to branched chain amino acids at 1ppm and aromatic amino acids at 7 ppm show little difference between the two spectra. Peaks are still well resolved with the capillary line inside the NMR tube and the typical TMSP peak width is around 2.5Hz when medium is supplemented with 10% serum.

5.5. Cells and Flow

Maintaining live cells adjacent to, or even inside the spectrometer presents many challenges. In particular, mammalian cells require a controlled environment such as constant temperature [173], buffered physiological pH and adequate oxygen supply [174]. The manner in which these parameters are controlled depends on where the cells are housed and the flow system offers three configurations based on cells being either inside or outside the spectrometer, or a combination of both. The first two are compatible with both adherent and suspension cultures, while the last is only usable with suspension cells:

1. The inlet and outlet capillary lines can be connected together, to close the system into a minimum volume loop. The cells could reside inside the NMR tube while the medium is circulated around the system. Depending on the volume and number of the cells used, the spectrum would reflect a mixture of intracellular metabolites and medium components.
2. A suitable vessel, such as a cell culture flask or bioreactor, could be used to maintain the cells outside the spectrometer. Cells would be prevented from entering the capillary flow lines by a filter/membrane while the medium is circulated around the system. The spectrum would reflect the metabolic footprint, providing information on the changing composition of the medium as nutrients are used and cellular by-products effluxed.
3. Cell lines that grow in suspension could be pumped around the whole system. The spectrum would reflect the mixture of metabolites inside and outside the cells, depending on the cell size and density.

5.5.1. Cells inside the spectrometer

Initial experiments investigated the possibility of loading the NMR tube with an aliquot of myeloid Kasumi-1 suspension cell culture. Cells very quickly formed a sediment at the bottom of the tube, just as they would in a normal cell culture flask (Figure 5.5, panel A). This is unsuitable for NMR as the sample is inhomogeneous, being composed of the cell pellet and the medium.

Moving forward, a low flow rate was used in an attempt to buoy the cells inside the detection region of the coil, with the aim of avoiding sedimentation of the cells and maintaining a homogenous sample. This would only be successful if the cells could be kept below the level of the outlet capillary line, otherwise they would be pumped out of the NMR tube. Unfortunately, we were unable to find a compromise between a flow rate low enough to keep the cells from reaching the outlet line and high enough to prevent sedimentation.

An alternative approach was to circulate the entire cell suspension around the system. This was attempted at a flow rate of 0.5ml/min, followed by 0.1ml/min. Unfortunately, both flow rates resulted in a stringy precipitate forming inside the tube (pictured Figure 5.5, panel B). This could have been due to the cells hitting the wall of the glass tube as they enter via the capillary inlet. The force of shear stress may have been sufficient to induce cell death and/or burst the cells, releasing DNA. Reversing the flow, pumping cells into the tube via the outlet capillary, did not improve viability.

The next method introduced a filter or membrane to keep the cells inside the NMR tube. The reusable filter frit (designed and manufactured by Bruker Ltd) was positioned at the top of the NMR tube and slid over the capillary line. The idea was to prevent any cells escaping while medium was perfused via the inlet line. The flow rate would keep the cells floating, without being forceful enough to push them against the frit. This setup was tested by slowly loading cells into the NMR tube via the inlet line. The flow rate was

then increased to buoy the cells and the system was left circulating medium overnight. After only a few hours the frit had become blocked and a stringy precipitate was visible in the tube. A close up taken using an optical microscope is shown in Figure 5.5, Panel D. This result was likely due to cells being broken apart by mechanical stress from flow inside the tube and against the filter frit. On removal of the flow tube a clear difference in medium colour could be seen (Figure 5.5 Panel C), indicating that the cells had been alive long enough to produce some lactate. An aliquot of suspension from the tube was taken for trypan blue staining. Most remaining intact cells appeared to be dead at this point.

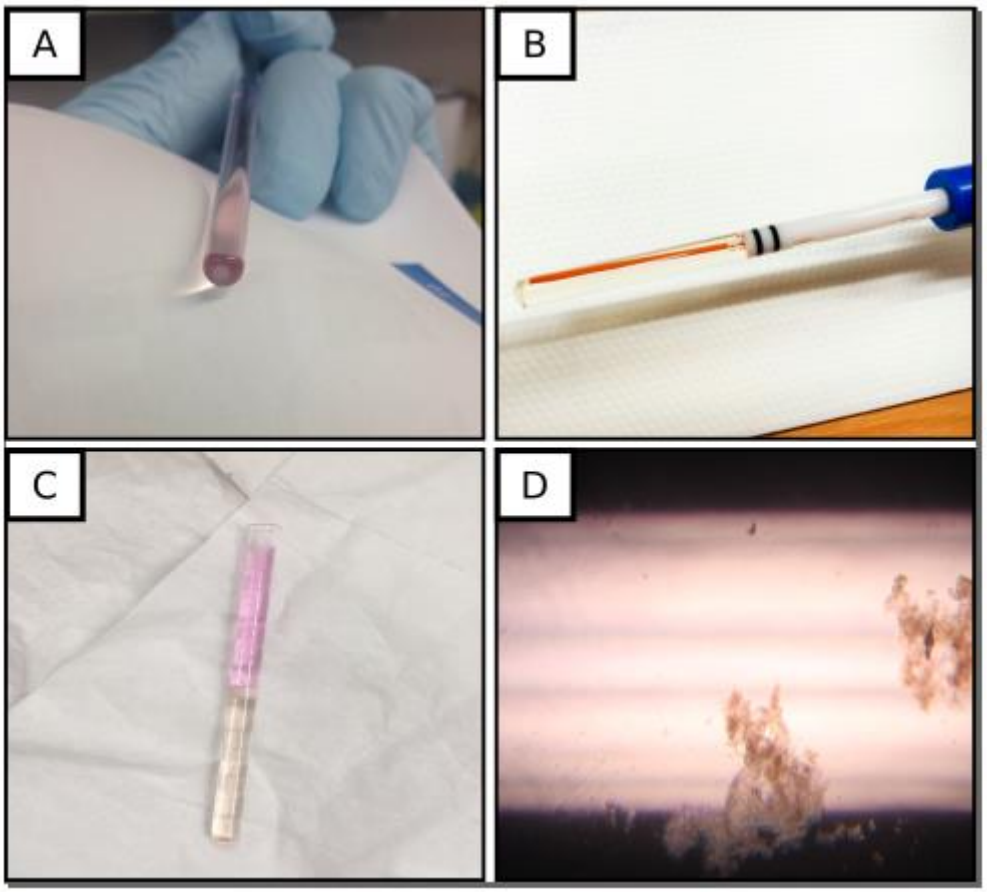

Figure 5.5 Problems with cells and shear stress due to fluid flow

(A): Cells pooled at the bottom of the NMR tube immediately after being aliquoted. (B): Precipitate formed from cell lysis inside capillary lines and NMR tube. (C): Filter frit blocked in the centre of the tube. While the medium contained in the upper part is cell free, the bottom is yellow due to cells acidifying the medium with metabolic by-products. (D): Close up of cell precipitate, likely to be DNA and chromatin. The shear forces from the flow were sufficient to cause cell clumping, death and eventual lysis.

Normal blood flow involves circulation of blood cells through arteries, veins and capillaries. Velocity of flow varies with pressure and site of circulation, with maximum turbulent flow in the aorta around 100 cm/s, while laminar flow in capillaries is around 1000 times slower [175]. While some cell types, particularly red blood cells, are quite robust and able to deform under the pressures of flow, others are more rigid and less elastic. However, the assumption that the various types of cell that constitute blood are able to withstand the forces associated with flow, as isolated cells, is incorrect. The immature myeloid precursors were likely vulnerable to flow due to the lack of other component cell types that would normally act as protective buffers [176].

Adherent cell types may be more amenable to direct exposure to flow. In many cellular systems the biomechanical force generated by blood flow, known as shear stress, stimulates cells to change morphology, activating cells to initiate particular functions and even induce stem cells to undergo differentiation [177,178]. While investigating changes associated with flow could be a useful application of the system it is not the aim of this project. Rather, the focus of this work was to study the metabolism of haematological cells. Consequently, the decision was made to concentrate on protecting cells from shear stress. The next steps involved investigation of methods to house the cells outside of the spectrometer bore, and circulate the medium into the NMR tube.

Mammalian cell lines are usually cultured at relatively low densities in comparison to bacteria and other eukaryotes, such as yeasts. For example, Kasumi-1 (around 1 pL in volume) are seeded at $3x10^5$ cells/ml and split around $1.2x10^6$ cells/ml, corresponding to a maximum intracellular volume of 0.3 µl in a sample size of 0.5 ml. Consequently it would not be possible to detect signals from molecules inside the cells and there is therefore no reason to keep them inside the detection region of the coil. Instead, uptake

of nutrients and efflux of metabolic by-products in the culture medium can be monitored for around thirty metabolites. While this would generate a metabolic footprint, rather than providing any intracellular data, it would allow cells to be kept in the same conditions as in a normal cell culture.

5.5.2. Cells outside the spectrometer

Maintaining cell cultures adjacent to the spectrometer facilitates non-invasive studies of live systems as environmental parameters can be controlled during NMR acquisitions. This is particularly important when monitoring metabolism as cells constantly adjust their nutrient usage in response to outside stimuli, and growth rates and survival are strongly affected by key variables of temperature, pH and oxygen levels [179,180,181]. Therefore a single static measurement can't replace the metabolic activity caused by constant turn-over of metabolites.

Model cell lines, such as immature myeloid cells, are not viable when exposed to flow in the context of a flow system. Consequently, it was necessary to engineer a system which can maintain cell cultures adjacent to the spectrometer. This was achieved using a cell culture incubator, Galaxy 48R (Eppendorf, UK), in which cell cultures were placed to maintain temperature, buffer pH and control oxygen concentration, as depicted in Figure 4.1.

In this set up the capillary flow lines enter the incubator via an access port on the rear side, which was sealed with a rubber cork and Parafilm™ in order to maintain a gas tight seal. A bioreactor or cell culture flask was attached to the capillary lines in order to perfuse medium through the bioreactor and the flow system. The incubator provides an optimal environment with a humidified atmosphere and controlled temperature. pH was

maintained at physiological levels, between pH 7.2 and pH 7.4 by using bicarbonate buffer system at concentrations of 5 to 10 % carbon dioxide.

5.6. Sterile Environment

A critical consideration in mammalian cell culture is a sterile environment. Cell cultures need to be kept free from microorganisms (bacteria, fungi, viruses) by using aseptic techniques and handling in laminar flow hoods. This avoids contamination by organisms that could otherwise influence behaviour of the living system under study or confound metabolism of the cell lines of interest which that of contaminants [182]. In order for real-time NMR analysis to maintain sterile conditions, it was necessary to develop a protocol to sterilise the InsightMR system and ensure that cells could be transported to and from the cell culture laboratory and the NMR facility without compromising the sterility of the sample.

5.6.1. Bioreactor

Cells are usually grown inside flasks, culture plates or dishes, depending on the number and type of cells. Plates and dishes are unsuitable for transport as their lids are not held firmly in place and fluid could escape during movement. Flasks have screw top lids and are more amenable to transport. They also offer the possibility to attach capillary flow lines through the lid. Initial experiments used this approach without success, as the flow lines seemed to damage cells. There was no simple way to fit filters to keep the cells inside the flask, and ultimately the flasks are limited due to the set sizes. Instead, a bioreactor was designed to transport and maintain the cells. While it is possible to buy prefabricated bioreactors the types available are not suitable for the constraints of the flow NMR experiment. Therefore, a bioreactor compatible with the flow system was

fashioned around the dimensions of a six-well plate. This set up is compatible with the use of commercially available Transwell inserts to protect the cells from flow.

The bioreactor design was tested by circulating medium through the system overnight. Cells were protected from shear stress by the membrane in one of two configurations:

1. Capillary lines are connected into the bioreactor under the membrane, as pictured in Figure 5.6. Cells are placed on top of the membrane, and metabolites can diffuse across the membrane into the flow system.

2. Cells sit on the plate surface and the capillary lines run into the top of the Transwell insert, above the membrane.

The design makes use of a gas permeable membrane on top of the bioreactor to allow gas exchange for oxygenation and buffering. In both cases the cells remained viable after 12 hour exposure to flow in the bioreactor.

The only difference between the two configurations is the mixing of the fluid either inside or underneath the Transwell insert. When the lines enter into the top of the insert the fluid underneath is not exposed to flow and consequently not well mixed.

By resting the insert directly above the flow lines the motion of the fluid encourages diffusion through the membrane, as anything moving through will be pulled out of the bioreactor into the flow lines.

This mixing and diffusion was tested by flushing the system with 1 mM TMSP (10 % D_2O), allowing the flow to equilibrate for around 20 minutes, followed by injection of a small aliquot of metabolite into the bioreactor. The signal intensity of the relevant metabolite was recorded as a function of time. When no membrane was used the

maximum metabolite signals were detected in the first spectrum after addition, therefore taking only 2 to 3 minutes to reach maximum intensity. When the Transwell insert was in place there was a lag time between injection of the metabolite and appearance of maximum intensity caused by diffusion through the membrane. It took around 20 minutes for the signal intensity to plateau, indicating that the aliquot had fully mixed with the total system volume. In each case we observed a slight kink in the signal intensity curve, as the initial bolus of metabolite entered the NMR tube before being fully diluted by the system volume.

In collaboration with Dr Lauren E. J. Thomas-Seale and Joseph Crolla, at the Department of Mechanical Engineering, a prototype bioreactor was produced using a design that is optimised to transfer samples between labs.

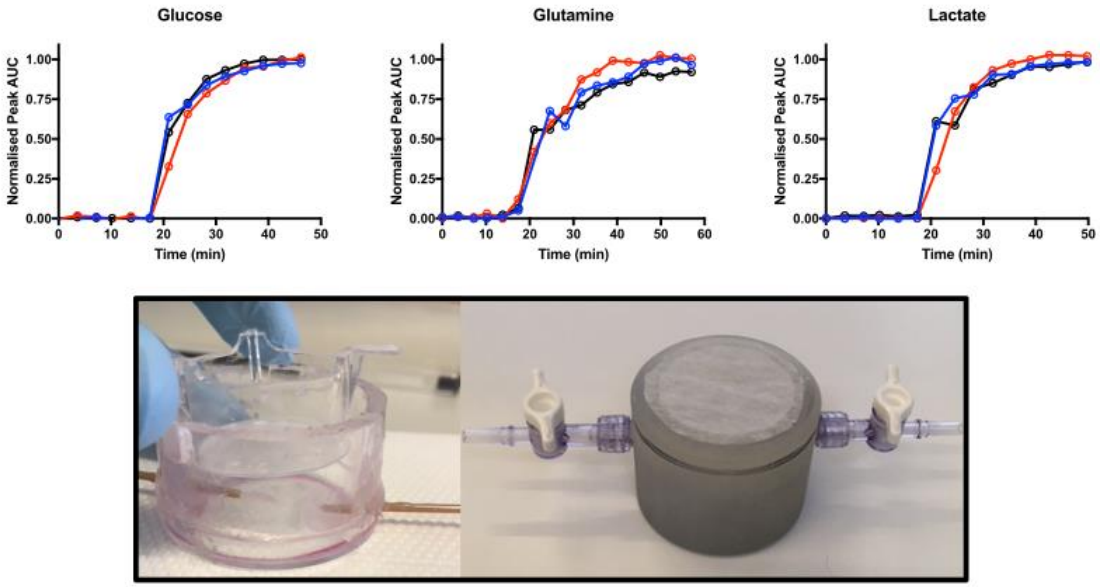

Figure 5.6 Bioreactor prototypes and Transwell membrane diffusion kinetics.

Transwell membrane diffusion kinetics (n = 3) for example metabolites. Plots show metabolite peak area (AUC) normalised to the TMSP standard for over time. The flow system was equilibrated for 20 minutes (i.e. from t = 0 to t = 20 minutes), following which a bolus of metabolite was injected (at t = 20 minutes). All tested metabolites reach a maximum peak intensity 20 minutes after injection (t = 40 minutes). While this is not fast enough to monitor reactions on a short time scale, it is adequate for the purposes of monitoring real time metabolism over many hours. Photo: Initial bioreactor design using cell culture plate with PEEK flow lines entering the bioreactor underneath the Transwell membrane. Prototype fabricated by Department of Mechanical Engineering. A gas permeable membrane covers the top of the bioreactor to allow oxygen and carbon dioxide gas exchange.

5.6.2. Sterile Conditions: Cleaning and Disinfection

A variety of approaches to decontaminate the flow system were considered and tested. The aim was to achieve a sterile environment inside the capillary lines and NMR tube, so that samples taken from the tissue culture laboratory would remain free from microorganisms. This was to ensure that cell behaviour would not be influenced by any contamination and that results would not be confounded by any non-mammalian metabolism. It was also necessary to clean the system after use, to avoid any carryover of material from one experiment to another, and to ensure that no hazardous biological waste remained.

Antimicrobial substances can be used to disinfect surfaces, meaning neutralising or removing most microorganisms, often with the exception of bacterial spores. This method is distinct from sterilisation, the process of destroying all viable life and its germinative elements. For the purpose of the flow system it would be sufficient to reduce any microorganisms to low numbers, i.e. undetectable levels. This could be confirmed by examining components under the microscope and keeping aliquots of medium to look for any subsequent growth.

When selecting methods for decontamination various factors have to be considered, including; spectrum of organisms to be inactivated, corrosive properties of substances used, and contact times required for efficacy.

Three approaches were considered for the flow system:

1. Autoclave. The components of InsightMR are made from PEEK, polytetrafluoroethylene (PTFE) and glass. All of which could be suitable for sterilisation under the heat and pressure of the autoclave.

2. Chemical disinfection. A range of antimicrobial fluids are compatible with the flow system. These could be pumped in and directly out, or left to soak over time.

3. Heat sterilisation. The flow unit has temperature controlled transfer lines, connected to a circulating pump, capable of heating the sheath fluid to temperatures sufficient to kill microorganisms.

Two of the three options were tested, as the autoclaving was not a practicable choice, since the flow unit would have to be disconnected from the sheath lines and transported to a separate building. While this process would not necessarily compromise the equipment and its cleanliness post-autoclave, it would be disruptive to routine work. Chemical disinfection was therefore considered as the next best option.

Three types of chemical disinfectant were tested; sodium azide, Distel and alcohol.

Biocides, such as sodium azide, are routinely used in NMR buffers to prevent microbial growth. Any acutely toxic compound presents a potential hazard to users via dermal and oral exposure. Azide also poses a risk through formation of explosive metal compounds when in contact with lead/copper surfaces, often when entering waste streams. Sodium azide (NaN_3) is unfortunately not easily NMR visible, as ^{14}N is very insensitive. It would therefore be difficult to know whether purged had removed all azide from the system before continuing with cell based experiments. This would make it difficult to assess the point at which the flow system could be used after decontamination. The azide ion binds Fe^{3+} in mitochondrial cytochrome oxidase, disrupting oxidative phosphorylation, and any carry over could therefore kill any eukaryotic cells [183,184].

The effectiveness of the azide solution was tested when there were visible levels of contamination (i.e. cloudy medium due to microorganism growth) in the flow lines and

NMR tube. After flushing the system with a solution of NaN_3 (2 %) and leaving overnight, a solution of RMPI medium was circulated around the equipment. This medium also turned cloudy, suggesting that exposure to NaN_3 was not sufficient to remove the contamination. Due to the lack of effectiveness, and associated risks of azides, this method of disinfection was not pursued any further.

Distel, a halogenated tertiary amine compound, is effective against a range of bacteria, fungi and viruses. It is commonly used in tissue culture laboratories to clean surfaces, removing biological material by destroying RNA and DNA [185]. Distel was tested on the flow system in a similar manner to azide; it was left circulating overnight (10 % solution, as recommend by the manufacturer). The system was flushed with sterile water to remove the Distel, followed by PBS, before reloading the system with RPMI medium. The RPMI was circulated for two hours while the incubator equilibrated to 37 °C and cells samples were prepared. Control cells were seeded in a plate and placed in the incubator. The bioreactor containing Kasumi-1 cells was seeded at the same density and connected to the flow unit and a spectrum acquired to check for any residual presence of Distel. The RPMI medium was left to circulate overnight and after 12 hours exposure the system was disconnected from the bioreactor and all samples taken back to the tissue culture laboratory for analysis. Staining with Trypan blue and comparing the cells from the bioreactor and plate, it was clear that cells inside the bioreactor had died, whereas those from the plate were alive and close to confluence, as pictured in Figure 5.7, panel B.

An aliquot of medium was taken from the bioreactor for NMR analysis. Residual Distel appeared in spectrum as a doublet at 1.18 ppm (See Figure 5.7, panel A). Although the flow unit had been flushed with several volumes of water, PBS and RPMI it still appeared to have a small amount of Distel still present, sufficient to kill the Kasumi-1 cells during such a long exposure time. The experiment was repeated, with a further

flushing of the system. However, the Distel resonance was present at the end of each overnight exposure. This suggested that it could not be flushed from the system, perhaps due to adsorption onto the capillaries or connections in the flow system. The long circulation of fluid provided sufficient time for it to desorb and enter the fluid flow.

Alcohol is used to sterilise surfaces and instruments for cell culture. The biocidal mechanism is thought to be due to denaturing proteins thereby destroying enzymes and structural molecules required for cell viability. It is generally used at concentrations between 50 to 80 % in water, in order to aid penetration into cells. At higher concentrations cell wall and membranes may coagulate on exposure to alcohol, forming a protective layer [[186]]. As an endogenous metabolite ethanol is often present in metabolic samples, so another solvent was chosen to disinfect the flow system. It has been noted that the efficacy of alcohols as biocides decreases with alkyl chain length [[187]]. For this reason two alcohols (methanol and isopropanol), and an alternative solvent (acetonitrile) were tested.

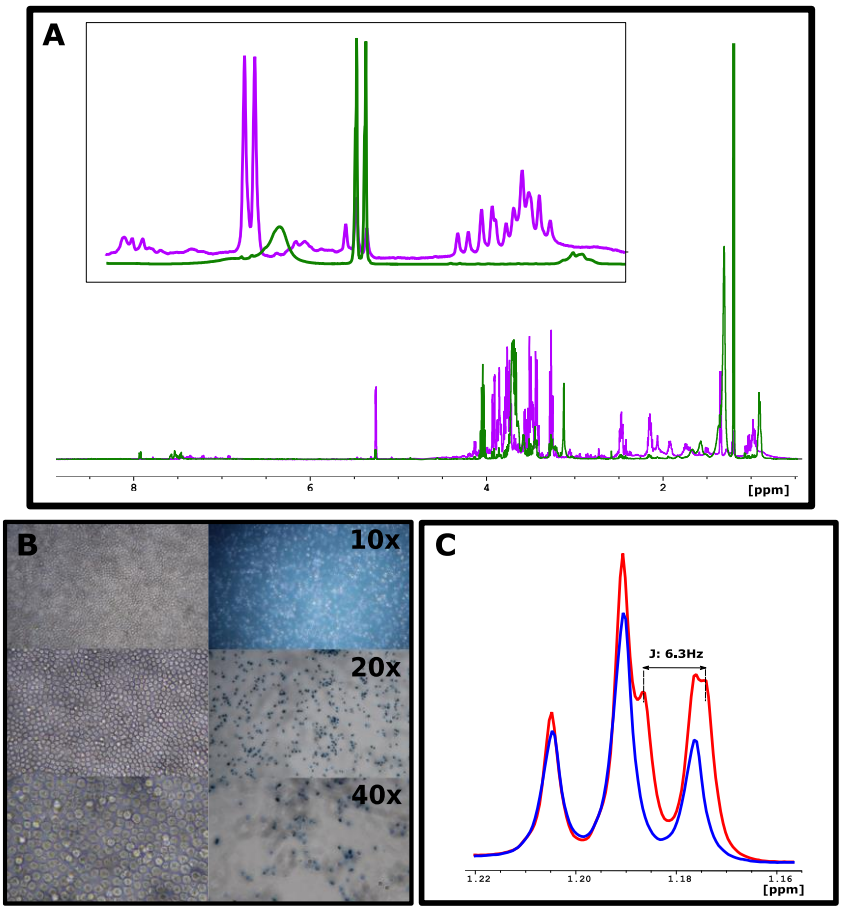

Figure 5.7 Disinfection of InsightMR flow system with Distel

Panel A: Spectrum of RPMI medium (purple) and Distel (green). The two most intense resonances are in the aliphatic region between 1 ppm and 2 ppm. Inset: zoom of most intense peak, with Distel spectrum scaled down to show overlap with ethanol triplet at 1.18 ppm . Panel B: Cells cultured in a sterile plate compared to cells maintained in the bioreactor after exposure to the flow system following disinfection with 10 % Distel. Trypan blue stain shows that most cells have taken up the dye and therefore have compromised membranes and are likely dead, or dying. Panel C: Comparison of two aliquots from the flow system. RPMI after 2 hour equilibration (blue) and RMPI after 12 hour overnight circulation (red). The doublet characteristic of Distel is present after the 12 hour circulation time.

Methanol has the advantage of being easily identifiable using the methyl proton resonance, a singlet at 3.35 ppm in an area of the medium spectrum with few other signals. As with the previous tests RPMI was flushed out of the system with water, and a solution of 70 % methanol was pumped in and allowed to circulate in the closed loop configuration overnight. The flow unit was then flushed with sterile water, followed by PBS, and set up for an experiment with cells. RPMI was allowed to equilibrate to temperature while flowing around the system. During this time it became clear that there was still a trace amount of methanol in the system. Over the duration of the 12 hour experiment the methanol peak increased in size, in a similar manner to the Distel peak previously.

This result seemed to suggest a hidden reservoir of solvent inside the system, either due to adsorption to surfaces or some artefact of the internal connections inside the system. The experiment was repeated with isopropanol and acetonitrile, in both cases the result was the same. After flushing the system with sterile water, followed by PBS, a solvent peak would reappear after several hours of circulation.

The two capillary lines are connected into the tube holder by two Fine Unified Screw Thread (UNF) fittings, shown in Figure 5.8. They enter and descend into the tube holder through a Y-shaped void before reaching the NMR tube. It is possible that fluid could become trapped in this area and gradually leach out over long circulation times.

The PTFE and PEEK tubing were both tested with the solvents to see if they adsorbed anything over long exposure times of 12 hours. Lines were filled with solvent and left overnight, then purged with water. Aliquots were taken and analysed for content by NMR. All tubing was free from solvent within minutes, and further soaking and flushing failed to recapitulate the phenomenon of reappearing solvent as seen with the flow unit.

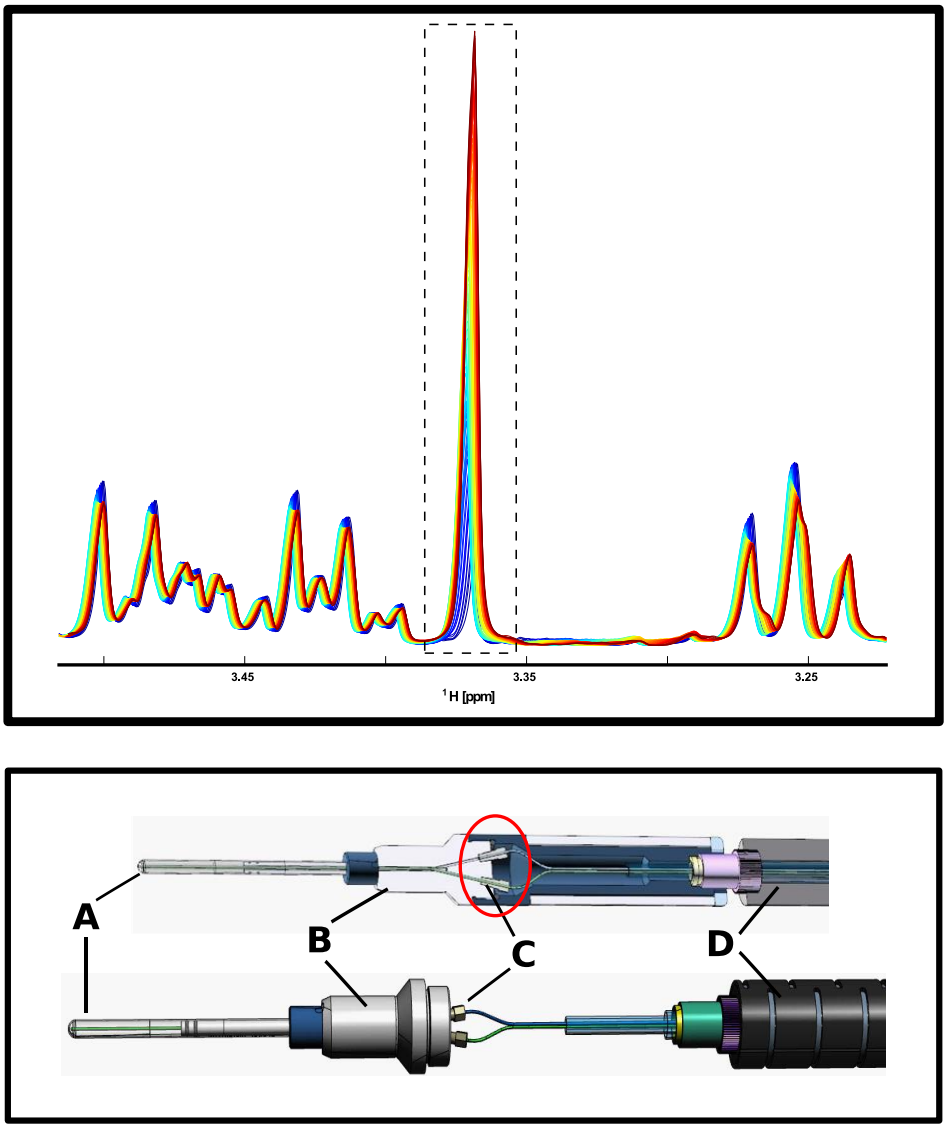

Figure 5.8 Solvent retention in NMR tube holder assembly.

Top Panel: methanol peak at 3.35 ppm increasing over time (initial spectrum blue, final spectrum red). Bottom panel: schematic of the InsightMR A: NMR tube, B: tube holder. C: UNF fitting, D: transfer sheath line. The area of potential stagnation, around the UNF fittings, where methanol may reside is highlighted.

Several attempts were made to modify the flow system in order to remove the potential reservoir inside the tube holder. This included trying to block off the area with resin and also forcing both capillary lines down into the NMR tube. No modifications were successful and the use of solvent for disinfection was abandoned.

Heat sterilisation was the final method tested. The flow system is made of thermally resistant materials capable of withstanding long durations of time at temperatures in excess of 100°C. The sheath fluid can be heated up and pumped around the capillary lines while the NMR tube can be placed into the heated waterbath. This approach was simple and effective; when the system was sterilised weekly no further contamination was seen.

The system was prepared for sterilisation by flushing out any residual material with several system volumes of isotonic PBS. This was to ensure that any cellular material residing in the lines would be flushed out, as osmotic shock could cause cells to burst and clump together, blocking the lines. To ensure that no debris was left inside the lines the NMR tube was disconnected and the capillary lines were blown through with compressed air. The NMR tube was reconnected and the system filled with water. The circulating pump was set to 95 °C and the NMR tube place in the water bath. The system was left to equilibrate for one hour, after which the water was pumped around the capillary lines for three further hours. This procedure was scheduled to coincide with the magnet nitrogen fill, so no spectrometer time was lost.

5.7. Data Acquisition

Monitoring live samples using 1D proton experiments requires a pulse sequence with solvent suppression. Three pulse sequences, using different water suppression approaches, were compared to establish which would be most suitable for real time acquisition. See Figure 5.9 for an overlay of example spectra.

While the 1D NOESY had a residual water peak in the spectrum, adjacent resonances were not adversely affected and the dynamic range of the digitiser was still sufficient to handle the large signal. The baseline was reasonably flat and peaks could be integrated. In contrast the excitation sculpting and WATERGATE sequences showed distortion of some resonances due to evolution of scalar coupling during delay periods.

In the complex spectra of real time samples, with a range of overlapping peaks from both known and unknown compounds, the integration of resonances is challenging. Any distortions to the peak shapes should be avoided

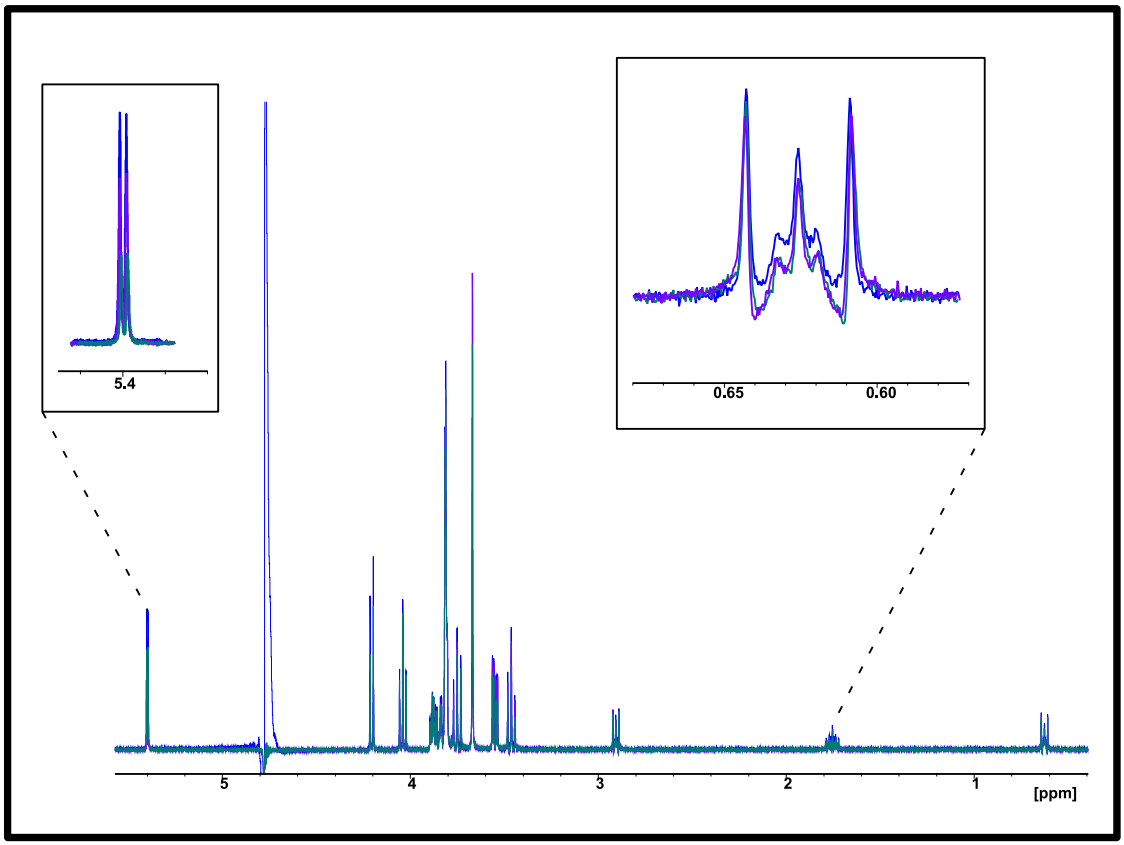

Figure 5.9 Comparison of water suppression using standard pulse sequences

Comparison of NOESY with presaturation (blue trace), excitation sculpting, and watergate pulse sequences applied to a sucrose standard. The zgesgp (purple trace) and w5 (green trace) pulse sequences completely remove the water resonance, whereas the NOESY-1D leaves a significant residual signal. The disadvantage of the zgesgp and w5 are the reduction in peak intensities around the water and peak distortion, as illustrated for the chemical shift standard DSS (inset). All sequences were from the Bruker library.

Live metabolic samples contain a mixture of large and small molecules, including; sugars, amino acids, lipids and proteins. All of these will contribute to the 1D ^{1}H NMR spectrum in some way. The small molecule metabolites will give distinct, sharp resonances, whereas the larger molecular species can contribute broad humps to the spectrum [188]. The serum component of medium, containing significant amounts of protein, is responsible for these interfering resonances (see top panel in Figure 5.10). The constituent proteins are crucial to maintain cell viability and cannot be completely replaced.

Overlaps of the broad signals can complicate integration as no signals can be baseline resolved, and in some cases protein resonances completely obscure smaller peaks. One method to reduce the macromolecular contribution from the spectrum is to use a Carr-Purcell-Meiboom-Gill (CPMG) pulse train of spin echoes. The CPMG sequence removes the protein signals using a relaxation filter, essentially exploiting the faster relaxation rates of large molecules [189]. The disadvantage of the CPMG sequence is that the total pulse train time influences the evolution of scalar coupling and can produce artefacts in peak shape. This distortion of multiplets from scalar coupled peaks is due to the development of antiphase magnetisation during the echo time.

Two parameters defining the relaxation filter in the CPMG are the T2 filter loop (L4) and echo time (d20). Together they define the total length of the pulse train as the sum of consecutive spin echoes. A set of spectra were acquired to compare the difference in protein contributions, and potential distortions in multiplets, as the spin echo time was increased (see bottom panel, Figure 5.10). In relation to a standard NOESY spectrum there is a considerable reduction in the broad baseline using the CPMG.

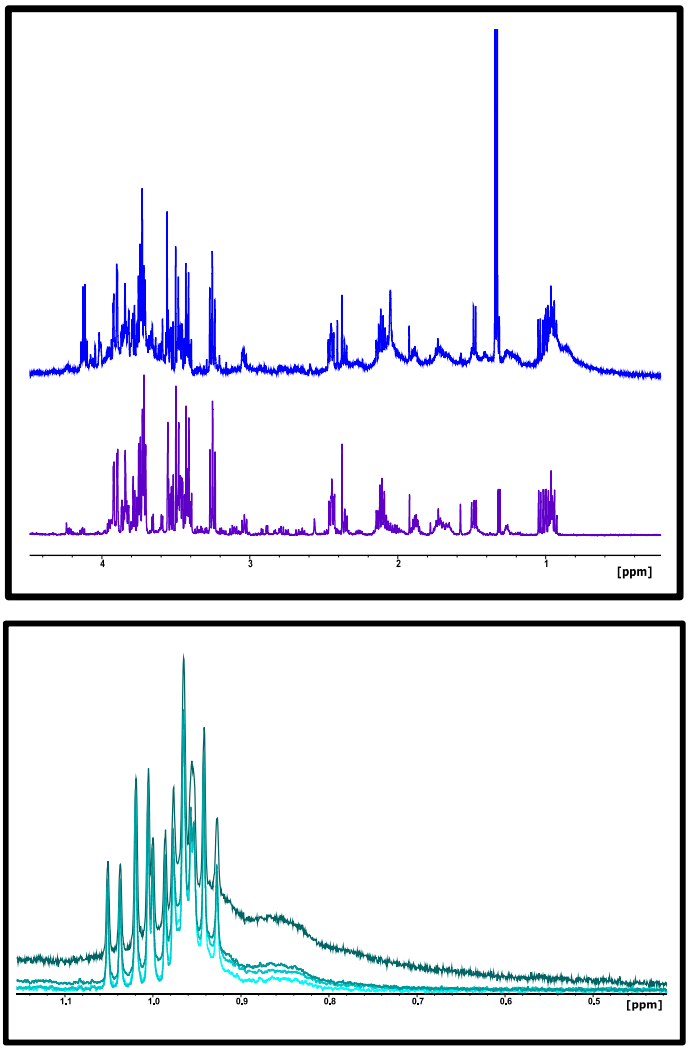

Figure 5.10 Protein contributions to media spectra

Top: Comparison of two medium samples with and without serum. Standard RPMI 1640 medium (purple trace) had a flat baseline, with sharp distinct peaks. The supplemented medium (blue trace) has broad baseline resonances due to the protein content in 10 % FBS. The metabolites present in the serum also contribute to the spectrum, for example lactate and alanine peak intensities are noticeably increased. Bottom: Expansion of region corresponding to the methyl resonances of the branched chain amino acids. NOSEY (noesygppr1d) (dark green trace) compared to CPMG acquisitions (cpmgpr1d, darker greens correspond to increasing T2 filter loop). Inset: basic CPMG pulse program.

A time course of twelve hours of data from a live cell sample was acquired using interleaved CPMG and NOESY spectra, with a data point acquired roughly every 45 minutes. Resonances corresponding to the branched chain amino acids, key carbon substrates and metabolic by-product were integrated. Results were compared to establish if the two pulse sequences yielded significantly different results.

While the metabolite intensity-time plots overlay, the CPMG data shows more variability for the metabolites whose resonances are affected by the macromolecular component of the medium (illustrated in Figure 5.11). This could be due to subtle distortion of peak shapes, or variations in peak intensity due to the length of spin echo. As there is no way to tailor the CPMG to all metabolites in the medium it was decided that NOESY was the better pulse sequence for acquisition.

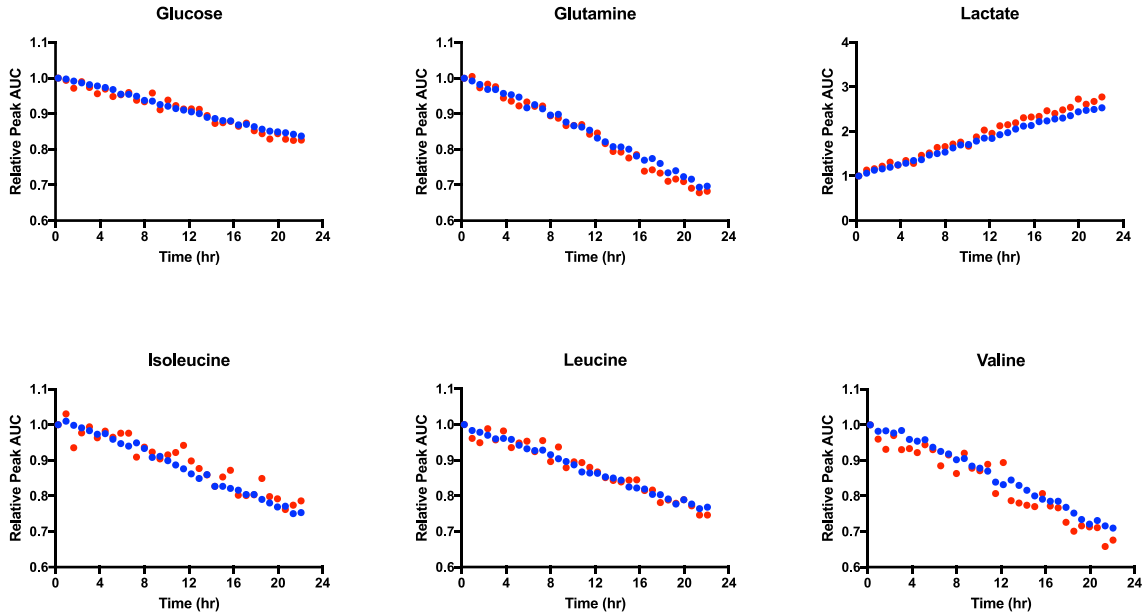

Figure 5.11 Metabolite intensity-time plots compared for CPMG and NOESY

Time course data was collected using live cells with interleaved CMPG (cpmgpr1d) and NOESY (noesygppr1d) acquisitions. Data quality was compared for metabolites across the ^{1}H ppm range, demonstrating that when samples have considerable protein content the baseline is distorted. Plots show metabolite peak areas (AUC) normalised to the TMSP standard over the time course of 24 hours. Representative metabolites show that the CPMG (red plot) is less consistent than the NOESY (blue plot), particularly when the resonances are situated in areas with the broad baseline humps due to protein (previously illustrated in Figure 5.10).

5.7.1. Calculating pH

Chemical shifts are dependent on the chemical environment and as such pH has an effect on resonances associated with acidic or basic groups which has the advantage of providing the spectroscopist with an inbuilt pH probe, as many compounds produce resonances that shift with changing pH.

RPMI 1640 medium contains the amino acid histidine at a concentration of 100 μM. This compound has an imidazole side chain containing two basic nitrogens (shown in Figure 5.12) which influences the chemical shifts of the adjacent protons. The relative chemical shifts of these protons can be used to construct a calibration curve to calculate pH of the sample [190]. Values were derived from data generated by K. Koczula using RPMI medium adjusted to a pH range of pH 3 to pH 9 [191].

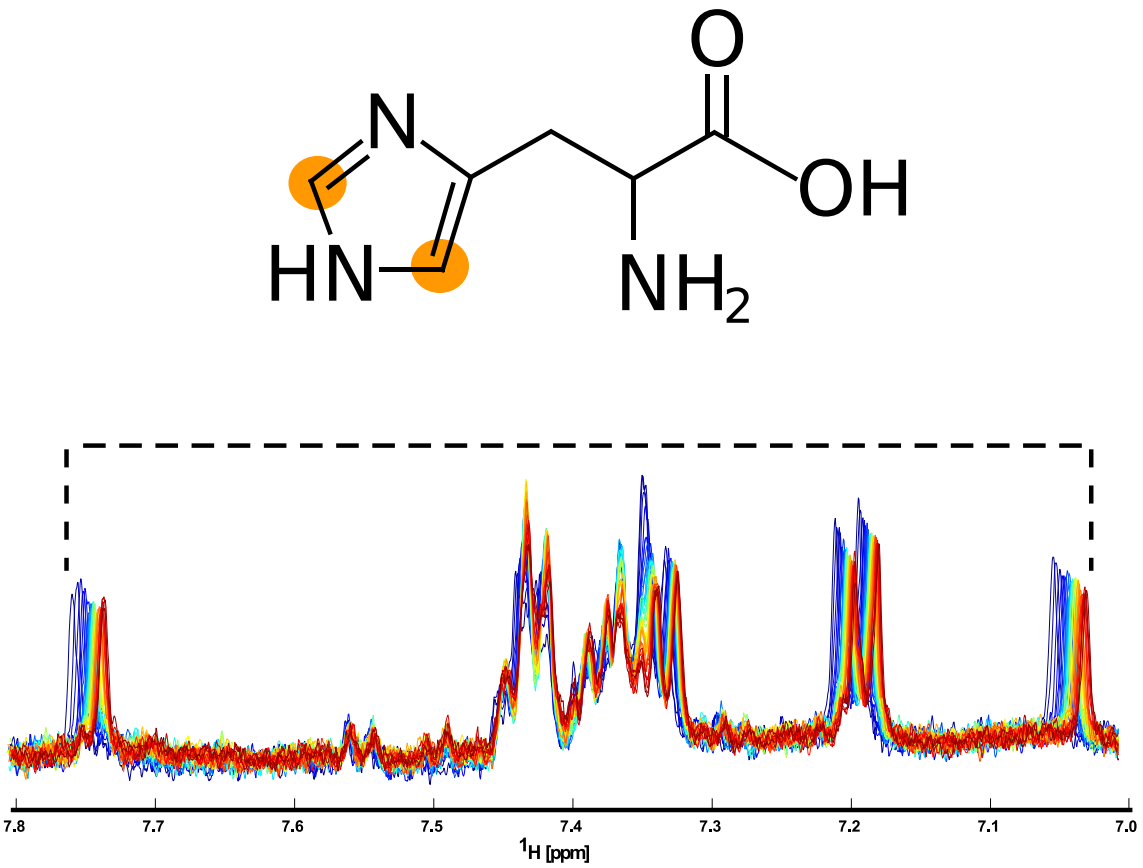

Figure 5.12 pH measurements using histidine proton resonances.

Imidazole resonances of histidine, highlighted in orange, can be used to calculate the pH of the sample. The relative shift of the two ring protons, shown as a dotted line here, can be calibrated to yield a pH measurement (see methods section 4.5.2 for calculation). The example spectrum shows an overlay of spectra acquired during a time course of 12 hour (initial spectrum is blue, final is red, with intermediate spectra transitioning though green, yellow and orange). The resonances shift over time as the culture medium becomes acidified due to metabolic by-products.

5.8. Workflow

The flow system is prepared by flushing the system lines with the same medium to be used in the experiment, in order to eliminate any carryover from previous experiments. The incubator is switched on and left to equilibrate to temperature while RPMI medium circulates in the 5 % CO_2 atmosphere and buffers to physiological pH.

Cells are then seeded into the bioreactor in the sterile environment of the tissue culture laboratory. The bioreactor is sealed with a gas permeable membrane, and then placed inside a thermally insulated box for transfer to the NMR facility. Once at the facility the bioreactor is placed inside the incubator and the InsightMR capillary flow lines are connected up. The culture medium is perfused around the system into and out of the NMR tube. The total volume of the system is comprised of the bioreactor, the NMR tube and the capillary flow lines, around 9 ml.

Over the duration of the 12 hour time course, data is acquired in the form of sequential 1D proton NOESY spectra. This data dense approach provides a continuous metabolic readout from the cell culture medium, a sampling strategy that may provide a better representation of the biological state than fewer, replicate measurements [192].

CHAPTER 6

MEASUREMENT OF REAL-TIME CELLULAR METABOLISM

6. Monitoring Cellular Metabolism with Flow NMR

This chapter describes the experiments performed to establish the metabolic changes that take place in cell culture medium under laboratory standard conditions. These results were used to guide the modifications to the flow system, and its associated components, together with the development of appropriate protocols for real-time flow NMR studies.

An example is made of the situation where metabolic changes are observed that do not correlate with the expected cell metabolism. This is used to illustrate the importance of validating the application of real-time flow NMR to mammalian cell metabolism, in order to be confident in the reliability and consistency of results.

6.1. Overview

The quantification of temporal changes in cell media, either with or without perturbation of cellular states, generates an overview of nutrient usage and overflow metabolism. Global changes include the consumption of carbon and nitrogen sources from the culture medium, such as glucose, glutamine and amino acids. Metabolic by-products are effluxed from cells, resulting in the accumulation of compounds in the medium, notably lactate and alanine in proliferative cells [193]. Concentrations of some species can fluctuate over time, as certain metabolites are effluxed then taken up again by cells later in a time course. This is a characteristic of co-cultured cells, where interactions between niche and malignant cells include exchange of metabolites, seen as efflux of excess carbon from one cell type subsequently taken up by adjacent stroma [194]. Meanwhile, some components of the medium will remain at a constant level, with no detectable variations in concentration over the duration of the experiment.

In order to interpret data correctly and attribute concentration changes to biological processes there should be confidence that the observed metabolic profiles are genuinely

a product of mammalian cell metabolism. When using the flow system this includes verifying that metabolic profiles are equivalent when cells are monitored outside the sterile cell culture laboratory compared to in the NMR facility. The work described in this chapter endeavoured to establish an understanding of what constitutes a normal metabolic footprint for cell lines cultured under standard conditions (exponential growth rate, 37 °C, pH 7.4, atmospheric O_2).

Two sets of experiments were set up in 75 cm^3 cell culture flasks to provide a basic overview of the major metabolic changes in the culture medium, with the following comparisons:

1. Cell-free media vs proliferative cell culture. This was to establish which changes in medium composition related to metabolic activity of cells, rather than thermal degradation of components, or other outside influences.

2. Various suspension cell cultures. These experiments generated a range of metabolic profiles to provide a scale of metabolic footprints in cancer cell lines. Further work was based on the differences observed compared to these initial profiles.

Cell culture flasks were maintained over 24 hours in the sterile environment of the tissue culture laboratory. Aliquots of cell medium were taken from cultures at different time points during the experiments and then analysed by ^1H NMR. Datasets were used for later comparisons with metabolic data generated during flow system development.

As described in Chapter 5 the development of the flow system presented a variety of challenges with respect to contamination from chemical and microbial sources. This

chapter describes the metabolic changes in cell culture medium observed during development of the cleaning and sterilisation methods. Initial experiments served to identify changes in medium concentration due to microbial metabolism and leaching from chemical components.

6.2. Metabolic Changes During Cell Culture

6.2.1. Medium Composition

Culture medium is designed to support cell growth and viability, and is often tailored to meet the individual requirements of specific cell lines. Media are typically composed of a variety of nutrients, osmolytes, vitamins, hormones, proteins, salts and buffers. The origin and concentrations of each substituent will depend on the biological application [195]. Commonly, chemically defined media are supplemented with fetal bovine serum (FBS), the cell-free liquid fraction of clotted blood, in order to provide a range of essential factors required for cell growth including protein carriers or chelators together with albumin, hormones, including insulin, and a range of cytokines.

Components of the medium degrade over time, a process that is slowed by storing media at 4 °C. Therefore, during real-time monitoring degradation of components could contribute to the metabolic footprint and mask changes in metabolite concentrations due to the presence of cellular activity. For example, the anapleurotic substrate glutamine is known to be thermally labile and breaks down non-enzymatically in aqueous media during storage [196]. Such degradation could also occur over the time scale of experiments using the flow system.

In order to understand the stability of the medium, and generate a comparative profile of live-cell related metabolism, a series of medium aliquots were taken from flasks maintained in a tissue culture environment. Four sets of flasks were set up, in triplicate, containing the following:

1. RPMI 1640 medium, the base formulation used for many cancer cell lines.
2. RPMI 1640 supplemented with 10% FBS.

3. Spent medium, the product of a previous culture where cells had been removed by centrifugation after a suitable culture period with supplemented RPMI 1640.
4. A suspension culture of JJN3 cells in supplemented RPMI 1640. JJN3 are a multiple myeloma line, established from the bone marrow of a patient with leukaemia [197].

A small panel of metabolites were chosen to represent the expected changes in cultured cancer cell lines, based on their metabolic importance and distinct ^{1}H NMR resonance. These compounds also covered a substantial spectral window, with proton resonances from 0.9 ppm to 8.5 ppm.

Primary carbon sources, glucose and glutamine, were chosen as readouts for glycolytic and anapleurotic TCA metabolism, characteristic of the Warburg effect. The proteogenic branched chain amino acids (isoleucine, leucine and valine) where chosen due to their association with myeloid cancer progression [198]. Key overflow metabolites (alanine, lactate, pyruvate and formate) were selected to reflect the metabolic fate of the main carbon sources. While these metabolites are not present in the base RPMI formulation they will be present in the FBS and therefore seen when medium is supplemented, or has previously supported cells.

The first experimental set compared the cell-free media with and without supplementation, and demonstrated consistent concentrations for all metabolites over time, as shown in Figure 6.1. We observed no appreciable degradation of glutamine over the 24 hour period of culture, indicating that the instability of this compound requires longer periods of time.

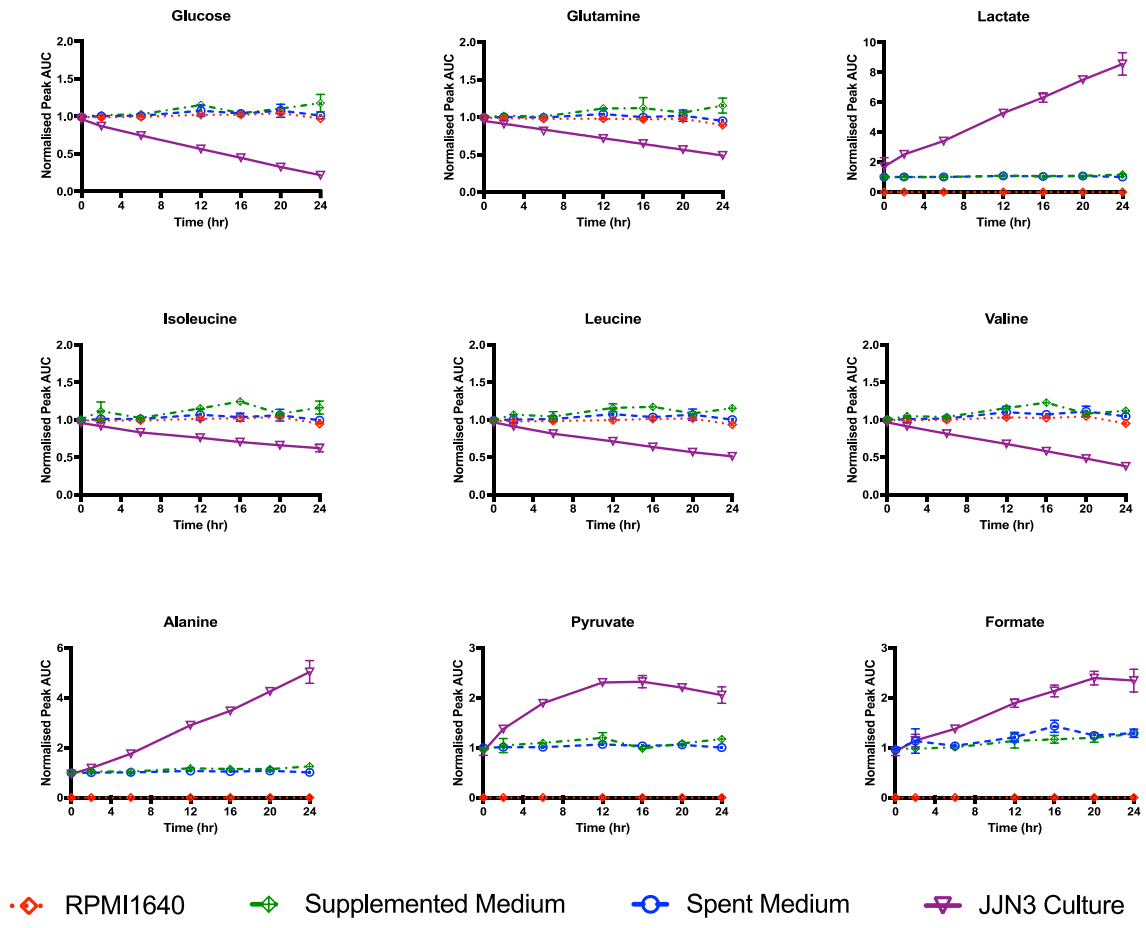

Figure 6.1 Metabolic changes in cell culture medium over 24 hours.

Plots show peak area (AUC) relative to TMSP standard over the 24 hours of cell culture. All peak areas are normalised to one at the start of the experiment, regardless of the absolute concentration. During the experiment cell-free media (red, green and blue) show no significant changes over time. RPMI 1640 is the basic medium formulation that does not contain lactate, alanine, pyruvate or formate. These spectra therefore did not contain the corresponding resonances, and the peak area was consequently zero. The supplemented and spent medium contains FBS and therefore has the additional small molecule metabolites. The culture containing live JJN3 cells (purple) shows consumption of main fuel substrates glucose, glutamine and branched chain amino acids. Lactate, alanine, pyruvate and formate are all effluxed and therefore concentrations gradually build up in the culture medium.

The spent medium could contain metabolic enzymes due to apoptotic release of cytoplasmic contents, a phenomena often used to assess viability [199]. The comparison of medium formulations between fresh and spent medium showed no significant changes, indicating that there was no significant release of enzymes into the medium that could confound results during the 24 hour experiment.

The culture containing JJN3 cells showed a variety of changes in composition compared to the cell-free media. The cells consumed nutrients and effluxed metabolic by-products, as expected. Glucose and branched chain amino acids were used up, while overflow of lactate, alanine and formate was observed. Pyruvate concentration increased over the first 12 hours of culture, after which it seemed to reach a plateau then decreased slightly in the latter 12 hours indicating that pyruvate was reabsorbed and used by JJN3 cells as a substrate. Pyruvate is known to protect cells against reactive oxygen species and consumption in cell culture medium has been shown to be linked to peroxide concentrations [200,201]. Cells are also known to uptake pyruvate, via moncarboxylate transporters (MCTs), and convert it to lactate by LDH [202].

6.2.2. Metabolic Footprints

A panel of metabolic changes, established under standard cell culture conditions, provides a point of reference for data collected using the flow unit. Any major deviations from the data generated in the tissue culture laboratory will point to potential contamination or perturbation of cell metabolism due to the use of the flow unit.

Three blood cancer cell lines were selected for the following experiments:

1. HL-60. A promyelocytic cell line established from a patient with chronic myeloid leukaemia in blast crisis [203]. It contains an amplified c-myc proto-oncogene [204].
2. Kasumi-1. A cell line established from the blast cells of a patient with relapsed t(8:21) acute myeloid leukaemia [205].
3. JJN3. A subclone of the JJN-1 line, established from the bone marrow of a patient with multiple myeloma leukaemia [206].

These cell lines are highly proliferative and can be seeded at low densities and grown up to generate cultures containing millions of cells per millilitre. Growth curves were generated to ensure that all three cell types could be maintained at similar densities for comparison of metabolic footprints, shown in Figure 6.2. This procedure ensured that metabolic changes could be detected in the medium, and cells would not rapidly exhaust the medium in too shorter time. Recommended cell densities for each culture are in the range of $1x10^5$ to $30x10^5$ per millilitre [207].

The myeloma cell line, JJN3, is more proliferative than HL-60 and Kasumi-1. The rate of proliferation of all three cell lines increases once cells reach a density of $30x10^4$/ml.

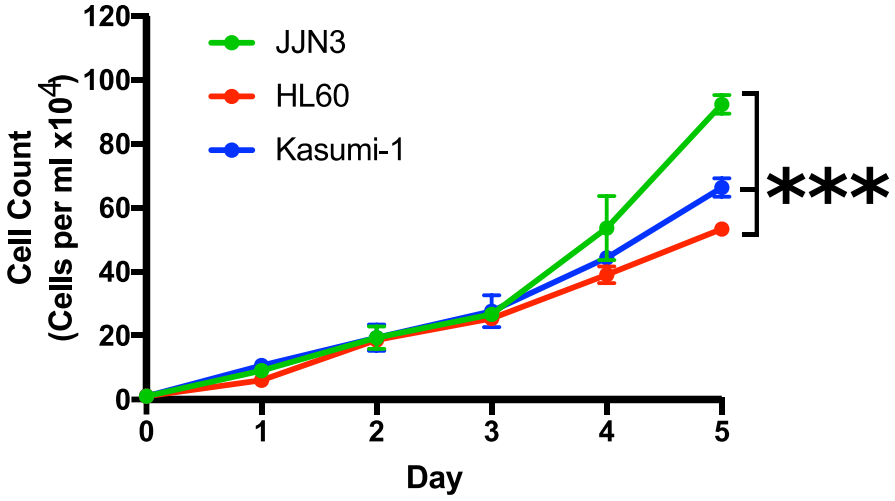

Figure 6.2 Growth rates of three cancer cell lines.

Three cell lines were grown over five days from a very low seed density. Medium was changed every day along with the cell count. Growth rates, and optimal culture densities, of the three cells lines were similar enough to use identical conditions for each cell line during metabolic experiments. The three cell lines were used to establish metabolic changes in cell culture medium during periods of 12 to 24 hours. At the end of a five day growth period cell numbers were significantly different for all three cell lines ($p < 0.001$).

For one experiment, three flasks were prepared for each cell line, seeding at a density of $5x10^5$ cells/ml. Aliquots of culture medium were taken over a 24 hour culture period. The same set of nine metabolites was used to build a metabolic footprint over time, as shown in Figure 6.3.

Comparison of data from each cell line produced a range of rates for the consumption and efflux of the main metabolic substrates and products. Each cell line demonstrated usage of nutrients such as glucose, glutamine, and amino acids. Effluxed metabolites included lactate, alanine, glutamate, pyruvate and formate.

As the most proliferative cell line, JJN3 cells showed a marked difference in the rate of glucose consumption and lactate production compared to Kasumi-1 and HL-60 cells, with growth rates roughly proportional to glucose usage and lactate production. Interestingly, all three cell lines used a similar amount of branched chain amino acids, such as leucine, valine and isoleucine.

Overflow metabolism was different for each cell line. While JJN3 produced several fold more alanine than the other cells lines, it produced less formate than both HL-60 and Kasumi-1 cells. HL-60 cells used more glucose and produced more lactate than Kasumi-1, but it did not show any significant efflux of alanine or pyruvate.

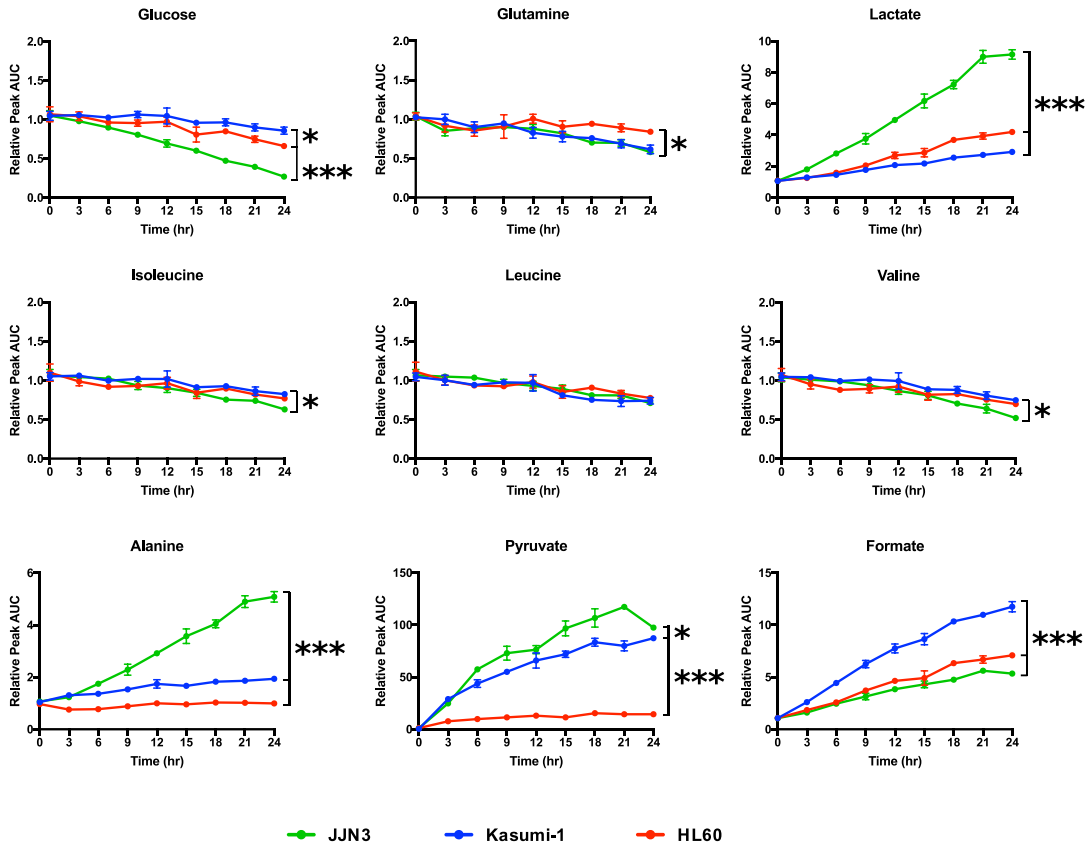

Figure 6.3 Metabolic features of proliferative suspension cell cultures

Plots show relative peak areas (AUC) normalised to the TMSP standard. All cell lines demonstrated detectable consumption of glucose, glutamine and branched chain amino acids. Overflow metabolism was different for each of the three cell lines. Efflux of lactate, alanine, pyruvate and formate varied significantly, with HL-60 cells producing very little alanine and formate. JJN3 produced a greater amount of lactate, alanine and formate than the other cell lines ($p < 0.001$). Together these metabolite changes provide a cell line specific reference profile to be replicated using the NMR flow system.

6.3. InsightMR: Sources of Contamination

Methods of analysis should not perturb the cell lines under investigation or introduce artefacts into the data. The flow unit should generate data comparable to standard cell culture conditions and observed differences in the metabolic footprint must come from the cell's metabolic processes. Unfortunately, during development of the flow system there were a variety of problems that resulted in datasets not reflecting the metabolic profiles generated under sterile conditions in the tissue culture laboratory.

Contamination from external sources can confound results. Three distinct sources were identified during the development and subsequent validation of the flow system:

1. Chemicals leaching from system components.
2. Microorganisms infecting cultures.
3. Residual material carrying over from previous analyses and cleaning procedures.

In order to ensure quality data is produced using the flow system, steps must be taken to confirm that observed metabolic changes are from cell activity not external factors. Care must be taken not to incorrectly attribute spectral changes to expected, or desired, metabolic processes.

6.3.1. Chemical Contamination

The flow system is composed of a variety of different materials. The NMR tube is glass, while most components and capillary lines and tubing connections are made from chemically inert PTFE and/or PEEK. Manufacturing processes can leave residue on new equipment, peristaltic force can degrade surfaces, while heat and exposure to chemicals

can damage surfaces. Therefore any component could contribute to contamination by chemical or physical degradation.

The first experiments with the flow system and live cells used the M6 pump, up until its failure, and subsequently all experiments were conducted with the peristaltic pump. During these acquisitions cell suspensions were pumped around the system, and as described in section 5.5, and underwent significant stress due to shear forces in the system. In the case of initial experiments using the M6 pump, the cells quickly died, and very little metabolic change was seen over the time course. Using the peristaltic pump cells survived slightly longer, but still died and formed a visible precipitate in the NMR tube. A signal at 1.92 ppm was detected. This peak was not present in medium from cells cultured in flasks, indicating that it could be related to perturbation by flow, or pumping mechanism. A singlet resonance at 1.92 ppm could correspond to acetate, a metabolite generated by central carbon pathways and effluxed from cells [208,209]. In order to clarify the source of this compound the experiment was repeated using cell-free RPMI medium. In this case the resonance at 1.92 ppm was still evident, suggesting that the source was not from cell metabolism, but likely related to the peristaltic pump tubing (shown in Figure 6.4).

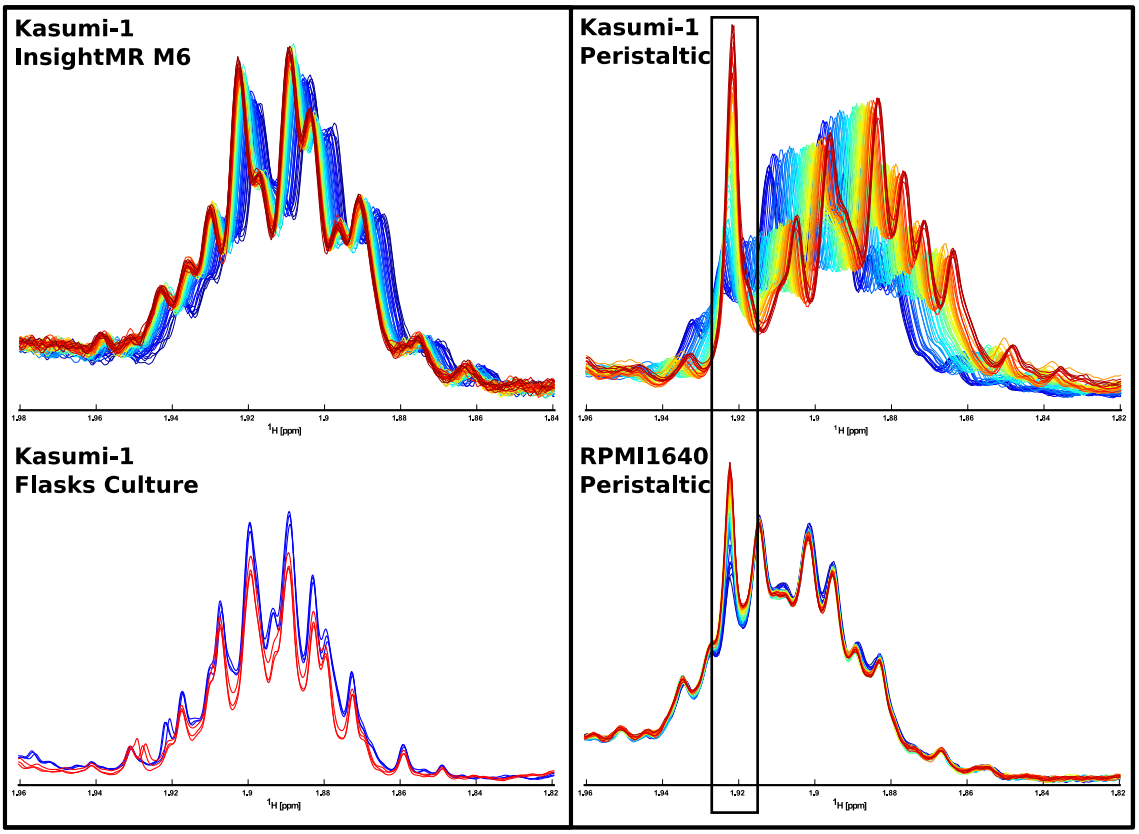

Figure 6.4 Real-time detection of a peristaltic tubing contaminant.

Comparison of data obtained using normal cell culture flask and the flow system with the M6 pump (top left) and the flow system with the peristaltic pump (right). Shear forces in the M6 pump may have accelerated cell death in comparison to the peristaltic pump and no significant metabolic changes were seen in these spectra. When the peristaltic pump was used a peak at 1.92 ppm increased over time, both with and without cells. In contrast aliquots of medium taken from a Kasumi-1 cell culture (bottom left) at 0 and 24 hours show no equivalent peak. This demonstrates that the contaminant was related to the use of the peristaltic pump. After the tubing was replaced the contaminant peak was no longer seen.

Moving forward, tubing compatible with the Masterflex peristaltic pump and InsightMR tubing connections were purchased based on chemical stability and robustness. The TygonE and Masterflex PharMed were selected for testing, based on advertised biocompatibility and resistance to solvents. Tubing sections were cut to size and washed with distilled water prior to use in order to remove any residues from manufacturing that could interfere with analysis. While degradation of the tubing material is expected over time, as peristalsis eventually removes the elasticity and reduces flow rate, this should not occur during the relatively short time frames of the real-time flow NMR experiments (12 to 24 hours).

Experiments conducted with the Tygon tubing all had the same resonance at 1.92 ppm, whereas once the tubing was changed to MasterFlex PharMed the contaminant was no longer seen. Previous studies with Tygon have questioned its biocompatibility, with one report also containing a small resonance at 1.9 ppm [^{210}]. PharMed tubing was used for further experiments, with the expectation that any resonance appearing at 1.9 ppm could be attributed to cell metabolism.

Other sources of chemical contamination include the sheath water used to control the temperature in the transfer lines between the reaction vessel and the spectrometer bore. This water is circulated around the outside of the transfer capillaries and could ingress into the system via the UNF fittings in the NMR tube holder (see Figure 6.5). UNF fittings, each with a PEEK retainer, hold the capillary lines in place as they enter and descend into the tube holder. If these fittings are not tight enough the sheath water can ingress through any gap and enter the NMR tube. The use of these components is complicated by an opposing thread, making it very easy to inadvertently unscrew during changing of the capillary lines.

Ethylene glycol is used as an additive in the waterbath, to protect against corrosion of the circulator pump and act as a biocide. If any of the fluid from the sheath lines enters the flow system the ethylene resonance will be visible at 3.7 ppm. This was indeed the case when the UNF fittings were initially reused and ingress of sheath fluid led to a detectable resonance at the end of the time course (shown in Figure 5.9). The ethylene glycol peak appeared and rapidly increased over time to become the most dominant peak in the spectrum. Exposure to ethylene glycol at these concentrations is likely to affect cells as its biocidal activity is linked to osmotic effects and membrane disruption [[211]]. Any experimental data collected during glycol ingress should therefore be discarded.

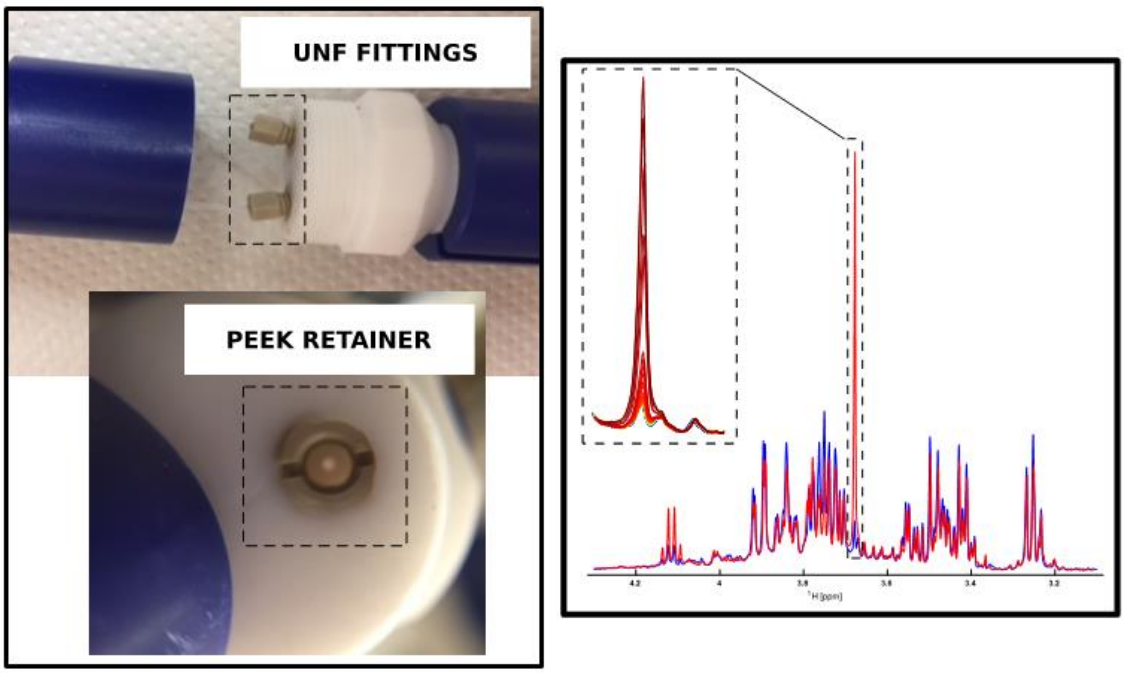

Figure 6.5 Ingress of sheath water into capillary flow lines

Left: Capillary flow lines connect to the NMR tube via the UNF fittings, which screw into PEEK retainers in the NMR tube holder. These components are all threaded. The UNF fittings screw into the retainer in the opposite sense to that of the retainer into the tube holder. Consequently, it is relatively easy to unscrew the retainer while connecting the UNF fittings. Right: Ethylene glycol resonance at 3.7 ppm is indicative of water ingress due to the compromised internal connections.

6.3.2. Microbial Contamination

Infection of cell cultures, with bacteria or fungi, is very rare under the strict conditions of the tissue culture laboratory. Routine cell culture work is undertaken in a sterile environment and a laminar flow hood is used to for all procedures, ensuring that only filtered, sterile air comes into contact with cultures. Aseptic technique is used to protect against contamination while materials are autoclaved, and surfaces are disinfected with 70 % ethanol as a further defence against microbial growth.

Cultured cells are often observed under an optical microscope in order to monitor cellular growth and viability, and to follow any changes in cell morphology over time. During each one of these procedures contamination by microorganisms would be seen as small cells, distinct from the mammalian cell line. In contrast, the flow system cannot be directly inspected for microbial contamination. Instead aliquots of medium have to be taken from the flow lines and transported to the tissue culture laboratory for analysis, with an associated lag time in understanding the status of the system.

6.3.3. Microbial metabolism

Initial experiments, during development of the flow system sterilisation protocol described in the previous chapter, were plagued by problems with microbial contamination. This provided an opportunity to identify which metabolic signatures are associated with bacteria and how they can be recognised when combined with mammalian cells under study.

After each attempt to sterilise the system, either by chemical means or application of heat, sterile cell-free medium was introduced via the capillary lines and circulated overnight. Testing for residual contamination was achieved by:

1. Monitoring the metabolic footprint of the medium during the overnight circulation (approx.12 hours). Sterile RPMI medium should not show any variation in metabolite concentrations during this time. Any significant changes can be attributed to microorganisms still alive in the system.

2. Taking an aliquot of medium from the flow system after the overnight circulation. Any contamination can be seen under the microscope, or in cases of established colonies, by direct visual inspection. In some cases there may be no metabolic changes detectable in the medium, even though microorganisms can be seen under the microscope. In this case the sterilisation procedure should be repeated until no further contamination can be observed.

3. If no contamination is evident the medium aliquot is stored at room temperature for several days. Any low level contamination should bloom within 24 to 48 hours and be visible under the microscope. Any data acquired during this time should be discarded as metabolic profiles may be influenced by an equivalent growth of microorganism in the flow unit.

After a variety of unsuccessful attempts to disinfect the flow unit with biocides and solvents, as described in section 5.6.2, several analytical runs demonstrated metabolic signatures contrary to those seen with mammalian cells in culture. This phenomenon was often twinned with the production of cloudy medium from the flow lines, indicating that the microorganisms were proliferating. Bacterial contamination was confirmed using optical microscopy, where small cells could be seen moving in the medium. In order to

verify that these cells were indeed alive and multiplying an aliquot of infected medium was taken from the flow system and cultured over several days. The aliquot was diluted with fresh, sterile RPMI and split into three replicates. Growth rate of the bacteria was assessed using optical density measurements, where the rate of proliferation was correlated to the OD_{600} (shown in Figure 6.6). The linear growth rate indicates that the bacteria are multiplying, but still in the lag phase and adapting to conditions outside the flow unit.

There are a limited number of ways the flow system can become contaminated. The two capillary lines are only transiently open to the air during connection and disconnection of the bioreactor. This may be enough time for micro-organisms, in the air or from contact with the user, to enter the system. Colonies can grow to the point they are dense enough to be visible and identified. At this point it would be likely that they would be sufficient in number to influence the observed metabolic profile, and therefore invalidate any data acquired. As such it is prudent to inspect medium at the end of a time course for any signs of non-mammalian cells. It can take time for microorganism populations to bloom and for the resulting contamination to be visible. Consequently, an aliquot of medium is retained after all experiments and kept for at least 48 hours after data acquisition. If no sign of micro organismal growth is seen post acquisition metabolic data can be considered reliable.

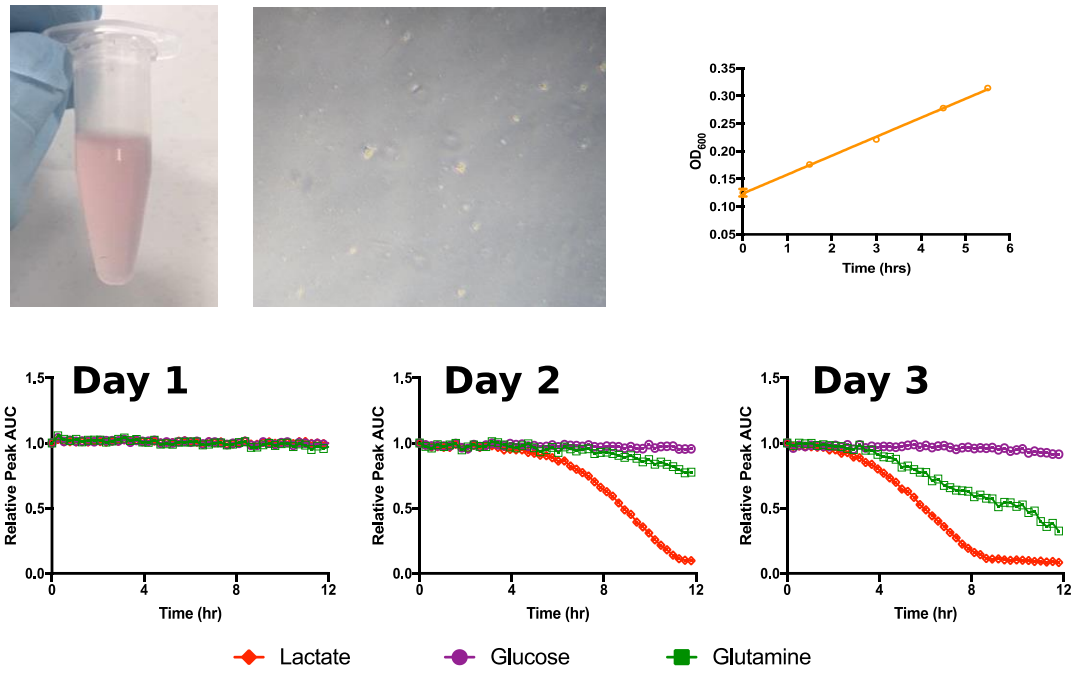

Figure 6.6 Bacterial Contamination of NMR Flow System

Top Panel: Aliquot of cloudy supplemented medium after circulation around flow system and magnification (20X), showing the small clusters of cells present. These motile cells are much smaller than any cultured mammalian cell used in this project. Bottom panel: Comparison of analytical runs over three consecutive days. A fresh aliquot of cell-free RPMI medium, supplemented with 10 % FSC, was circulated each night. (Left) No changes in main metabolites over time. At this point the system does not show any macroscopic sign of contamination, even though it still contains a small bacterial population. (Middle) Lactate consumption starts around the half-way point, while glutamine concentrations decrease nearer the end of the time course. Glucose concentration is stable. (Right) Consumption of all three metabolites occurs. Initially lactate and glutamine, with glucose concentrations starting to show a decrease in the final hours after exhaustion of lactate. These differing profiles reflect the blooming bacterial population.

6.4. Real-Time Flow NMR: Observing Metabolic Profiles

The myeloma cell line JJN3 was used to evaluate metabolic profiles generated using the flow system during development of the sterilisation protocol. Data from cultures maintained in a sterile environment, summarised in Figures 6.1 and 6.3, should be reproducible using the flow system. Profiles for three main metabolites were used to assess the system, with the expectation that a 12 hour time course should show consumption of glucose and glutamine, and concomitant production of lactate.

Initial experiments showed some curious metabolic behaviour whereby glucose and glutamine were consumed and lactate fluctuated. This was due to the co-culture of JJN3 and bacteria, with the bacteria consuming the lactate produced by the proliferative JJN3 cells. While it is possible for some mammalian cell lines to use lactate as an alternative carbon source [212], it was not expected for the JJN3 as previous experiments demonstrated lactate build-up over 24 hours.

Reliable data were only obtained after heat sterilisation, consequently this procedure was used weekly for the rest of the project.

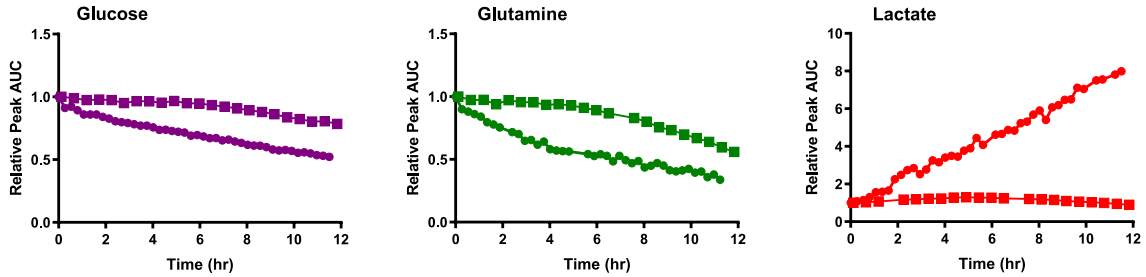

Figure 6.7 Establishing Metabolic Profiles of Mammalian Cells

Comparison of analytical runs before (squares) and after (circles) successful sterilisation. Plots show peak area (AUC) relative to the TMSP standard. Over the 12 hour time course glucose and glutamine were consumed. The unexpected profile for lactate without sterilisation was due to bacteria using the lactate produced by JJN3 cells. Without prior knowledge of expected metabolism, or investigation into the sterilisation of the flow system, this data would have been interpreted as JJN3 not showing overflow metabolism.

CHAPTER 7

APPLICATIONS OF REAL-TIME MONITORING USING FLOW NMR

7. Metabolic Signatures in Disease

This chapter explores the applications of the flow system in the context of monitoring cellular metabolism associated with disease. Initial experiments use a panel of cell lines to demonstrate that real-time NMR is capable of detecting different metabolic phenotypes. From this panel two cell lines are chosen to explore the possibility of measuring responses to therapeutic agents using the flow system.

Further experiments show metabolic changes measured over longer time courses, with the flow system used to monitor changes in a leukaemia cell line with an shRNA targeting a gene responsible for the proliferative leukaemic cell type.

Clinical applications of the flow system are also explored, with a focus on how best to prepare samples when using patient cells with the flow system. The utility of real-time monitoring is demonstrated for proliferating patient cells.

7.1. Overview

The central dogma of biology, as first proposed by Crick [213] "DNA makes RNA makes protein", reflects the culmination of cellular information passing through genomic, epigenetic, transcriptomic and proteomic processes. All cellular functions are governed by the genome via changes in gene expression, which in turn, drives alterations in biomolecule production. The metabolome forms the final layer of this cascade, and consequently metabolism provides a read out of biological status of the cell, for example, whether it is healthy or diseased. [214,215].

Metabolic biomarkers can be used to diagnose disease, differentiate morbidities, and predict severity of conditions [216]. There is more than just a correlation between disease mechanisms and metabolism, in fact metabolic dysregulation as a result of disease processes directly influences disease pathogenesis and progression [217,218,219].

Understanding the altered metabolic states in disease and how multiple metabolic pathways are linked to cellular functions, such as gene regulation, cell signalling and cell growth, requires technologies capable of detection and quantification of metabolites [220]. Due to the broad range of molecule types in complex biological matrices, sampling, extracting, and analysing the entire metabolome is challenging. Different analytical techniques demand different approaches to sample handling and preparation, depending on physical and chemical properties of the analyte [221]. While NMR lacks the sensitivity to detect the entire complement of endogenous small molecules, it has the advantage of being able to non-destructively identify the more abundant metabolites in complex mixtures. The non-invasive nature of the technique also allows collection of time course of data to be built up as samples can be reanalysed without being perturbed or destroyed.

A range of NMR methodologies can be applied to live samples to investigate metabolic signatures associated with disease. One such signature, known to accompany proliferative expansion of cell populations, is a distinctive phenotype seen in many cancers called the Warburg effect [222], which is characterised by a shift towards lactate production from glycolysis rather than feeding pyruvate into the TCA cycle.

7.2. Metabolic Hallmarks in Cancer

Cancer is a catch all term used to describe a variety of different malignancies that can occur in, and affect, any tissue of higher organisms. Often the tumour site of origin is used to name the disease, as genetic mutations directing oncogenic transformations act predominantly in a tissue specific fashion [223]. These alterations to the genetic code can drive malignant changes that result in alterations coupled to cellular metabolism [224].

The hallmarks of cancer are recognised as characteristics and functional capabilities that enable disease progression through deregulation of gene expression, cellular survival, proliferation and dissemination [225]. Reprogramming of cellular metabolism is considered as such an emerging hallmark, altering cell growth by replacing the normal metabolic programs in healthy cells with a regime that meets the requirements of uncontrolled proliferation[226].

Leukaemia is a group of haematological malignancies characterised by the build-up of immature blood cells [227]. This group of neoplasms display a range of genetic abnormalities, combined with a highly diverse and flexible metabolism [228,229,230]. These highly proliferative, multipotent cells need to fuel cell growth and division and therefore provide a good model for monitoring nutrient consumption.

7.2.1. Exometabolome

The untargeted metabolic footprint observed using the flow system provides information on the changes occurring in culture medium over time. Monitoring the consumption of substrates while simultaneously detecting the build-up of effluxed metabolites provides a real-time read out of cell status.

A panel of four acute myeloid leukaemia (AML) cell lines were chosen in order to compare metabolic profiles and investigate distinct features for each cell line. These included HL-60 and Kasumi-1, used previously to establish metabolic profiles under standard conditions in section 6.2.2, and two further leukaemia lines:

1. SKM-1, derived from a patient with monoblastic leukaemia following myelodysplastic syndrome [231]. Chromosomal abnormalities involve the p53 anti-oncogene [232].

2. MOLM-14, an acute monocytic leukaemia established from peripheral blood of a patient with AML-M5a at relapse [233]. This line contains a chromosomal insertion ins(11;9), a FLT3 internal tandem duplication and the fusion gene MLL-AF9.

Cells were placed in the bioreactor at a concentration of $5x10^5$ cells/ml and medium was perfused around the flow system at 1 ml/min. The metabolic footprint was monitored over 12 hours by acquiring consecutive 1D ^{1}H NMR spectra. To ensure consistent results were obtained each culture was treated in the same manner, using identical culture medium, prepared freshly each day. This guaranteed that the composition of culture medium was the same for each experiment, enabling relative peak areas to be compared across triplicates and between cell lines. The panel of nine metabolites, used in section 6.2.1, was again used to compare the cell lines.

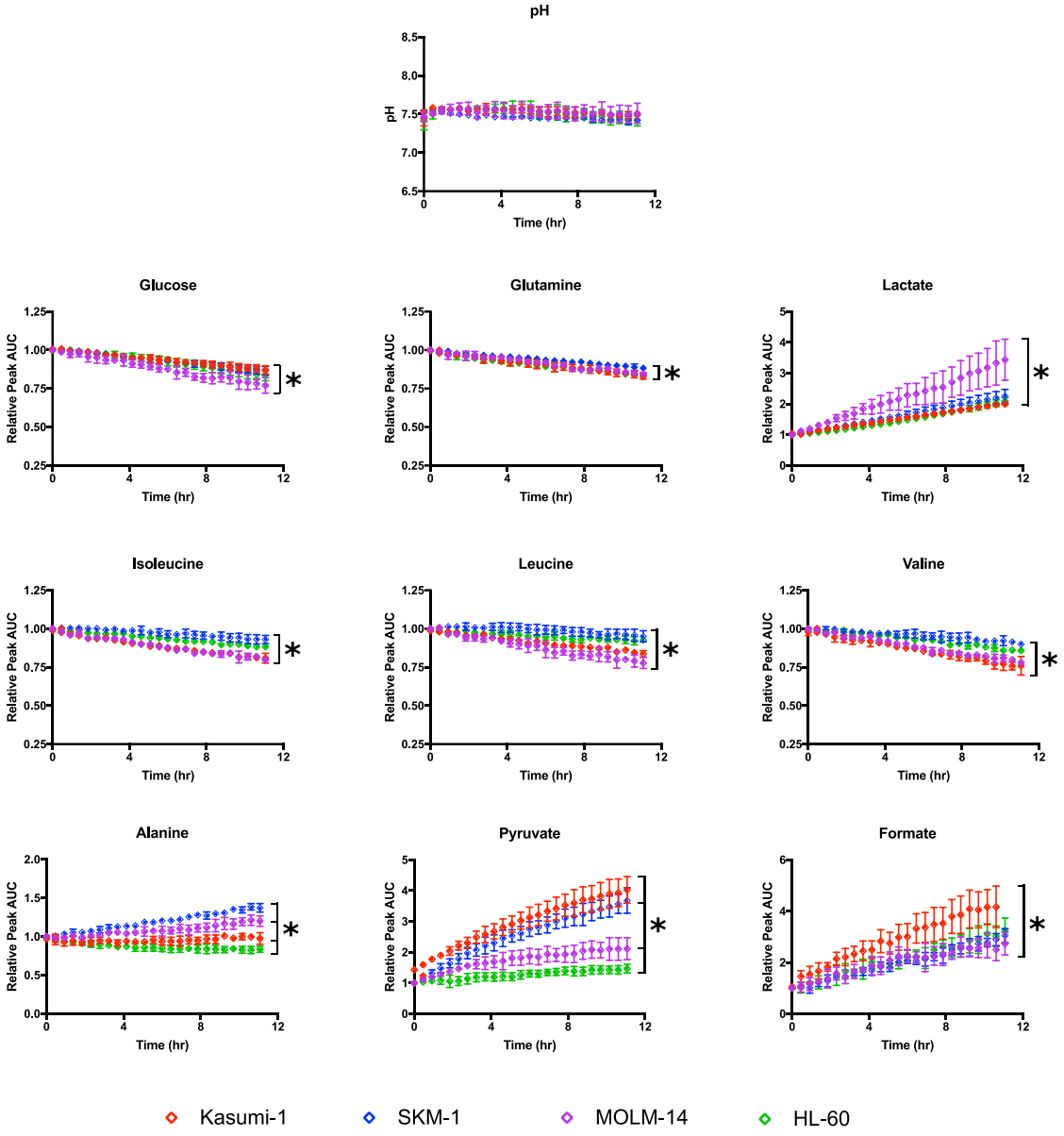

Figure 7.1 Real-Time Metabolic Profiles of Leukaemia Cells Lines

Four cell lines were chosen to investigate the metabolic phenotypes associated with leukaemia cells. Plots show relative peak areas (AUC) normalised to the TMSP standard, over the time course of 12 hours. These metabolite-intensity plots demonstrate that the acquisition technique is sensitive enough to detect metabolic changes and distinguish the cell lines based on usage of main substrates and overflow metabolism. Significant differences in final concentrations were measured for at least one cell line per metabolite ($p<0.05$).

All cell lines used glucose, glutamine and branched chain amino acids (BCAA). MOLM-14 consumed glucose at a slightly faster rate than other cell lines, and both MOLM-14 and Kasumi-1 used more BCAAs than SKM-1 and HL-60 cells. Glutamine consumption was similar for all cell lines, with SKM-1 having a slightly slower rate of usage.

A distinct, cell specific signature was evident as all cells effluxed lactate and other overflow metabolites at different rates. In particular MOLM-14 showed significantly more lactate production than the other cell lines, accompanied by a slightly faster rate of glucose consumption. Clearly, in all these cell lines the glycolytic pathway is active as glucose is metabolised with concomitant efflux of lactate. However, the usage of glutamine also suggests that this occurs in parallel with the TCA cycle.

There were distinct differences in overflow metabolism between the four cell lines, with Kasumi-1 and SKM-1 both effluxing pyruvate at a much faster rate than either MOLM-14 or HL-60. The efflux of pyruvate is thought to protect cells from oxidative stress by direct scavenging of hydrogen peroxide [234,235]. The mechanism involves a non-enzymatic decarboxylation of pyruvate by the activated peroxide ion [236].

Formate was universally effluxed, with Kasumi-1 generating slightly more than the other three cell lines. Formate overflow has been reported as a product of one-carbon metabolism, fuelled by medium serine [237].

Alanine production was evident for SKM-1 and MOLM-14, while HL-60 consumed a small amount from the medium. In experiments with Kasumi-1 cells no significant change in alanine levels was detected. The secretion of alanine is linked to glutamine catabolism via the TCA cycle [238].

Overall HL-60s showed the lowest levels of nutrient usage and metabolic efflux, while MOLM-14 had the highest.

7.3. Metabolic Response to Therapeutics

Comparing the metabolic profiles of different cell types can provide insight into relative activity of metabolic pathways. This data can be used to identify possible metabolic liabilities, as substrate usage can indicate a reliance on fuel substrates [239].

Targeting dysregulated metabolism as an anticancer therapy is an attractive option, as all cancer cells rely on rewired pathways for proliferation. Malignant phenotypes can be similar even when the underlying genetic drivers are completely different. Successful treatments may therefore be applicable to a range of cancer types. Multipharmacy approaches could twin metabolic inhibitors with other targeted therapies to improve efficacy.

Metabolic readouts, such as differences in glycolytic activity, could be used as early indicators of treatment efficacy before any major clinicopathological changes are detectable [240]. Testing new therapeutic strategies on live cells also allows the identification of chemoresistance due to metabolic plasticity. Conversely, limited metabolic flexibility can also be uncovered as cells unable to adjust metabolism will be sensitised to particular treatments.

Cancer cells are known to rewire cellular metabolism in order to undergo uncontrolled proliferation. Proliferating cells provide an ideal system for testing metabolic therapies as they multiply over short time scales. For example, in human haematopoiesis blood cells can be generated at a rate of two million cells each second [241]. The oncogenes responsible for metabolic plasticity that allow cells to produce excess biomass also result in potential therapeutic liabilities due to the stress on activated biosynthetic pathways. For example, the reliance of proliferating cells on glucose can be leveraged with the drug 2-deoxyglucose (2-DG). It inhibits glycolysis by out competing glucose and for access to hexokinase. The resulting phosphorylated 2-DG cannot be metabolised by cells and

accumulates. It competitively inhibits hexokinase, resulting in decreased glucose uptake and has shown an anti-proliferative effect in preclinical studies [242].

The flow system can be used to monitor real-time cellular responses induced by treatments in order to gain insight into the effects of drugs and determine the optimal therapeutic strategy based on metabolic dependencies. Metabolite-intensity plots can be used to indicate the efficacy of metabolic inhibitors or anti-neoplastic agents as spectral changes, relative to a control sample, correlate with metabolic effects.

The biguanide metformin impacts cellular respiration through inhibition of mitochondrial metabolism. Direct inhibition of respiratory chain complex 1 is responsible for antineoplastic activity observed in a variety of cancer cell lines [243,244]. Downstream effects due to reduced activity of the electron transport chain include activation of AMPK through changes in ATP/AMP ratio. Overall both glucose and glutamine metabolism have been shown to change as a consequence of metformin treatment [245].

Two cell lines were used to compare metabolic changes; Kasumi-1 and HL-60. These were chosen on the basis of their differing rates of overflow metabolism. While HL-60 produced the least pyruvate, Kasumi-1 produced the most. Cells were resuspended in medium with or without metformin (1 μM) and placed in the bioreactor at a concentration of $5x10^5$ cells/ml. The medium was perfused around the flow system at 1 ml/min and the subsequent metabolic footprint was monitored over 12 hours. To ensure consistent results were obtained each culture was treated in the same manner, and fresh medium was prepared for each experiment.

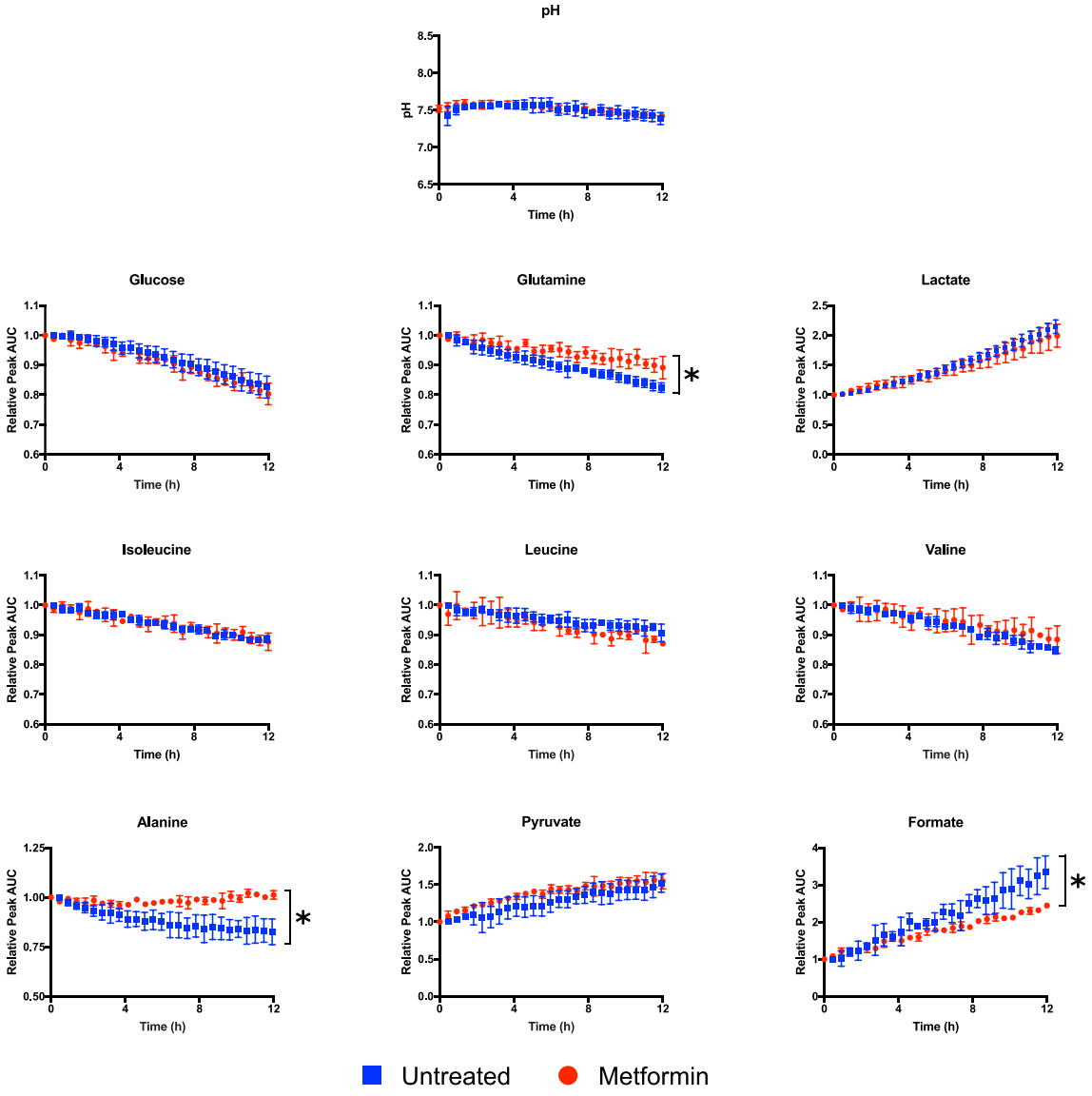

Figure 7.2 Real-Time Monitoring of HL-60 Response to Metformin Treatment

Metabolite-intensity plots show metabolic changes following metformin treatment (red plot) compared to no treatment (blue plot). Plots show relative peak areas (AUC) normalised to the TMSP standard, over the time course of 12 hours. There were no significant changes in other metabolites shown here.

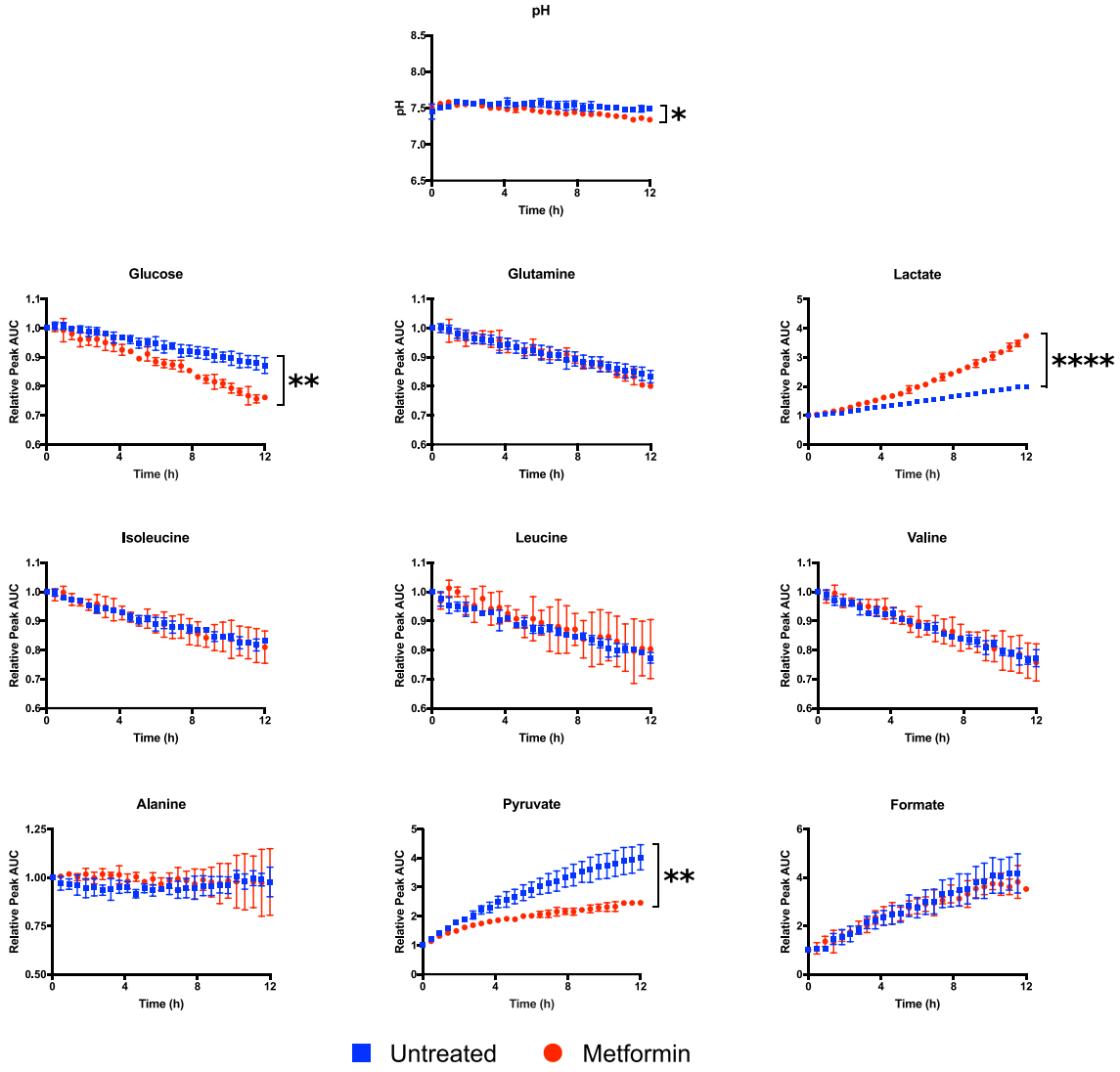

Figure 7.3 Real-Time Monitoring of Kasumi-1 Response to Metformin Treatment

Metabolite-intensity plots show metabolic changes following metformin treatment (red plot) compared to no treatment (blue plot). Plots show relative peak areas (AUC) normalised to the TMSP standard, over the time course of 12 hours. There are no significant changes in other metabolites shown here.

7.4. Monitoring Changes in Cell State

The metabolic phenotype associated with AML is a direct reflection of the accumulation of proliferative multipotent progenitors, unable to differentiate to functional, mature blood cells. Upregulated glycolysis and overflow metabolism fuel the malignant state by supplying the cells with nutrients, energy and redox equivalents.

In Kasumi-1 cells the t(8:21) translocation produces the RUNX1/ETO fusion protein responsible for the block in differentiation. Using shRNA to target the mRNA for this protein prevents expression, and allows cells move away from the immature phenotype and begin to differentiate.

This Kasumi-1 system has two markers to monitor expression of the shRNA. A green fluorescent protein (GFP) is constitutively expressed in the cells, while a DsRed fluorophore is only active when the doxycycline induced transcript is formed. Flow cytometry can therefore be used to assess knockdown of the target gene and sort cells expressing the shRNA, as shown in Figure 7.4. Reduction in RUNX1/ETO mRNA expression after 24 hours of doxycycline treatment was confirmed using qPCR.

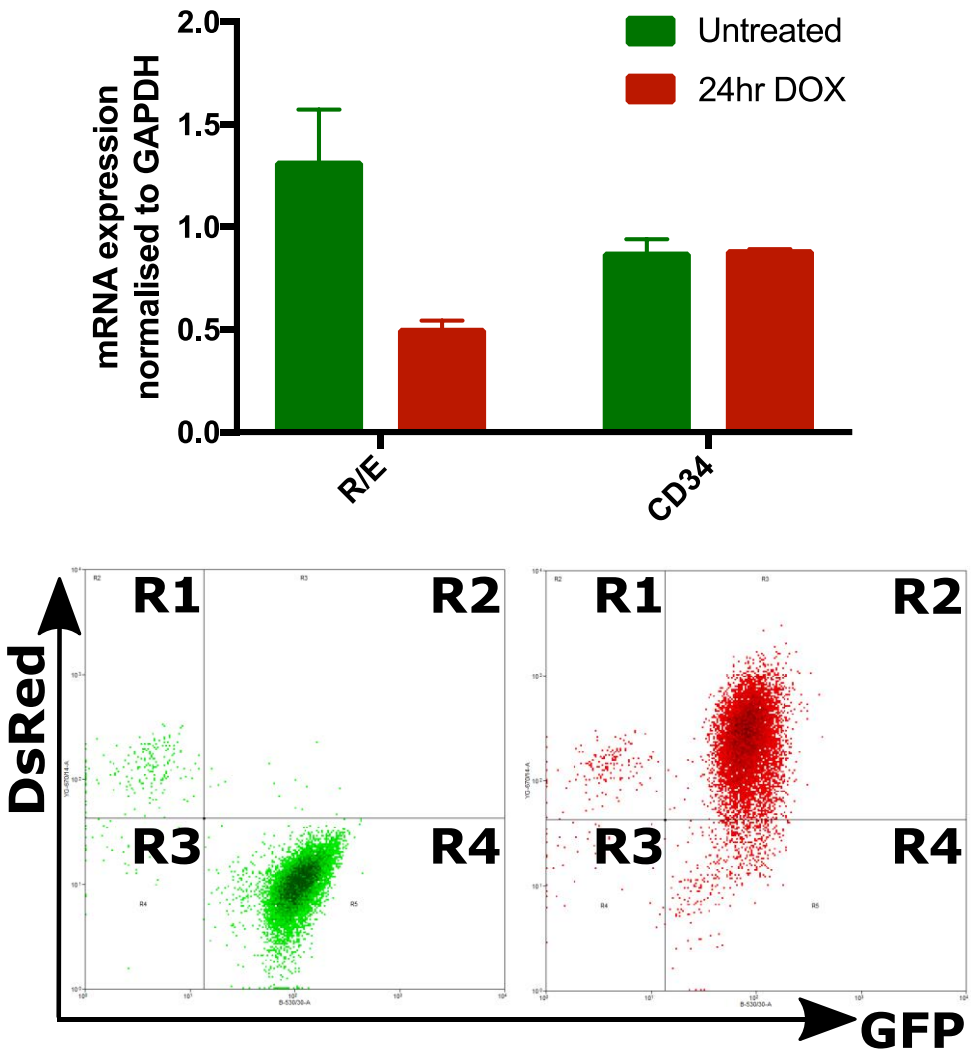

Figure 7.4 Doxycycline induction of shRNA targeting RUX1/ETO in Kasumi-1.

Doxycyline inducible TET activator system allows selective ablation of the RUNX1/ETO fusion protein in Kasumi-1 cells. Fluorescent markers GFP and DsRed demonstrate induction of the shRNA 24 hours after treatment commences, with protein expression confirmed by qPCR analysis. Cells express the GFP protein constitutively and treatment with doxycycline induces the expression of the DsRed marker, as shown by a shift from R4 to R2 quadrant.

7.4.1. Metabolic Changes Associated with RUNX1/ETO Ablation

Real-time monitoring can be used to detect alterations to metabolism post-knockdown, as selective removal of RUNX1/ETO leads to inhibition of the leukemic stem cell phenotype. As cells begin to differentiate the proliferation rate should decrease and consequently metabolism will change as demand for nutrients decreases and the related overflow metabolism is affected.

A control cell line, containing a mismatch shRNA, was used to confirm that there were no metabolic effects associated with doxycycline treatment. This construct has no target gene so expression levels should be unaffected and therefore no changes in cell state should be seen.

Both Kasumi-1 cell lines (shRE containing the RUNX1/ETO shRNA, and shMM containing the mismatch shRNA) were treated with doxycycline over a seven day time course. Cell aliquots where taken for analysis using the flow system at three time points:

1. Day Zero. Cells were monitored prior to treatment with doxycycline to establish a baseline metabolism in their most proliferative state.
2. Day Two. After 48 hours exposure to doxycycline cells were monitored to look for initial changes in metabolism after induction of the shRNA.
3. Day Seven. After a full week of exposure to doxycycline cells were monitored to investigate the metabolic changes associated with the onset of differentiation.

Cell aliquots were taken from a bulk culture and resuspended at $50x10^4$ cells/ml in medium containing doxycycline (1 μg/ml) where applicable. The medium was perfused around the flow system at 1 ml/min and the subsequent metabolic footprint was monitored over 12 hours. Fresh medium was prepared daily to ensure consistent results.

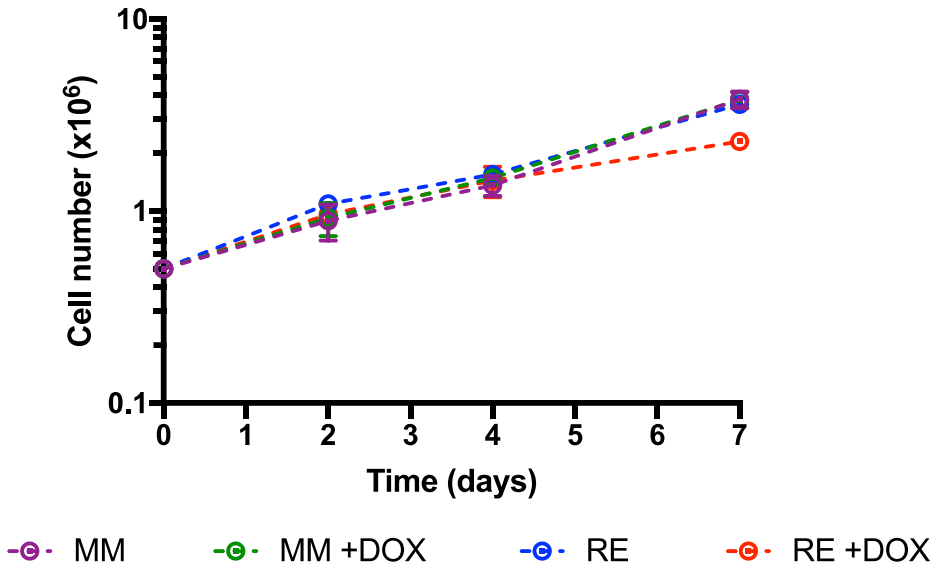

Figure 7.5 Kasumi-1 growth during treatment with doxycycline.

Cell growth was monitored over the duration of the seven day time course. Doxycycline was administered on day zero and every 48 hours thereafter. Ablation of RUNX1/ETO reduce proliferation rate of the Kasumi-1 cells by day seven.

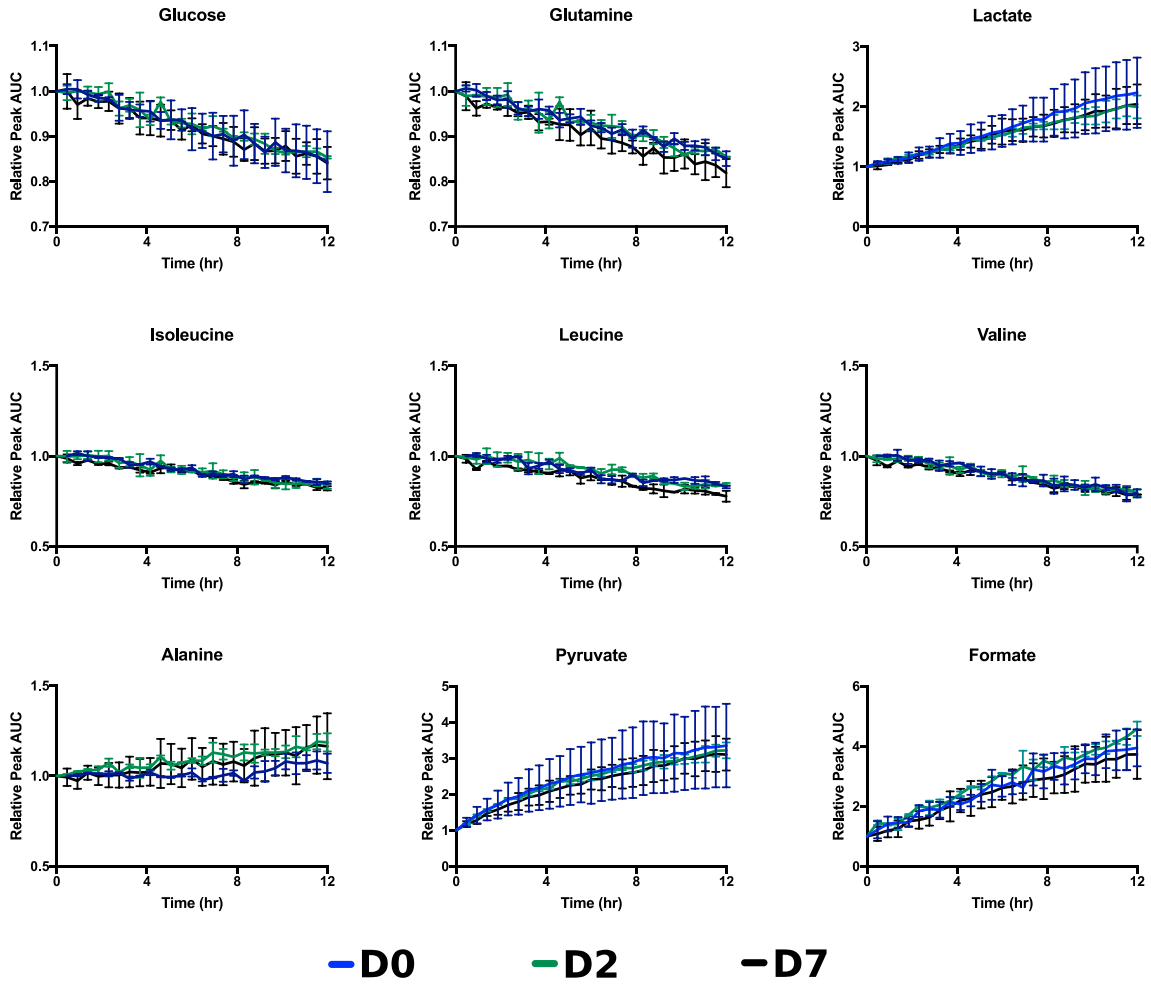

Figure 7.6 Kasumi-1 metabolism after induction of mismatch shRNA

Metabolite-intensity plots show metabolic changes following doxycycline induction of shMM over a course of seven days. Doxycycline was administered on day zero (blue plot) and every 48 hours thereafter. Metabolite intensity plots are consistent for all metabolites. Plots show relative peak areas (AUC) normalised to the TMSP standard, over the time course of 12 hours.

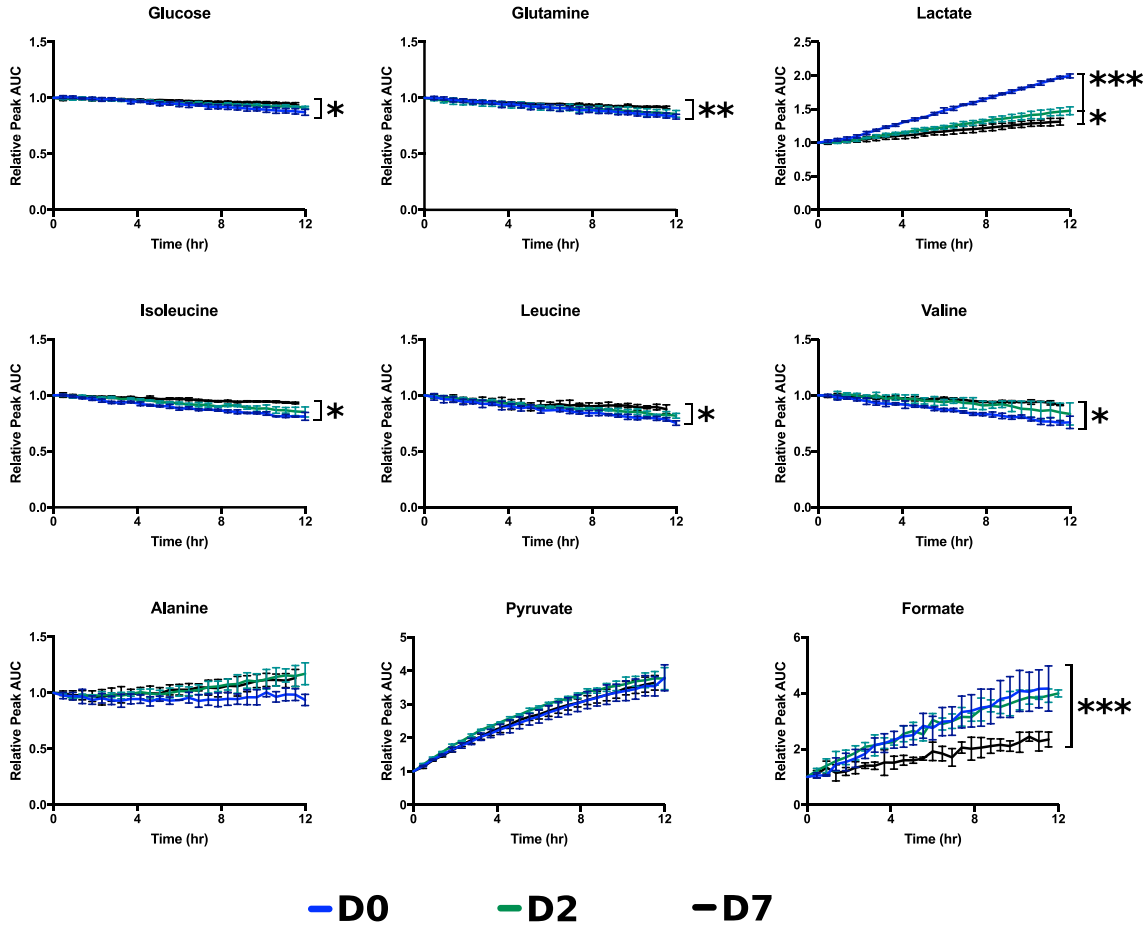

Figure 7.7 Kasumi-1 metabolism after shRNA knockdown of RUNX1/ETO.

Metabolite-intensity plots show metabolic changes following doxycycline induction of shRE over a course of seven days. Doxycycline was administered on day zero (blue plot) and every 48 hours thereafter. Plots show relative peak areas (AUC) normalised to the TMSP standard, over the time course of 12 hours. Significant changes in metabolism were seen after induction of the shRNA targeting RUNX1/ETO. Consumption of glucose and glutamine decreased from day two ($p<0.05$) and at day seven ($p<0.05$). Lactate efflux increased significantly from day two ($p<0.05$) and at day seven ($p<00001$). Consumption of BCAA decreased between day zero and day seven ($p<0.05$). While formate efflux increased significantly between day zero and day seven ($p<0.001$).

7.5. Clinical Applications

Cells can be purified from biopsies or blood and analysed using real-time monitoring. This provides the opportunity to compare metabolic phenotypes, and to test therapeutic strategies on patient derived material. Individual responses could then be used to personalise therapies as results from live cell monitoring informs on drug efficacy. This approach is not dissimilar to pharmacometabonomics where pre-dose metabolite profiling and chemometrics are used to predict patient responses [246].

A specific application would use patient samples to investigate chemoresistance in cancer therapy. The problem of drug resistance occurs as activation of cell membrane transporters reduces the effectiveness of xenobiotics over time [247]. Here, resistance to cell death correlated with altered metabolic phenotypes.

7.5.1. Sample Storage and Cell Viability for Real Time NMR

Many genomic and epigenetic studies require only a small number of cells, with some techniques using only a few thousand cells per sample [248]. In contrast, real-time monitoring of metabolic footprints requires much higher cell numbers in order to see changes in medium composition due to cellular activity. This can be challenging when working with patient samples where cell numbers are limited.

Often, samples from patients are taken and frozen for later bioanalysis which allows collection of all samples so analysis can proceed under the same conditions, an approach particularly important with techniques such as mass spectrometry where results can vary from batch to batch [249]. Unfortunately, the freeze/thaw cycle can kill a significant number of cells, even when samples are stored in cryoprotectants that stabilise cell membranes, such as DMSO. In order to reduce intracellular ice formation suspension

cells are cooled relatively slowly, around 1 °C per min. The DMSO can then diffuse into cells and reduce osmotic shock during freezing and thawing [250].

To assess the feasibility of real-time NMR using frozen cells a patient sample was defrosted, purified for $CD34^+$ cells, and prepared for use with the flow system to investigate the suitability of freezing samples for later analysis. See methods section 4.2.4 for details of defrost and preparation. Cells were suspended at a concentration of $5x10^5$ live cells/ml. Medium was perfused around the flow system at 1ml/min, and the metabolic footprint was monitored over 12 hours. During this time no change in metabolite intensities were detectable.

Subsequent analysis of cell viability using flow cytometry with annexinV (AV) and propidium iodide (PI) showed that most cells were undergoing apoptosis (70 %) or dead (25 %), as shown in Figure 7.8. AV binds to phosphatidylserine, a lipid that translocates to cell surface membranes during apoptosis, and PI enters cells with compromised membranes to bind to DNA.

Further experiments used fresh cells to avoid problems associated with freezing and thawing.

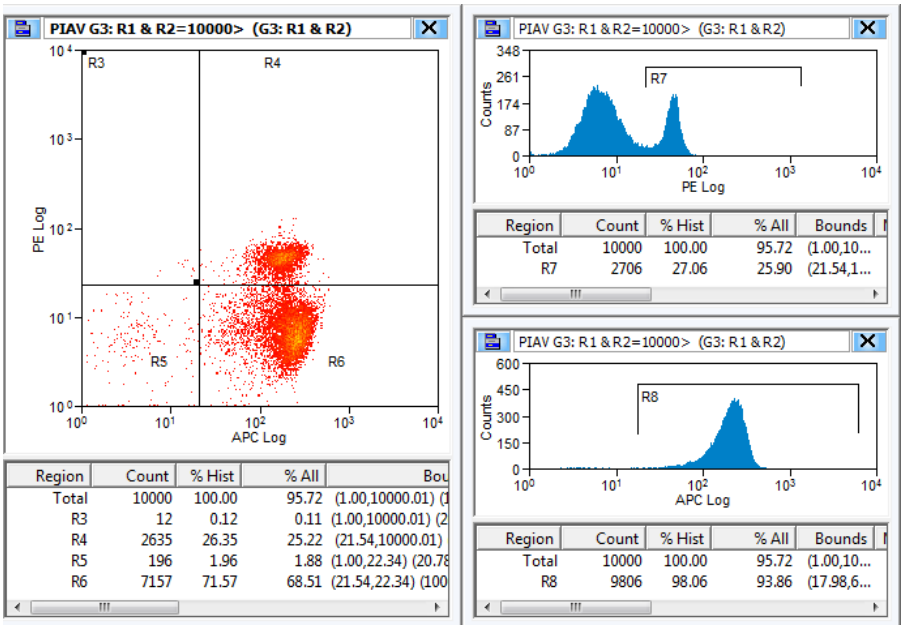

Figure 7.8 Freeze-Thawing Patient Samples.

To assess the feasibility of using previously frozen cells with the flow system a patient sample was defrosted and prepared for use with the bioreactor. After the 12 hour time course no metabolic changes were seen. Subsequent flow cytometry using an AV/PI stain demonstrated that most cells were apoptotic or dead.

7.5.2. Metabolic Activity is Associated with the Cell Cycle

The location of the NMR facility, adjacent to the hospital and biomedical institute, means that transport of live samples is relatively straightforward. A blood sample can be taken from a patient in the hospital and transferred to the biomedical institute for purification. The cells of interest can then be prepared for analysis and transported to the NMR facility. In this manner the real-time analysis commences only a few hours after the cells are taken from the patient.

To test this approach an AML sample was taken from a patient by a clinician and immediately processed by a member of the Bonifer lab using density centrifugation. Mononuclear cells were separated out from a peripheral blood sample and flow cytometry was used to confirm the presence of cell type using the CD34+ stem marker. A magnetic bead sort ensured that a purity of greater than 95% was achieved in the final sample. An aliquot of these cells was used ($5x10^5$ live cells/ml) for real-time analysis. Medium was perfused around the flow system at 1 ml/min and the metabolic footprint was monitored over 12 hours.

During the time course no clear metabolic response was seen in the sample; metabolite concentrations remained constant over time. Post-acquisition analysis by flow cytometry demonstrated that these cells were indeed alive, as shown in Figure 7.9.

Region	Stain	Status	Count	% Hist	% All
Total	-	-	9600	100	87.78
R3	PI	Dead	13	0.14	0.12
R4	PI/AV	Dead	111	1.16	1.01
R5	none	Alive	9041	94.18	82.66
R6	AV	Apoptotic	435	4.53	3.98

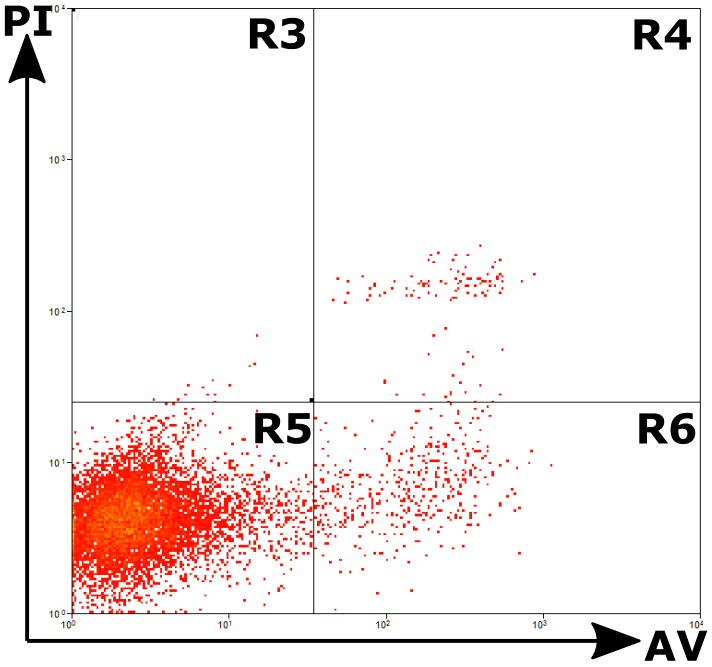

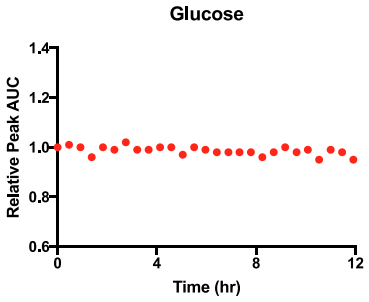

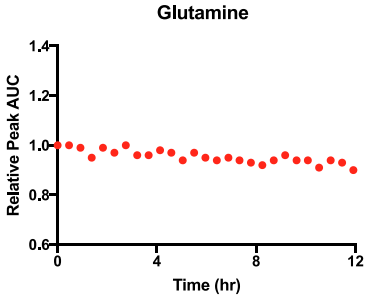

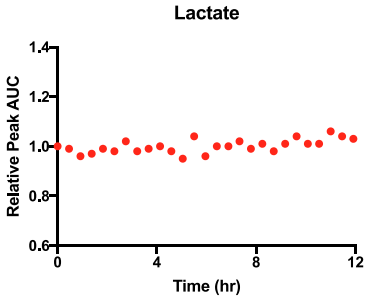

Figure 7.9 Metabolically Inactive Fresh Patient Sample.

Post-NMR acquisition flow cytometry analysis by AV/PI stain shows that most cells are still alive (95 %). However, there are no detectable changes in metabolite levels during the 12 hour time course. Representative metabolite intensity plots shown for main carbon sources glucose and glutamine, and common overflow product lactate show no significant changes.

Further analysis indicted that the majority of these cells were in the G0/G1 phase of the cell cycle (see Figure 7.10). This indicates that they were not proliferating, but in a dormant state of either quiescence or senescence. The difference between these states depends on the cells ability to re-enter the cell cycle. Senescent cells have completely lost their proliferative potential, whereas quiescent cells retain their capacity to divide after appropriate activation [[251],[252]]. The cells that still possess the ability to proliferate can re-enter the cell cycle, grow and divide at a later point in time.

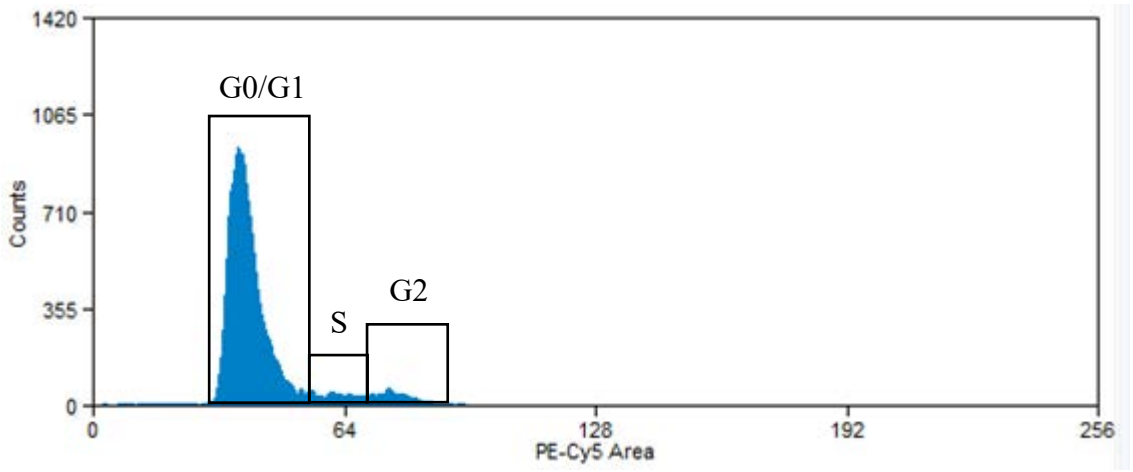

Figure 7.10 Quiescent patient sample resting in G0/G1

The DNA dye 7-amino actinomycin D (7-AAD) was used to stain cells to establish the relative populations of the stages of the cell cycle. Gating separates cells into G0/G1, S and G2 phases. In this case most cells were quiescent, resting in the G0/G1 stage.

7.5.3. Real-Time Metabolic Changes in Live Patient Cells

As fresh patient cells did not show metabolic changes, a proliferative primary patient cell line was used to investigate metabolic activity. A surplus of cells from a diagnostic patient sample was sorted for the cell surface marker CD34+, as described in methods section 4.2.5. Cells were cultured on stroma and expanded over a period of several weeks to yield sufficient numbers for a triplicate analysis by real-time monitoring.

This cell line is an AML double mutant for CEBPA (CCAAT/enhancer binding protein alpha), with two distinct mutations resulting in proliferative activity [253].The first mutation, in the C-terminal region, disrupts binding to DNA. The second mutation, in the N-terminal, produces a short isoform that lacks the transactivation domain. Normally this transcription factor plays a part in differentiation, and initiating commitment to myeloid lineages [254]. It also acts as a tumour suppressor inhibiting cell proliferation [255].

Cell aliquots were taken from the bulk culture and resuspended at $5x10^5$ cells/ml in medium supplemented with a serum free mixture of human cytokines. The medium was perfused around the flow system at 1 ml/min and the subsequent metabolic footprint was monitored over 12 hours. Fresh medium was prepared daily to ensure consistent results.

Data quality in this sample was lower than previous samples due to the protein content of the medium. This proprietary mixture contains a selection of cytokines and growth factors vital for viability, unfortunately these proprietary factors bind to the analytical standard. This resulted in variable data, as indicated by large error bars for some metabolites (see Figure 7.11), as normalisation was affected by the apparent reduced peak area of TMSP.

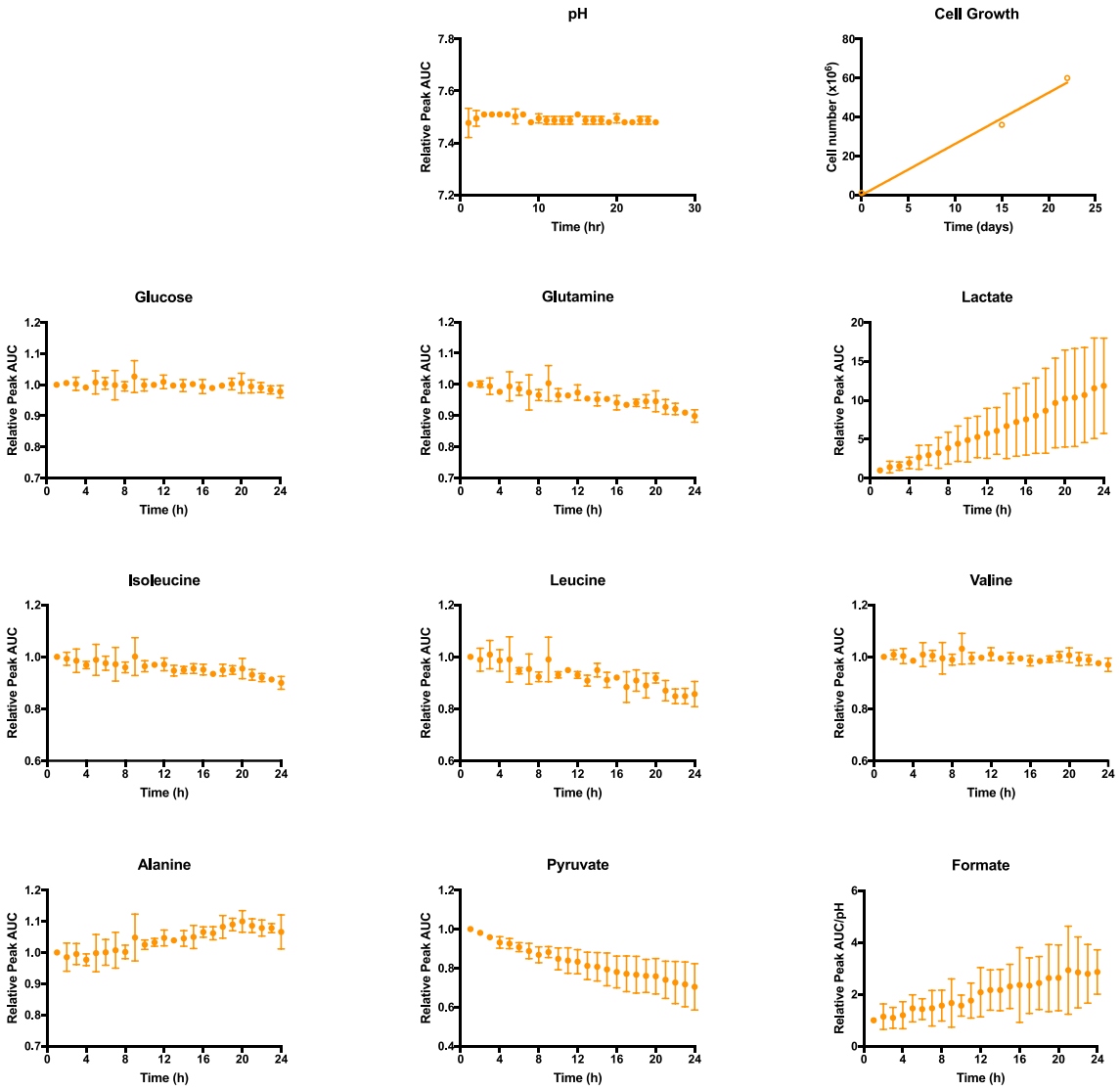

Figure 7.11 Proliferating Patient AML Cells Show Metabolic Activity

Metabolite intensity plots show metabolic changes associated with AML cells grown from a patient sample. Plots show relative peak areas (AUC) normalised to the TMSP standard, over the time course of 24 hours. Cell growth plot demonstrates that cells were proliferating in culture. Pyruvate appears to be the main carbon source, as glucose levels remain constant. Glutamine and branched chain amino acids are consumed from the medium, while lactate is effluxed over the duration of the 24 hour time course.

CHAPTER 8

DISSCUSSION

8. Discussion

Real-time analysis of physiological parameters at the cellular level, such as metabolism, requires a non-disruptive method of maintaining live cells. The flow system achieved this by successfully integrating a cell culture incubator in a controlled environment suitable for the study of mammalian cells. The development of a bioreactor prototype facilitated the sterile transfer of samples from the cell culture laboratory to the NMR facility with minimum disturbance to the live cell samples.

The study of metabolic overflow phenotypes in real-time was achieved by monitoring the exometabolome in cancer cell lines and patient derived cells. This chapter seeks to interpret the data generated during this project, followed by discussion of further work in the area of metabolic analysis by real-time NMR.

8.1. Metabolic Profiles of Cultured Cells

8.1.1. Metabolic Stability of Culture Medium

The first experimental data set used a standard cell culture methodology to compare the cell-free media with and without serum supplementation. A series of flasks containing media were prepared and incubated for 24 hours. This experiment demonstrated consistent concentrations for all metabolites over time, as shown in Figure 6.1. In particular, we observed no appreciable degradation of glutamine, over the 24 hour period of culture, indicating that the breakdown of this compound requires longer periods of time.

The spent medium could contain metabolic enzymes due to apoptotic release of cytoplasmic contents, a phenomena often used to assess viability [256]. The comparison of medium formulations between fresh and spent medium showed no significant changes,

indicating that there was no significant release of enzymes into the medium that could confound results during the 24 hour period of the experiment.

The same, standard cell culture approach was used to determine the metabolic profile of culture medium, with live cells. Flasks were used to maintain a live cell culture in an incubator for 24 hours in order to establish changes in the exometabolome due to cellular activites. The culture containing JJN3 cells showed a variety of changes in the small molecule composition of the medium compared to the cell-free media. Nutrients were consumed and metabolic by-products were effluxed by the JJN3 cells. Glucose and branched chain amino acids were used up, while the overflow of lactate, alanine and formate was observed. Formate overflow has been reported as a product of one-carbon metabolism, fuelled by medium serine [257]. Pyruvate concentration increased over the first 12 hours of culture, after which it seemed to reach a plateau then decreased slightly in the latter 12 hours, indicating that pyruvate was reabsorbed and used by JJN3 cells as a substrate. Pyruvate is known to protect cells against reactive oxygen species (ROS), and consumption in cell culture medium has been shown to be linked to peroxide concentrations [258,259]. Cells are also known to uptake pyruvate, via moncarboxylate transporters, and convert it to lactate by lactate dehydrogenase (LDH) as illustrated in Figure 1.4 [260]. This maintains cytosolic redox potential by regenerating NAD+ and ensures that glycolysis can continue to consume redox equivalents.

8.1.2. Metabolic Signatures of Live Cells

The metabolic profiles generated in section 6.2.2 demonstrate that growth rate roughly correlates with rate of usage of substrates and subsequent production of overflow products. JJN3, the faster growing cell line, used more glucose and produced more lactate in comparison to the two slower growing lines.

The type of overflow metabolism varied with each cell line, providing a unique profile based on just a few metabolites. JJN3 produced most alanine and pyruvate but least formate, while HL-60 secreted almost no alanine or pyruvate, and only a small amount of formate. Kasumi-1 produced an intermediate amount of alanine and pyruvate, but significantly more formate than either HL-60 or JJN3.

8.2. Real-Time Response to Metformin

The value of monitoring live systems lies in the dynamic nature of the information obtained; instantaneous responses to external stimuli can be observed and followed over time. This was demonstrated using real-time NMR to follow the initial metabolic reaction in leukaemia cells to the drug metformin, described in section 7.3.

A variety of studies on metformin-induced metabolic effects have been reported, with a range of results in the literature, as different cell lines respond to impaired mitochondrial metabolism in different ways [261,262]. Under normal conditions mitochondria produce ATP through oxidative phosphorylation. Other important functions include generating redox equivalents, namely NADH and $FADH_2$, and precursors for anabolism. Metformin treatment is expected to impair these processes and result in alterations to the TCA cycle.

During metformin treatment each of the two examined cell types displayed a distinctly different metabolic response, as illustrated in Figure 7.2 and Figure 7.3. Kasumi-1 cells showed no change in glutamine usage, but glycolysis was significantly upregulated as glucose consumption and lactate production increased over the time course. In contrast the HL-60 cells showed no significant change in glycolysis, instead overflow metabolism changed and glutamine usage decreased with metformin treatment. Less formate was effluxed by these cells during treatment, indicating that mitochondrial metabolism may

have been impaired. In Kasumi-1 cells the formate production was unchanged, suggesting that either mitochondrial metabolism was unaffected or that the cytosolic pathway can compensate for dysregulated mitochondrial metabolism by using serine, either directly from the medium or via glycolysis [263].

HL-60 also used less alanine and showed no change in BCAA usage or pyruvate secretion. In Kasumi-1 there were no changes in BCAA metabolism or formate efflux, while pyruvate secretion was significantly reduced during treatment.

The differences between Kasumi-1 and HL-60 cells could be indicative of metabolic flexibility, or different metabolic strategies to in response to the effects of metformin. The upregulation of glycolysis by Kasumi-1 could compensate for the lack of ATP produced by compromised mitochondria. The reduced overflow of pyruvate could be indicative of a redirection of metabolic flux, as formation of lactate would regenerate NAD+.

8.3. Leukemic Phenotype: Effect of RUNX1/ETO

Metabolism influences all cellular activities, pervading all aspects of biology, from regulatory mechanism to signal transduction and differentiation. Enzymes that control gene regulation use substrates derived from cellular metabolism. It is therefore unsurprising that any shift from the normal physiological state will also be accompanied by some form of metabolic perturbation. Understanding the precise relationship between metabolic processes and disease is an ongoing field of work.

The experiments in section 7.4 demonstrated that real-time NMR has the sensitivity to detect the changes in metabolic phenotype associated with cellular state. In this case the Kasumi-1 model was used to monitor metabolic effects during the alleviation of a block in differentiation. Cells were treated with doxycycline over a seven day period in order to ablate RUNX1/ETO expression and real time NMR analysis of the resulting phenotype was undertaken at three time points; day zero, day two and day seven.

The control cell line, shMM, showed no metabolic change over the course of seven days doxycycline treatment, illustrated in Figure 7.6. This confirms that induction of the expression system has no off target metabolic effects over the duration of the time course. All metabolites had the same rate of substrate consumption and metabolite efflux at each time point.

In contrast, the shRE cell line demonstrated that ablation of RUNX1/ETO changed the metabolic phenotype of the cells over the seven day period, as shown in Figure 7.7. During the first 48 hours following doxycycline treatment there was a distinct drop in the rate of lactate efflux, coupled with a decrease in consumption of glucose, glutamine and branched chain amino acids. While pyruvate secretion was unchanged over time the level of formate efflux dropped significantly between day two and day seven. These results demonstrate the potential of the flow system to monitor metabolic changes

associated with cell state during the course of differentiation. From these experiments it is also becoming increasingly clear that a static snapshot of metabolism is of limited scope, as it is often the rate of metabolic turn-over for specific mechanisms that is affected by cancer related metabolic changes in cells.

8.4. Challenges Associated with Live Patient Cells

The clinical applications for real-time NMR were explored using cells derived from patient blood. The initial attempt, to use a previously frozen patient sample, was unsuccessful as there were not sufficient numbers of live cells in the sample after the freeze/thaw process. It is possible to isolate live cells and expand the culture to reach the cell numbers required for real time NMR, however this is time consuming, potentially expensive and may not yield a similar cell population to the original sample. Further attempts tried to circumvent this problem by using fresh blood, or allowing cells to recover after the freeze/thaw process.

8.4.1. Quiescent Cells

Cells taken and directly processed for real-time NMR were stuck in the G0/G1 phase of the cell cycle, as shown in Figure 7.10. For the duration of the experiment these cells rested in a non-proliferative state of dormancy with no detectable metabolic signature.

Live samples may also have a mixture of cells in different stages of the cell cycle. It could be advantageous to ensure that all cells are in the same stage before starting a metabolic analysis.

While this result illustrates the challenges of analysing live cell samples it also opens up another area of clinically relevant experimentation. In AML the high relapse rate is due to a small population of cells surviving chemotherapy, remaining unaffected by anti-

mitotic drugs that target proliferative cells by virtue of their suspended growth. Cells remain alive and non-dividing for significant time frames until resuming proliferation, resulting in recurrent disease.

The flow system could be used to probe the mechanisms underlying drug resistance in certain cell populations by monitoring responses to cell cycle inhibitors and stimulators. Cells could be stimulated to proliferate and then the flow system would be an ideal platform to test therapies using metabolic response as a read out. However, selective modification of the cell cycle may be quite challenging, depending on the cell type.

8.4.2. Patient Phenotype Differs From Cultured Cells

The patient derived AML cells displayed an interesting phenotype of low glycolytic activity, different to any of the cultured cell lines. While lactate was effluxed, glucose was not consumed as the major carbon source, instead pyruvate seemed to be the primary substrate taken up by the cells. While most was converted to lactate, it is also possible that some was used in the TCA cycle. This reliance on pyruvate could be a result of the in vivo niche; AML cells home to the endosteal region of the bone marrow where they can maintain dormant, supported by distinct molecular mechanisms [264]. Being sequestered inside the niche environment, where cellular architecture protects circulating cells, malignant cells have been shown to stimulate secretion of pyruvate in surrounding stroma and take up the pyruvate [265]. The patient derived cells also had a much lower proliferation rate in comparison to the cultured cell lines.

8.5. Future work

The power of NMR spectroscopy lies in the ability to interrogate live systems with minimal perturbation. Studies of live systems have major potential to aid in the development and evaluation of therapeutics as clinical applications may evolve to include the use of benchtop spectrometers in the future. It is also possible to use the flow system with tissues or organs, and experiments using perfusion could be easily set up with the incubator.

Further improvements in the methodology of real-time monitoring are immediately obvious. Peak overlap can potentially be reduced at higher fields, signal-to-noise can be improved with more sensitive hardware and stable isotope labelling studies can be used to prove metabolite specific information [266].Together with a move to higher field to improve resolution, and moving from room temperature probe to a cryo-probe, the spectral quality can be greatly enhanced.

NMR tubes compatible with the InsightMR system are not limited to the larger volume 5mm. The tube holder used in this work mimics a conventional 5mm tube and spinner, however a smaller 3mm tube size is now available, reducing the volume from 550 µl to 180 µl. Reducing the overall volume of the system by decreasing the bioreactor size would allow smaller cell numbers to be monitored, and therefore make the technique more amenable to patient samples.

Equally, the volume of the system could be increased for cell line work so multiple samples could be taken from the flowing medium during acquisition. This offers the possibility to combine methodologies to take parallel samples. Aliquots of the flowing suspension could be taken during the time course and extracted to provide intracellular metabolite levels, providing a complementary set of data points to elucidate metabolic

pathways [267]. Information on intracellular metabolic processes is vital to truly understand the biological system under study.

Techniques such as DNP can be combined with bioreactor systems to enhance sensitivity and provide detailed information on dynamic fluxes [268].

Alternative acquisition methods can be used to reduce peak overlap, such as using 2D NMR, in order to confidently assign and quantify more metabolites [269]. Another approach would be to use stable isotope labelling to determine active metabolic pathways. We have demonstrated the use of ^{13}C filtering to monitor cell metabolism in a live cell sample, obtaining ^{13}C incorporations from difference spectra [270]. Other fast acquisition techniques, such as 2D HSQC spectra could be used to overcome spectral crowding and trace ^{13}C substrate usage [271].

Another point to consider is the inherently unphysiological nature of cell culture. Normally cells are seeded at low densities, allowed to grow and harvested when medium is near exhaustion. The flow system can be altered to provide a continuous flow of fresh medium, maintaining a stable environment that recapitulates the in vivo niche. It is also possible to alter medium formulations to reflect the physiological state, rather than the supraphysiological concentrations often encountered for immortalised cell lines [272].

Overall the type of design of bioreactors in this work opens avenues to work with human cells under conditions that resemble those of well-established lab experiments. It enables monitoring metabolism in primary patient cells as demonstrated for AML cells. Most importantly this work shows that metabolic turn-over considerably enhances the metabolic information, as continuous flux in live cells can be monitored in real-time.

REFERENCES

[1] Heald R, Cohen-Fix O. Morphology and function of membrane-bound organelles. Curr Opin Cell Biol. 2014;26:79-86.

[2] Lunt SY, Heiden MGV. Aerobic Glycolysis: Meeting the Metabolic Requirements of Cell Proliferation. Annual Review of Cell and Developmental Biology. 2011;27(1):441-64.

[3] KEGG PATHWAY Database http://www.genome.jp/kegg/

[4] Cao Y, Wang RH. Associations among Metabolism, Circadian Rhythm and Age-Associated Diseases. Aging Dis. 2017;8(3):314–333.

[5] Panda S. Circadian physiology of metabolism. Science. 2016;354(6315):1008-15.

[6] Flamholz A, Noor E, Bar-Even A, Liebermeister W, Milo R. Glycolytic strategy as a tradeoff between energy yield and protein cost. Proc Natl Acad Sci U S A. 2013;110(24):10039-44.

[7] Vale RD, Milligan RA. The Way Things Move: Looking Under the Hood of Molecular Motor Proteins. Science. 2000;288(5463):88-95.

[8] Nagel ZD, Klinman JP. A 21st century revisionist's view at a turning point in enzymology. Nat Chem Biol. 2009;5(8):543-50.

[9] Rutter J, Winge DR, Schiffman JD. Succinate dehydrogenase – Assembly, regulation and role in human disease. Mitochondrion. 2010;10(4):393-401.

[10] Hosios AM, Vander Heiden MG. The redox requirements of proliferating mammalian cells. J Biol Chem. 2018;293(20):7490-8.

[11] Hahn A, Parey K, Bublitz M, Mills DJ, Zickermann V, Vonck J, et al. Structure of a Complete ATP Synthase Dimer Reveals the Molecular Basis of Inner Mitochondrial Membrane Morphology. Mol Cell. 2016;63(3):445-56.

[12] Liu Y, Fiskum G, Schubert D. Generation of reactive oxygen species by the mitochondrial electron transport chain. Journal of neurochemistry. 2002;80(5):780-7.

[13] Indo HP, Yen HC, Nakanishi I, et al. A mitochondrial superoxide theory for oxidative stress diseases and aging. J Clin Biochem Nutr. 2015;56(1):1–7.

[14] Chauvin JR, Pratt DA. On the Reactions of Thiols, Sulfenic Acids, and Sulfinic Acids with Hydrogen Peroxide. Angew Chem Int Ed Engl. 2017;56(22):6255-9.

[15] Xie W, Ma W, Liu P, Zhou F. Overview of thioredoxin system and targeted therapies for acute leukemia. Mitochondrion. 2019;47:38-46.

[16] Lehninger AL, Cox MM, Nelson DL. 2008. Principles of Biochemistry. W.H. Freeman and Company, New York

[17] Mueckler M, Thorens B. The SLC2 (GLUT) family of membrane transporters. Mol Aspects Med. 2013;34(2-3):121-38.

[18] Wilson JE. Isozymes of mammalian hexokinase: structure, subcellular localization and metabolic function. J Exp Biol. 2003;206(Pt 12):2049-57.

[19] Berg JM, Tymoczko JL, Stryer L. 2002. Biochemistry. W.H. Freeman and Company, New York

[20] Amelio I, Cutruzzolá F, Antonov A, Agostini M, Melino G. Serine and glycine metabolism in cancer. Trends Biochem Sci. 2014;39(4):191–198.

[21] Reitzer LJ, Wice BM, Kennell D. Evidence that glutamine, not sugar, is the major energy source for cultured HeLa cells. J Biol Chem. 1979;254(8):2669-76.

[22] Locasale JW, Cantley LC. Metabolic flux and the regulation of mammalian cell growth. Cell Metab. 2011;14(4):443-51.

[23] Efeyan A, Comb WC, Sabatini DM. Nutrient-sensing mechanisms and pathways. Nature. 2015;517(7534):302-10.

[24] Wellen KE, Thompson CB. Cellular metabolic stress: considering how cells respond to nutrient excess. Mol Cell. 2010 Oct 22;40(2):323-32.

[25] Lindsley JE, Rutter J. Nutrient sensing and metabolic decisions. Comparative Biochemistry and Physiology Part B: Biochemistry and Molecular Biology. 2004;139(4):543-59.

[26] Li F, Xu W, Zhao S. Regulatory roles of metabolites in cell signaling networks. J Genet Genomics. 2013;40(7):367-74.

[27] Etchegaray J-P, Mostoslavsky R. Interplay between Metabolism and Epigenetics: A Nuclear Adaptation to Environmental Changes. Molecular Cell. 2016;62(5):695-711.

[28] Pietrocola F, Galluzzi L, Bravo-San Pedro José M, Madeo F, Kroemer G. Acetyl Coenzyme A: A Central Metabolite and Second Messenger. Cell Metabolism. 2015;21(6):805-21.

[29] Shyh-Chang N, Locasale JW, Lyssiotis CA, Zheng Y, Teo RY, Ratanasirintrawoot S, et al. Influence of Threonine Metabolism on S-Adenosylmethionine and Histone Methylation. Science. 2013;339(6116):222-6.

[30] Yuan H-X, Xiong Y, Guan K-L. Nutrient Sensing, Metabolism, and Cell Growth Control. Molecular Cell. 2013;49(3):379-87.

[31] Crozet P, Margalha L, Confraria A, Rodrigues A, Martinho C, Adamo M, et al. Mechanisms of regulation of SNF1/AMPK/SnRK1 protein kinases. Frontiers in Plant Science. 2014;5(190).

[32] Xiao B, Heath R, Saiu P, Leiper FC, Leone P, Jing C, et al. Structural basis for AMP binding to mammalian AMP-activated protein kinase. Nature. 2007;449(7161):496-500.

[33] Barnes K, Ingram JC, Porras OH, Barros LF, Hudson ER, Fryer LG, et al. Activation of GLUT1 by metabolic and osmotic stress: potential involvement of AMP-activated protein kinase (AMPK). J Cell Sci. 2002;115(Pt 11):2433-42.

[34] Wolfson RL, Sabatini DM. The Dawn of the Age of Amino Acid Sensors for the mTORC1 Pathway. Cell Metab. 2017;26(2):301-9.

[35] Goberdhan DC, Wilson C, Harris AL. Amino Acid Sensing by mTORC1: Intracellular Transporters Mark the Spot. Cell Metab. 2016;23(4):580-9.

[36] Pernicova I, Korbonits M. Metformin—mode of action and clinical implications for diabetes and cancer. Nature Reviews Endocrinology. 2014;10(3):143-56.

[37] Ast T, Mootha VK. Oxygen and mammalian cell culture: are we repeating the experiment of Dr. Ox? Nature Metabolism. 2019;1(9):858-60.

[38] Weidemann A, Johnson RS. Biology of HIF-1α. Cell Death & Differentiation. 2008;15(4):621-7.

[39] Koczula KM, Ludwig C, Hayden R, et al. Metabolic plasticity in CLL: adaptation to the hypoxic niche. Leukemia. 2016;30(1):65–73.

[40]Busa WB, Nuccitelli R. Metabolic regulation via intracellular pH. American Journal of Physiology-Regulatory, Integrative and Comparative Physiology. 1984;246(4):R409-R38.

[41] Webb BA, Chimenti M, Jacobson MP, Barber DL. Dysregulated pH: a perfect storm for cancer progression. Nat Rev Cancer. 2011;11(9):671-7.

[42] Slavov N, Budnik BA, Schwab D, Airoldi EM, van Oudenaarden A. Constant growth rate can be supported by decreasing energy flux and increasing aerobic glycolysis. Cell Rep. 2014;7(3):705-14.

[43] Liberti MV, Locasale JW. The Warburg Effect: How Does it Benefit Cancer Cells? Trends Biochem Sci. 2016;41(3):211-8.

[44] Pietzke M, Arroyo SF, Sumpton D, Mackay GM, Martin-Castillo B, Camps J, et al. Stratification of cancer and diabetes based on circulating levels of formate and glucose. Cancer Metab. 2019;7:3.

[45] Brosnan ME, Brosnan JT. Formate: The Neglected Member of One-Carbon Metabolism. Annu Rev Nutr. 2016;36:369-88.

[46] Brosnan ME, MacMillan L, Stevens JR, Brosnan JT. Division of labour: how does folate metabolism partition between one-carbon metabolism and amino acid oxidation? Biochem J. 2015;472(2):135-46.

[47] Meiser J, Schuster A, Pietzke M, Vande Voorde J, Athineos D, Oizel K, et al. Increased formate overflow is a hallmark of oxidative cancer. Nat Commun. 2018;9(1):1368.

[48] Whitten ST, García-Moreno E. B, Hilser VJ. Local conformational fluctuations can modulate the coupling between proton binding and global structural transitions in

proteins. Proceedings of the National Academy of Sciences of the United States of America. 2005;102(12):4282-7.

[49] Halestrap AP. Monocarboxylic acid transport. Compr Physiol. 2013;3(4):1611-43.

[50] Bröer S, Schneider HP, Bröer A, Rahman B, Hamprecht B, Deitmer JW. Characterization of the monocarboxylate transporter 1 expressed in Xenopus laevis oocytes by changes in cytosolic pH. Biochem J. 1998;333 (Pt 1):167-74.

[51] Dimmer KS, Friedrich B, Lang F, Deitmer JW, Bröer S. The low-affinity monocarboxylate transporter MCT4 is adapted to the export of lactate in highly glycolytic cells. Biochem J. 2000;350(pt 1):219–227.

[52] Halestrap AP. The SLC16 gene family - structure, role and regulation in health and disease. Mol Aspects Med. 2013;34(2-3):337-49.

[53] Carpenter L, Halestrap AP. The kinetics, substrate and inhibitor specificity of the lactate transporter of Ehrlich-Lettre tumour cells studied with the intracellular pH indicator BCECF. Biochem J. 1994;304 (Pt 3)(Pt 3):751-60.

[54] Hong CS, Graham NA, Gu W, et al. MCT1 Modulates Cancer Cell Pyruvate Export and Growth of Tumors that Co-express MCT1 and MCT4. Cell Rep. 2016;14(7):1590–1601.

[55] Hanahan D, Weinberg RA. The hallmarks of cancer. Cell. 2000;100(1):57-70.

[56] Cancer Research UK, https://www.cancerresearchuk.org/health-professional/cancer-statistics/worldwide-cancer/incidence, Accessed Jan 2020

[57] WHO (2017) Cancer. World Health Organization. https://www.who.int/en/news-room/fact-sheets/detail/cancer, Accessed Jan 2020

[58] Hoelder S, Clarke PA, Workman P. Discovery of small molecule cancer drugs: successes, challenges and opportunities. Mol Oncol. 2012;6(2):155-76.

[59] http://gco.iarc.fr/today/fact-sheets-cancers, Accessed Jan 2020

[60] Warburg O, Wind F, Negelein E. The Metabolism of Tumors in the body. J Gen Physiol. 1927;8(6):519–530.

[61] Warburg O. On the origin of cancer cells. Science. 1956;123(3191):309–14.

[62] Martinez-Outschoorn UE, Peiris-Pagés M, Pestell RG, Sotgia F, Lisanti MP. Cancer metabolism: a therapeutic perspective. Nat Rev Clin Oncol. 2017;14(1):11-31.

[63] Mullard A. FDA approves first-in-class cancer metabolism drug. Nat Rev Drug Discov. 2017;16(9):593.

[64] Altenberg B, Greulich KO. Genes of glycolysis are ubiquitously overexpressed in 24 cancer classes. Genomics. 2004;84(6):1014-20.

[65] Ying H, et al. Oncogenic Kras maintains pancreatic tumors through regulation of anabolic glucose metabolism. Cell. 2012;149:656–670.

[66] Wise DR, et al. Myc regulates a transcriptional program that stimulates mitochondrial glutaminolysis and leads to glutamine addiction. Proc Natl Acad Sci USA. 2008;105:18782–18787

[67]Yuan TL, Cantley LC. PI3K pathway alterations in cancer: variations on a theme. Oncogene. 2008;27(41):5497-510.

[68] Fruman DA, Chiu H, Hopkins BD, Bagrodia S, Cantley LC, Abraham RT. The PI3K Pathway in Human Disease. Cell. 2017;170(4):605–635.

[69] Lee YR, Chen M, Pandolfi PP. The functions and regulation of the PTEN tumour suppressor: new modes and prospects. Nat Rev Mol Cell Biol. 2018;19(9):547-62.

[70] Cully M, You H, Levine AJ, Mak TW. Beyond PTEN mutations: the PI3K pathway as an integrator of multiple inputs during tumorigenesis. Nat Rev Cancer. 2006;6(3):184-92.

[71] Ackerman D, Simon MC. Hypoxia, lipids, and cancer: surviving the harsh tumor microenvironment. Trends Cell Biol. 2014;24(8):472-8.

[72] Finicle BT, Jayashankar V, Edinger AL. Nutrient scavenging in cancer. Nat Rev Cancer. 2018;18(10):619-33.

[73] Rabinowitz JD, White E. Autophagy and metabolism. Science. 2010;330(6009):1344-8.

[74] Commisso C, Davidson SM, Soydaner-Azeloglu RG, Parker SJ, Kamphorst JJ, Hackett S, et al. Macropinocytosis of protein is an amino acid supply route in Ras-transformed cells. Nature. 2013;497(7451):633-7.

[75] Walenta S, Snyder S, Haroon ZA, Braun RD, Amin K, Brizel D, et al. Tissue gradients of energy metabolites mirror oxygen tension gradients in a rat mammary carcinoma model. Int J Radiat Oncol Biol Phys. 2001;51(3):840-8.

[76] Gatenby RA, Gawlinski ET, Gmitro AF, Kaylor B, Gillies RJ. Acid-mediated tumor invasion: a multidisciplinary study. Cancer Res. 2006;66(10):5216-23.

[77] Doherty JR, Cleveland JL. Targeting lactate metabolism for cancer therapeutics. J Clin Invest. 2013;123(9):3685–3692.

[78] Yan H, Parsons DW, Jin G, et al. IDH1 and IDH2 mutations in gliomas. N Engl J Med. 2009;360(8):765–773.

[79] Dang L, White DW, Gross S, et al. Cancer-associated IDH1 mutations produce 2-hydroxyglutarate. Nature. 2009;462(7274):739–744.

[80] Ng AP, Alexander WS. Haematopoietic stem cells: past, present and future. Cell Death Discovery. 2017;3(1):17002.

[81] Ito K, Suda T. Metabolic requirements for the maintenance of self-renewing stem cells. Nat Rev Mol Cell Biol. 2014;15(4):243-56.

[82] Goode DK, Obier N, Vijayabaskar MS, Lie ALM, Lilly AJ, Hannah R, et al. Dynamic Gene Regulatory Networks Drive Hematopoietic Specification and Differentiation. Dev Cell. 2016;36(5):572-87.

[83] Greaves M, Maley CC. Clonal evolution in cancer. Nature. 2012;481(7381):306-13.

[84] Arber DA, Orazi A, Hasserjian R, Thiele J, Borowitz MJ, Le Beau MM, et al. The 2016 revision to the World Health Organization classification of myeloid neoplasms and acute leukemia. Blood. 2016;127(20):2391-405.

[85] Youn BS, Mantel C, Broxmeyer HE. Chemokines, chemokine receptors and hematopoiesis. Immunological reviews. 2000;177:150-74.

[86] Kumar CC. Genetic abnormalities and challenges in the treatment of acute myeloid leukemia. Genes Cancer. 2011;2(2):95–107.

[87] Forster VJ, Nahari MH, Martinez-Soria N, Bradburn AK, Ptasinska A, Assi SA, et al. The leukemia-associated RUNX1/ETO oncoprotein confers a mutator phenotype. Leukemia. 2016;30(1):250-3.

[88] Martinez-Soria N, McKenzie L, Draper J, Ptasinska A, Issa H, Potluri S, et al. The Oncogenic Transcription Factor RUNX1/ETO Corrupts Cell Cycle Regulation to Drive Leukemic Transformation. Cancer Cell. 2018;34(4):626-42 e8.

[89] Heidenreich O, Krauter J, Riehle H, Hadwiger P, John M, Heil G, et al. AML1/MTG8 oncogene suppression by small interfering RNAs supports myeloid differentiation of t(8;21)-positive leukemic cells. Blood. 2003;101(8):3157-63.

[90] Fire A, Xu S, Montgomery MK, Kostas SA, Driver SE, Mello CC. Potent and specific genetic interference by double-stranded RNA in Caenorhabditis elegans. Nature. 1998;391(6669):806-11.

[91] Elbashir SM, Lendeckel W, Tuschl T. RNA interference is mediated by 21- and 22-nucleotide RNAs. Genes Dev. 2001;15:188–200

[92] Kappel S, Matthess Y, Kaufmann M, Strebhardt K. Silencing of mammalian genes by tetracycline-inducible shRNA expression. Nat Protoc. 2007;2(12):3257-69.

[93] Levitt, M. H. Spin Dynamics : Basics of Nuclear Magnetic Resonance. 2008. John Wiley & Sons.

[94] Kostidis S, Addie RD, Morreau H, Mayboroda OA, Giera M. Quantitative NMR analysis of intra- and extracellular metabolism of mammalian cells: A tutorial. Anal Chim Acta. 2017;980:1-24.

[95] Gebregiworgis T, Powers R. Application of NMR metabolomics to search for human disease biomarkers. Comb Chem High Throughput Screen. 2012;15(8):595-610.

[96] Beckonert O, Keun HC, Ebbels TM, Bundy J, Holmes E, Lindon JC, et al. Metabolic profiling, metabolomic and metabonomic procedures for NMR spectroscopy of urine, plasma, serum and tissue extracts. Nat Protoc. 2007;2(11):2692-703.

[97] Lian Y, Jiang H, Feng J, Wang X, Hou X, Deng P. Direct and simultaneous quantification of ATP, ADP and AMP by 1H and 31P Nuclear Magnetic Resonance spectroscopy. Talanta. 2016;150:485-92.

[98] Glunde K, Ackerstaff E, Natarajan K, Artemov D, Bhujwalla ZM. Real-time changes in 1H and 31P NMR spectra of malignant human mammary epithelial cells during treatment with the anti-inflammatory agent indomethacin. Magn Reson Med. 2002;48(5):819-25.

[99] Claridge, Timothy DW. High-Resolution NMR Techniques in Organic Chemistry. 2016. Elsevier.

[100] Huang H, Yu Y, Yi X, Zhang Y. Nitrogen metabolism of asparagine and glutamate in Vero cells studied by (1)H/ (15)N NMR spectroscopy. Appl Microbiol Biotechnol. 2007;77(2):427-36.

[101] Martinelle K, Doverskog M, Jacobsson U, Chapman BE, Kuchel PW, Häggström L. Elevated glutamate dehydrogenase flux in glucose-deprived hybridoma and myeloma cells: evidence from 1H/15N NMR. Biotechnol Bioeng. 1998;60(4):508-17.

[102] Saborano R, Eraslan Z, Roberts J, Khanim FL, Lalor PF, Reed MAC, et al. A framework for tracer-based metabolism in mammalian cells by NMR. Sci Rep. 2019;9(1):2520.

[103] Lee S, Wen H, An YJ, Cha JW, Ko Y-J, Hyberts SG, et al. Carbon Isotopomer Analysis with Non-Unifom Sampling HSQC NMR for Cell Extract and Live Cell Metabolomics Studies. Analytical Chemistry. 2017;89(2):1078-85.

[104] Patching S. NMR-Active Nuclei for Biological and Biomedical Applications. Journal of Diagnostic Imaging in Therapy. 2016; 7–48.

[105] R. J. Abraham, J. Fisher and P. Loftus. Introduction to NMR spectroscopy. 1988. Wiley, Chichester.

[106] Freeman, R. Spin Choreography Basic Steps in High Resolution NMR.1996. Oxford University Press.

[107] Bharti SK, et al. Improved quantification from H-1-NMR spectra using reduced repetition times. Metabolomics 2008;4(4): 367-376.

[108] Evilia RF. Quantitative NMR Spectroscopy. Analytical Letters. 2001;34(13): 2227-2236.

[109] Hore P. NMR: The Toolkit : How Pulse Sequences Work. 2015. Oxford University Press.

[110] Freeman, R. Handbook of Nuclear Magnetic Resonance. 1987. United States.

[111] Hoult DI, Richards RE. Critical Factors in the Design of Sensitive High Resolution Nuclear Magnetic Resonance Spectrometers. Proceedings of the Royal Society of London Series A, Mathematical and Physical Sciences. 1975;344(1638):311-40.

[112] Barker P, Freeman R. Pulsed field gradients in NMR. An alternative to phase cycling. Journal of Magnetic Resonance (1969). 1985;64(2):334-8.

[113] Zheng G, Price WS. Solvent signal suppression in NMR. Prog Nucl Magn Reson Spectrosc. 2010;56(3):267-88.

[114] Giraudeau P, Silvestre V, Akoka S. Optimizing water suppression for quantitative NMR-based metabolomics: a tutorial review. Metabolomics. 2015;11(5):1041-55.

[115] Hwang TL, Shaka AJ. Water Suppression That Works. Excitation Sculpting Using Arbitrary Wave-Forms and Pulsed-Field Gradients. Journal of Magnetic Resonance, Series A. 1995;112(2):275-9.

[116] Piotto M, Saudek V, Sklenář V. Gradient-tailored excitation for single-quantum NMR spectroscopy of aqueous solutions. Journal of Biomolecular NMR. 1992;2(6):661-5.

[117] Liu M, Mao X-a, Ye C, Huang H, Nicholson JK, Lindon JC. Improved WATERGATE Pulse Sequences for Solvent Suppression in NMR Spectroscopy. Journal of Magnetic Resonance. 1998;132(1):125-9.

[118] McKay RT. How the 1D-NOESY suppresses solvent signal in metabonomics NMR spectroscopy: An examination of the pulse sequence components and evolution. Concepts in Magnetic Resonance Part A. 2011;38A(5):197-220.

[119] Van QN, Issaq HJ, Jiang Q, Li Q, Muschik GM, Waybright TJ, et al. Comparison of 1D and 2D NMR Spectroscopy for Metabolic Profiling. Journal of Proteome Research. 2008;7(2):630-9.

[120] Mandal PK, Majumdar A. A comprehensive discussion of HSQC and HMQC pulse sequences. Concepts in Magnetic Resonance Part A. 2004;20A(1):1-23.

[121] Keeler, J. Understanding NMR Spectroscopy. 2010. John Wiley and Sons.

[122] Chmurny GN, Hoult DI. The Ancient and Honourable Art of Shimming. Concepts in Magnetic Resonance. 1990;2(3):131-49.

[123] Kovacs H, Moskau D, Spraul M. Cryogenically Cooled Probes — A Leap in NMR Technology. Progress in Nuclear Magnetic Resonance Spectroscopy - Prog Nucl Magn Reson Spectros. 2005;46:131-55.

[124] Styles P, Soffe NF, Scott CA, Crag DA, Row F, White DJ, et al. A high-resolution NMR probe in which the coil and preamplifier are cooled with liquid helium. Journal of Magnetic Resonance (1969). 1984;60(3):397-404.

[125] Odeblad E, Lindstrom G. Some preliminary observations on the proton magnetic resonance in biologic samples. Acta radiol. 1955;43(6):469-76.

[126] Freedberg DI, Selenko P. Live cell NMR. Annu Rev Biophys. 2014;43:171-92.

[127] Bancroft Brown, J, Sriram, R, VanCriekinge, M, et al. NMR quantification of lactate production and efflux and glutamate fractional enrichment in living human prostate biopsies cultured with [1,6-$^{13}C_2$]glucose. Magn Reson Med. 2019; 82: 566– 576

[128] van den Thillart G, Körner F, van Waarde A, Erkelens C, Lugtenburg J. A flow-through probe for in Vivo31P NMR spectroscopy of unanesthetized aquatic vertebrates at 9.4 tesla. Journal of Magnetic Resonance. 1989;84(3):573-9.

[129] Alshamleh I, Krause N, Richter C, Kurrle N, Serve H, Günther UL, et al. Real-Time NMR Spectroscopy for Studying Metabolism. Angew Chem Int Ed Engl. 2020;59(6):2304-8.

[130] Sellick CA, Hansen R, Stephens GM, Goodacre R, Dickson AJ. Metabolite extraction from suspension-cultured mammalian cells for global metabolite profiling. Nat Protoc. 2011;6(8):1241-9.

[131] Sakakibara D, Sasaki A, Ikeya T, Hamatsu J, Hanashima T, Mishima M, et al. Protein structure determination in living cells by in-cell NMR spectroscopy. Nature. 2009;458(7234):102-5.

[132] Wen H, An YJ, Xu WJ, Kang KW, Park S. Real-time monitoring of cancer cell metabolism and effects of an anticancer agent using 2D in-cell NMR spectroscopy. Angew Chem Int Ed Engl. 2015;54(18):5374-7.

[133] Barbieri L, Luchinat E, Banci L. Characterization of proteins by in-cell NMR spectroscopy in cultured mammalian cells. Nat Protoc. 2016;11(6):1101-11.

[134] Serber Z, Selenko P, Hänsel R, Reckel S, Löhr F, Ferrell JE, Jr., et al. Investigating macromolecules inside cultured and injected cells by in-cell NMR spectroscopy. Nat Protoc. 2006;1(6):2701-9.

[135] Dzatko S, Krafcikova M, Hänsel-Hertsch R, Fessl T, Fiala R, Loja T, et al. Evaluation of the Stability of DNA i-Motifs in the Nuclei of Living Mammalian Cells. Angew Chem Int Ed Engl. 2018;57(8):2165-9.

[136] Yamaoki Y, Kiyoishi A, Miyake M, Kano F, Murata M, Nagata T, et al. The first successful observation of in-cell NMR signals of DNA and RNA in living human cells. Physical Chemistry Chemical Physics. 2018;20(5):2982-5.

[137] Selenko P, Frueh DP, Elsaesser SJ, Haas W, Gygi SP, Wagner G. In situ observation of protein phosphorylation by high-resolution NMR spectroscopy. Nat Struct Mol Biol. 2008;15(3):321-9.

[138] Inomata K, Kamoshida H, Ikari M, Ito Y, Kigawa T. Impact of cellular health conditions on the protein folding state in mammalian cells. Chem Commun (Camb). 2017;53(81):11245-8.

[139] Hembram DS, Haremaki T, Hamatsu J, Inoue J, Kamoshida H, Ikeya T, et al. An in-cell NMR study of monitoring stress-induced increase of cytosolic Ca2+ concentration in HeLa cells. Biochem Biophys Res Commun. 2013;438(4):653-9.

[140] Kubo S, Nishida N, Udagawa Y, Takarada O, Ogino S, Shimada I. A gel-encapsulated bioreactor system for NMR studies of protein-protein interactions in living mammalian cells. Angew Chem Int Ed Engl. 2013;52(4):1208-11.

[141] Liu L, Loutherback K, Liao D, Yeater D, Lambert G, Estévez-Torres A, et al. A microfluidic device for continuous cancer cell culture and passage with hydrodynamic forces. Lab on a Chip. 2010;10(14):1807-13.

[142] Pohlscheidt M, Jacobs M, Wolf S, Thiele J, Jockwer A, Gabelsberger J, et al. Optimizing capacity utilization by large scale 3000 L perfusion in seed train bioreactors. Biotechnol Prog. 2013;29(1):222-9.

[143] van den Thillart G, Körner F, van Waarde A, Erkelens C, Lugtenburg J. A flow-through probe for in Vivo31P NMR spectroscopy of unanesthetized aquatic vertebrates at 9.4 tesla. Journal of Magnetic Resonance. 1989;84(3):573-9.

[144] Torres AM, Price WS. Common problems and artifacts encountered in solution-state NMR experiments. Concepts in Magnetic Resonance Part A. 2016;45A(2):e21387.

[145] Zhang Y, Stobbe P, Silvander CO, Chotteau V. Very high cell density perfusion of CHO cells anchored in a non-woven matrix-based bioreactor. J Biotechnol. 2015;213:28-41.

[146] Chandrasekaran P, Seagle C, Rice L, Macdonald J, Gerber DA. Functional analysis of encapsulated hepatic progenitor cells. Tissue engineering. 2006;12(7):2001-8.

[147] Carvalho J, Alves S, Castro MMCA, Geraldes CFGC, Queiroz JA, Fonseca CP, et al. Development of a bioreactor system for cytotoxic evaluation of pharmacological compounds in living cells using NMR spectroscopy. J Pharmacol Toxicol Methods. 2019;95:70-8.

[148] Ben-Tchavtchavadze M, Chen J, Perrier M, Jolicoeur M. A noninvasive technique for the measurement of the energetic state of free-suspension mammalian cells. Biotechnology progress. 2010;26(2):532-41.

[149] Jeffries RE, Gamcsik MP, Keshari KR, Pediaditakis P, Tikunov AP, Young GB, et al. Effect of oxygen concentration on viability and metabolism in a fluidized-bed bioartificial liver using ^{31}P and ^{13}C NMR spectroscopy. Tissue Eng Part C Methods. 2013;19(2):93-100.

[150] Knazek RA, Gullino PM, Kohler PO, Dedrick RL. Cell Culture on Artificial Capillaries: An Approach to Tissue Growth in vitro. Science. 1972;178(4056):65-7.

[151] Gillies RJ, Scherer PG, Rachunand N, Okerlund LS, Martinez-Zacuilan R, Hesterberg L, et al. Iteration of hybridoma growth and productivity in hollow fiber bioreactors using 31P NMR. Magnetic Resonance in Medicine. 1991;18(1):181-92.

[152] 1. Girard PR, Nerem RM. Shear stress modulates endothelial cell morphology and F-actin organization through the regulation of focal adhesion-associated proteins. J Cell Physiol. 1995;163(1):179-93.

[153]Stolberg S, McCloskey KE. Can shear stress direct stem cell fate? Biotechnol Prog. 2009;25(1):10-9.

[154] Hagmann S, Moradi B, Frank S, Dreher T, Kämmerer PW, Richter W, et al. Different culture media affect growth characteristics, surface marker distribution and chondrogenic differentiation of human bone marrow-derived mesenchymal stromal cells. BMC Musculoskelet Disord. 2013;14:223.

[155] Kalfe A, Telfah A, Lambert J, Hergenröder R. Looking into Living Cell Systems: Planar Waveguide Microfluidic NMR Detector for in Vitro Metabolomics of Tumor Spheroids. Anal Chem. 2015;87(14):7402-10.

[156] Foley DA, Bez E, Codina A, Colson KL, Fey M, Krull R, et al. NMR flow tube for online NMR reaction monitoring. Anal Chem. 2014;86(24):12008-13.

[157] Günther UL, Ludwig C, Rüterjans H. NMRLAB—advanced NMR dataprocessing in Matlab. J Magn Reson. 2000;145:201–8.

[158] Ludwig C, Günther UL. MetaboLab-advanced NMR data processing and analysis for metabolomics. BMC Bioinformatics. 2011;12:366.

[159] Wishart DS, Jewison T, Guo AC, Wilson M, Knox C, Liu Y, et al. HMDB 3.0--The Human Metabolome Database in 2013. Nucleic Acids Res. 2013;41(Database issue):D801-D7.

[160] Benjamini Y, Krieger AM, Yekutieli D. Adaptive linear step-up procedures that control the false discovery rate. Biometrika. 2006;93(3):491-507.

[161] Koczula. K. Real-Time Metabolic Flux In Chronic Lymphocytic Leukaemia Cells Adapting To The Hypoxic Niche. PhD thesis. 2015 University of Birmingham.

[162] Schechter AN, Sachs DH, Heller SR, Shrager RI, Cohen JS. Nuclear magnetic resonance titration curves of histidine ring protons. 3. Ribonuclease. J Mol Biol. 1972;71(1):39-48.

[163] Banci L, Barbieri L, Calderone V, Cantini F, Cerofolini L, Ciofi-Baffoni S, et al. Biomolecular NMR at 1.2 GHz. preprint arXiv:191007462. 2019.

[164] Gouilleux B, Charrier B, Danieli E, Dumez JN, Akoka S, Felpin FX, et al. Real-time reaction monitoring by ultrafast 2D NMR on a benchtop spectrometer. Analyst. 2015;140(23):7854-8.

[165] Silva Elipe MV, Milburn RR. Monitoring chemical reactions by low-field benchtop NMR at 45 MHz: pros and cons. Magnetic Resonance in Chemistry. 2016;54(6):437-43.

[166].Foley DA, Dunn AL, Zell MT. Reaction monitoring using online vs tube NMR spectroscopy: seriously different results. Magn Reson Chem. 2016;54(6):451-6.

[167] Gomez MV, de la Hoz A. NMR reaction monitoring in flow synthesis. Beilstein J Org Chem. 2017;13:285-300.

[168]https://commons.m.wikimedia.org/wiki/File:Nuclear_magnetic_resonance_(NMR)

[169] Levenspie O. Chemical Reaction Engineering. 199l. Wiley.

[170] Hall AMR, Chouler JC, Codina A, Gierth PT, Lowe JP, Hintermair U. Practical aspects of real-time reaction monitoring using multi-nuclear high resolution FlowNMR spectroscopy. Catalysis Science & Technology. 2016;6(24):8406-17.

[171] Sudmeier JL, Günther UL, Albert K, Bachovchin WW. Sensitivity Optimization in Continuous-Flow FTNMR. Journal of Magnetic Resonance, Series A. 1996;118(2):145-56.

[172] Hall AMR, Chouler JC, Codina A, Gierth PT, Lowe JP, Hintermair U. Practical aspects of real-time reaction monitoring using multi-nuclear high resolution FlowNMR spectroscopy. Catalysis Science & Technology. 2016;6(24):8406-17.

[173] Ducommun P, Ruffieux P, Kadouri A, von Stockar U, Marison IW. Monitoring of temperature effects on animal cell metabolism in a packed bed process. Biotechnol Bioeng. 2002;77(7):838-42.

[174] Vallejos JR, Brorson KA, Moreira AR, Rao G. Dissolved oxygen and pH profile evolution after cryovial thaw and repeated cell passaging in a T-75 flask. Biotechnology and bioengineering. 2010;105(6):1040-7.

[175] Garcia J, van der Palen RLF, Bollache E, Jarvis K, Rose MJ, Barker AJ, et al. Distribution of blood flow velocity in the normal aorta: Effect of age and gender. J Magn Reson Imaging. 2018;47(2):487-98.

[176] Egan K, Cooke N, Kenny D. Living in shear: platelets protect cancer cells from shear induced damage. Clin Exp Metastasis. 2014;31(6):697-704.

[177] Chistiakov DA, Orekhov AN, Bobryshev YV. Effects of shear stress on endothelial cells: go with the flow. Acta Physiol (Oxf). 2017;219(2):382-408.

[178] Bilgen B, Odabas S. Effects of Mechanotransduction on Stem Cell Behavior. 2016. Wiley.

[179] Yoon SK, Choi SL, Song JY, Lee GM. Effect of culture pH on erythropoietin production by Chinese hamster ovary cells grown in suspension at 32.5 and 37.0 degrees C. Biotechnol Bioeng. 2005;89(3):345-56.

[180] Osman JJ, Birch J, Varley J. The response of GS-NS0 myeloma cells to pH shifts and pH perturbations. Biotechnol Bioeng. 2001;75(1):63-73.

[181] Eales KL, Hollinshead KE, Tennant DA. Hypoxia and metabolic adaptation of cancer cells. Oncogenesis. 2016;5(1):e190.

[182] Yu T, Wang Y, Zhang H, Johnson CH, Jiang Y, Li X, et al. Metabolomics reveals mycoplasma contamination interferes with the metabolism of PANC-1 cells. Anal Bioanal Chem. 2016;408(16):4267-73.

[183] Stannard JN, Horecker BL. The in vitro inhibition of cytochrome oxidase by azide and cyanide. J Biol Chem. 1948;172(2):599-608.

[184] Tom R, Thalappil P. Interaction of Azide Ion with Hemin and Cytochrome c Immobilized on Au and Ag Nanoparticles. Langmuir : the ACS journal of surfaces and colloids. 2006;21:11896-902.

[185] DNA RNA degradation study: Distel high-level disinfectant https://www.tristel.com/uk/tristel-products/distel-for-labs Accessed Dec 2019

[186] Maris P. Modes of action of disinfectants. Rev Sci Tech. 1995;14(1):47-55.

[187] Tilley FW, Schaffer JM. Relation between the chemical constitution and germicidal activity of the monohydric alcohols and phenols. J Bacteriol. 1926;12(5):303-9.

[188] Beckonert O, Keun HC, Ebbels TM, Bundy J, Holmes E, Lindon JC, et al. Metabolic profiling, metabolomic and metabonomic procedures for NMR spectroscopy of urine, plasma, serum and tissue extracts. Nat Protoc. 2007;2(11):2692-703.

[189] Meiboom S, Gill D. Modified Spin Echo Method for Measuring Nuclear Relaxation Times. Review of Scientific Instruments. 1958;29(8):688-91.

[190] Gasparovic C, Barba I, Born J, Barton S, Arus C, Mann P. A study of imidazole-based nuclear magnetic resonance probes of cellular pH. Anal Biochem. 1998;261(1):64-72.

[191] Koczula KM, Ludwig C, Hayden R, Cronin L, Pratt G, Parry H, et al. Metabolic plasticity in CLL: adaptation to the hypoxic niche. Leukemia. 2016;30(1):65-73.

[192] Sefer E, Kleyman M, Bar-Joseph Z. Tradeoffs between Dense and Replicate Sampling Strategies for High-Throughput Time Series Experiments. Cell Syst. 2016;3(1):35-42.

[193] Feron O. Pyruvate into lactate and back: from the Warburg effect to symbiotic energy fuel exchange in cancer cells. Radiother Oncol. 2009;92(3):329-33.

[194] Fiaschi T, Marini A, Giannoni E, Taddei ML, Gandellini P, De Donatis A, et al. Reciprocal Metabolic Reprogramming through Lactate Shuttle Coordinately Influences Tumor-Stroma Interplay. Cancer Res. 2012;72(19):5130-40.

[195] Yao T, Asayama Y. Animal-cell culture media: History, characteristics, and current issues. Reprod Med Biol. 2017;16(2):99-117.

[196] Arii K, Kobayashi H, Kai T, Kokuba Y. Degradation kinetics of L-glutamine in aqueous solution. Eur J Pharm Sci. 1999;9(1):75-8.

[197] Jackson N, Lowe J, Ball J, et al. Two new IgA1-kappa plasma cell leukaemia cell lines (JJN-1 & JJN-2) which proliferate in response to B cell stimulatory factor 2. Clinical and Experimental Immunology. 1989 Jan;75(1):93-99.

[198] Hattori A, Tsunoda M, Konuma T, Kobayashi M, Nagy T, Glushka J, et al. Cancer progression by reprogrammed BCAA metabolism in myeloid leukaemia. Nature. 2017;545(7655):500-4.

[199] Racher AJ, Looby D, Griffiths JB. Use of lactate dehydrogenase release to assess changes in culture viability. Cytotechnology. 1990;3(3):301-7.

[200] Andrae U, Singh J, Ziegler-Skylakakis K. Pyruvate and related alpha-ketoacids protect mammalian cells in culture against hydrogen peroxide-induced cytotoxicity. Toxicol Lett. 1985;28(2-3):93-8.

[201] Giandomenico AR, Cerniglia GE, Biaglow JE, Stevens CW, Koch CJ. The importance of sodium pyruvate in assessing damage produced by hydrogen peroxide. Free Radic Biol Med. 1997;23(3):426-34.

[202] Harris T, Eliyahu G, Frydman L, Degani H. Kinetics of hyperpolarized 13C1-pyruvate transport and metabolism in living human breast cancer cells. Proceedings of the National Academy of Sciences. 2009;106(43):18131-6.

[203] 1. Collins SJ, Gallo RC, Gallagher RE. Continuous growth and differentiation of human myeloid leukaemic cells in suspension culture. Nature. 1977;270(5635):347-9.

[204] Birnie GD. The HL60 cell line: a model system for studying human myeloid cell differentiation. Br J Cancer Suppl. 1988;9:41–45.

[205] Asou H, Tashiro S, Hamamoto K, Otsuji A, Kita K, Kamada N. Establishment of a human acute myeloid leukemia cell line (Kasumi-1) with 8;21 chromosome translocation. Blood. 1991;77(9):2031-6.

[206] Jackson N, Lowe J, Ball J, Bromidge E, Ling NR, Larkins S, et al. Two new IgA1-kappa plasma cell leukaemia cell lines (JJN-1 & JJN-2) which proliferate in response to B cell stimulatory factor 2. Clin Exp Immunol. 1989;75(1):93-9.

[207] https://www.lgcstandards-atcc.org https://www.dsmz.de/dsmz Accessed Jan 2020

[208] Vazquez A, Beg QK, Demenezes MA, Ernst J, Bar-Joseph Z, Barabási AL, et al. Impact of the solvent capacity constraint on E. coli metabolism. BMC Syst Biol. 2008;2:7.

[209] Liu X, Cooper DE, Cluntun AA, Warmoes MO, Zhao S, Reid MA, et al. Acetate Production from Glucose and Coupling to Mitochondrial Metabolism in Mammals. Cell. 2018;175(2):502-13 e13.

[210] Jiang X, Jeffries RE, Acosta MA, Tikunov AP, Macdonald JM, Walker GM, et al. Biocompatibility of Tygon® tubing in microfluidic cell culture. Biomedical Microdevices. 2015;17(1):20.

[211] Neihof RA, Bailey CA. Biocidal properties of anti-icing additives for aircraft fuels. Appl Environ Microbiol. 1978;35(4):698–703.

[212] Whitaker-Menezes D, Martinez-Outschoorn UE, Lin Z, Ertel A, Flomenberg N, Witkiewicz AK, et al. Evidence for a stromal-epithelial "lactate shuttle" in human

tumors: MCT4 is a marker of oxidative stress in cancer-associated fibroblasts. Cell Cycle. 2011;10(11):1772-83.

[213] Crick FH. On protein synthesis. Symp Soc Exp Biol. 1958;12:138-63.

[214] Karczewski KJ, Snyder MP. Integrative omics for health and disease. Nat Rev Genet. 2018;19(5):299-310.

[215] Patti GJ, Yanes O, Siuzdak G. Innovation: Metabolomics: the apogee of the omics trilogy. Nat Rev Mol Cell Biol. 2012;13(4):263-9.

[216] Holmes E, Wilson ID, Nicholson JK. Metabolic phenotyping in health and disease. Cell. 2008;134(5):714-7.

[217] Newgard CB, An J, Bain JR, Muehlbauer MJ, Stevens RD, Lien LF, et al. A branched-chain amino acid-related metabolic signature that differentiates obese and lean humans and contributes to insulin resistance. Cell Metab. 2009;9(4):311-26.

[218] Punzo C, Xiong W, Cepko CL. Loss of daylight vision in retinal degeneration: are oxidative stress and metabolic dysregulation to blame? J Biol Chem. 2012;287(3):1642-8.

[219] DeBerardinis RJ, Thompson CB. Cellular metabolism and disease: what do metabolic outliers teach us? Cell. 2012;148(6):1132-44.

[220] Newgard CB. Metabolomics and Metabolic Diseases: Where Do We Stand? Cell Metab. 2017;25(1):43-56.

[221] Beltran A, Suarez M, Rodriguez MA, Vinaixa M, Samino S, Arola L, et al. Assessment of compatibility between extraction methods for NMR- and LC/MS-based metabolomics. Anal Chem. 2012;84(14):5838-44.

[222] Intlekofer AM, Finley LWS. Metabolic signatures of cancer cells and stem cells. Nat Metab. 2019;1(2):177-88.

[223] Haigis KM, Cichowski K, Elledge SJ. Tissue-specificity in cancer: The rule, not the exception. Science. 2019;363(6432):1150-1.

[224] Boroughs LK, DeBerardinis RJ. Metabolic pathways promoting cancer cell survival and growth. Nat Cell Biol. 2015;17(4):351-9.

[225] Hanahan D, Weinberg RA. Hallmarks of cancer: the next generation. Cell. 2011;144(5):646-74.

[226] Pavlova NN, Thompson CB. The Emerging Hallmarks of Cancer Metabolism. Cell Metab. 2016;23(1):27-47.

[227] Jan M, Majeti R. Clonal evolution of acute leukemia genomes. Oncogene. 2013;32(2):135-40.

[228] Kreitz J, Schönfeld C, Seibert M, et al. Metabolic Plasticity of Acute Myeloid Leukemia. Cells. 2019;8(8):805.

[229] Hattori A, Tsunoda M, Konuma T, Kobayashi M, Nagy T, Glushka J, et al. Cancer progression by reprogrammed BCAA metabolism in myeloid leukaemia. Nature. 2017;545(7655):500-4.

[230] Dang L, White DW, Gross S, Bennett BD, Bittinger MA, Driggers EM, et al. Cancer-associated IDH1 mutations produce 2-hydroxyglutarate. Nature. 2009;462(7274):739-44.

[231] Nakagawa T, Matozaki S, Murayama T, Nishimura R, Tsutsumi M, Kawaguchi R, et al. Establishment of a leukaemic cell line from a patient with acquisition of chromosomal abnormalities during disease progression in myelodysplastic syndrome. British Journal of Haematology. 1993;85(3):469-76.

[232] Nakagawa, T. and S. Matozaki. The SKM-1 Leukemic Cell Line Established from a Patient with Progression to Myelomonocytic Leukemia in Myelodysplastic Syndrome

(MDS)-Contribution to Better Understanding of MDS. Leukemia & Lymphoma 1995;17(3-4): 335-339.

[233] Matsuo Y, MacLeod RA, Uphoff CC, Drexler HG, Nishizaki C, Katayama Y, et al. Two acute monocytic leukemia (AML-M5a) cell lines (MOLM-13 and MOLM-14) with interclonal phenotypic heterogeneity showing MLL-AF9 fusion resulting from an occult chromosome insertion, ins(11;9)(q23;p22p23). Leukemia. 1997;11(9):1469-77.

[234] Constantopoulos G, Barranger JA. Nonenzymatic decarboxylation of pyruvate. Anal Biochem. 1984;139(2):353-8.

[235] O'Donnell-Tormey J, Nathan CF, Lanks K, DeBoer CJ, de la Harpe J. Secretion of pyruvate. An antioxidant defense of mammalian cells. J Exp Med. 1987;165(2):500-14.

[236] Lopalco A, Dalwadi G, Niu S, Schowen RL, Douglas J, Stella VJ. Mechanism of Decarboxylation of Pyruvic Acid in the Presence of Hydrogen Peroxide. J Pharm Sci. 2016;105(2):705–713.

[237] Meiser J, Tumanov S, Maddocks O, Labuschagne CF, Athineos D, Van Den Broek N, et al. Serine one-carbon catabolism with formate overflow. Science Advances. 2016;2(10):e1601273.

[238] DeBerardinis RJ, Mancuso A, Daikhin E, Nissim I, Yudkoff M, Wehrli S, et al. Beyond aerobic glycolysis: Transformed cells can engage in glutamine metabolism that exceeds the requirement for protein and nucleotide synthesis. Proceedings of the National Academy of Sciences. 2007;104(49):19345-50.

[239] Tennant DA, Durán RV, Gottlieb E. Targeting metabolic transformation for cancer therapy. Nat Rev Cancer. 2010;10(4):267-77.

[240] Rodrigues TB, Serrao EM, Kennedy BW, Hu DE, Kettunen MI, Brindle KM. Magnetic resonance imaging of tumor glycolysis using hyperpolarized 13C-labeled glucose. Nat Med. 2014;20(1):93–97.

[241] Chen K, Liu J, Heck S, Chasis JA, An X, Mohandas N. Resolving the distinct stages in erythroid differentiation based on dynamic changes in membrane protein expression during erythropoiesis. Proc Natl Acad Sci U S A. 2009;106(41):17413–17418.

[242] Zhang D, Li J, Wang F, Hu J, Wang S, Sun Y. 2-Deoxy-D-glucose targeting of glucose metabolism in cancer cells as a potential therapy. Cancer Lett. 2014;355(2):176-83.

[243] Owen MR, Doran E, Halestrap AP. Evidence that metformin exerts its anti-diabetic effects through inhibition of complex 1 of the mitochondrial respiratory chain. Biochem J. 2000;348 Pt 3(Pt 3):607–614.

[244] El-Mir M-Y, Nogueira V, Fontaine E, Avéret N, Rigoulet M, Leverve X. Dimethylbiguanide Inhibits Cell Respiration via an Indirect Effect Targeted on the Respiratory Chain Complex I. Journal of Biological Chemistry. 2000;275(1):223-8.

[245] Fendt SM, Bell EL, Keibler MA, Davidson SM, Wirth GJ, Fiske B, et al. Metformin decreases glucose oxidation and increases the dependency of prostate cancer cells on reductive glutamine metabolism. Cancer Res. 2013;73(14):4429-38.

[246] Clayton TA, Lindon JC, Cloarec O, Antti H, Charuel C, Hanton G, et al. Pharmaco-metabonomic phenotyping and personalized drug treatment. Nature. 2006;440(7087):1073-7.

[247] Schinkel AH. The physiological function of drug-transporting P-glycoproteins. Seminars in Cancer Biology. 1997;8(3):161-70.

[248] Skene PJ, Henikoff JG, Henikoff S. Targeted in situ genome-wide profiling with high efficiency for low cell numbers. Nat Protoc. 2018;13(5):1006-19.

[249] Sánchez-Illana Á, Piñeiro-Ramos JD, Sanjuan-Herráez JD, Vento M, Quintás G, Kuligowski J. Evaluation of batch effect elimination using quality control replicates in LC-MS metabolite profiling. Anal Chim Acta. 2018;1019:38-48.

[250] Lovelock JE, Bishop MWH. Prevention of Freezing Damage to Living Cells by Dimethyl Sulphoxide. Nature. 1959;183(4672):1394-5.

[251] Kuilman T, Michaloglou C, Mooi WJ, Peeper DS. The essence of senescence. Genes Dev. 2010;24(22):2463-79.

[252] Sagot I, Laporte D. Quiescence, an individual journey. Curr Genet. 2019;65(3):695-9.

[253] Pabst T, Mueller BU, Zhang P, Radomska HS, Narravula S, Schnittger S, et al. Dominant-negative mutations of CEBPA, encoding CCAAT/enhancer binding protein-alpha (C/EBPalpha), in acute myeloid leukemia. Nat Genet. 2001;27(3):263-70.

[254] Umek R, Friedman A, McKnight S. CCAAT-enhancer binding protein: a component of a differentiation switch. Science. 1991;251(4991):288-92.

[255] Watkins PJ, Condreay JP, Huber BE, Jacobs SJ, Adams DJ. Impaired Proliferation and Tumorigenicity Induced by CCAAT/Enhancer-binding Protein. Cancer Res. 1996;56(5):1063-7.

[256] Racher AJ, Looby D, Griffiths JB. Use of lactate dehydrogenase release to assess changes in culture viability. Cytotechnology. 1990;3(3):301-7.

[257] Meiser J, Tumanov S, Maddocks O, Labuschagne CF, Athineos D, Van Den Broek N, et al. Serine one-carbon catabolism with formate overflow. Science Advances. 2016;2(10):e1601273.

[258] Andrae U, Singh J, Ziegler-Skylakakis K. Pyruvate and related alpha-ketoacids protect mammalian cells in culture against hydrogen peroxide-induced cytotoxicity. Toxicol Lett. 1985;28(2-3):93-8.

[259] Giandomenico AR, Cerniglia GE, Biaglow JE, Stevens CW, Koch CJ. The importance of sodium pyruvate in assessing damage produced by hydrogen peroxide. Free Radic Biol Med. 1997;23(3):426-34.

[260] Harris T, Eliyahu G, Frydman L, Degani H. Kinetics of hyperpolarized 13C pyruvate transport and metabolism in living human breast cancer cells. Proceedings of the National Academy of Sciences. 2009;106(43):18131-6.

[261] Janzer A, German NJ, Gonzalez-Herrera KN, Asara JM, Haigis MC, Struhl K. Metformin and phenformin deplete tricarboxylic acid cycle and glycolytic intermediates during cell transformation and NTPs in cancer stem cells. Proc Natl Acad Sci U S A. 2014;111(29):10574-9.

[262] Liu X, Romero IL, Litchfield LM, Lengyel E, Locasale JW. Metformin Targets Central Carbon Metabolism and Reveals Mitochondrial Requirements in Human Cancers. Cell Metab. 2016;24(5):728-39.

[263] Ducker GS, Chen L, Morscher RJ, Ghergurovich JM, Esposito M, Teng X, et al. Reversal of Cytosolic One-Carbon Flux Compensates for Loss of the Mitochondrial Folate Pathway. Cell Metab. 2016;23(6):1140-53.

[264] Bruns I, Lucas D, Pinho S, Ahmed J, Lambert MP, Kunisaki Y, et al. Megakaryocytes regulate hematopoietic stem cell quiescence through CXCL4 secretion. Nat Med. 2014;20(11):1315-20.

[265] Sakamoto A, Kunou S, Shimada K, Tsunoda M, Aoki T, Iriyama C, et al. Pyruvate secreted from patient-derived cancer-associated fibroblasts supports survival of primary lymphoma cells. Cancer Sci. 2019;110(1):269-78.

[266] Bruntz RC, Lane AN, Higashi RM, Fan TW. Exploring cancer metabolism using stable isotope-resolved metabolomics (SIRM). J Biol Chem. 2017;292(28):11601-9.

[267] Chong M, Jayaraman A, Marin S, Selivanov V, de Atauri Carulla PR, Tennant DA, et al. Combined Analysis of NMR and MS Spectra (CANMS). Angew Chem Int Ed Engl. 2017;56(15):4140-4.

[268] Keshari KR, Kurhanewicz J, Jeffries RE, Wilson DM, Dewar BJ, Van Criekinge M, et al. Hyperpolarized ^{13}C spectroscopy and an NMR-compatible bioreactor system for the investigation of real-time cellular metabolism. Magn Reson Med. 2010;63(2):322-9.

[269] Hansen AL, Li D, Wang C, Bruschweiler R. Absolute Minimal Sampling of Homonuclear 2D NMR TOCSY Spectra for High-Throughput Applications of Complex Mixtures. Angew Chem Int Ed Engl. 2017;56(28):8149-52.

[270] Reed MAC, Roberts J, Gierth P, Kupče Ē, Günther UL. Quantitative Isotopomer Rates in Real-Time Metabolism of Cells Determined by NMR Methods. Chembiochem. 2019;20(17):2207-11.

[271] Smith TB, Patel K, Munford H, Peet A, Tennant DA, Jeeves M, et al. High-Speed Tracer Analysis of Metabolism (HS-TrAM). Wellcome Open Res. 2018;3:5.

[272] Vande Voorde J, Ackermann T, Pfetzer N, Sumpton D, Mackay G, Kalna G, et al. Improving the metabolic fidelity of cancer models with a physiological cell culture medium. Science Advances. 2019;5(1):7314.